Reparative Cells are Recruited to Sites of Gastric Injury: Lessons from Oxidative Stress and Innate Immune Responses

By

Anne R. Meyer

Dissertation

Submitted to the Faculty of the

Graduate School of Vanderbilt University

In partial fulfillment of the requirements

for the degree of

DOCTOR OF PHILOSOPHY

in

Cell and Developmental Biology

August 31, 2020

Nashville, Tennessee

Approved:

Matthew Tyska, PhD

Maureen Gannon, PhD

Vivian Gama, PhD

R. Stokes Peebles, MD

ACKNOWLEDGEMENTS

I first must acknowledge and thank my mentor, Dr. Jim Goldenring. I am forever grateful for Jim's guidance and support throughout my doctoral training. Jim was a better mentor than I could have possibly imagined. As a result of his leadership, I feel that I possess the knowledge, tools, and confidence to have success moving forward. In addition to having a wonderful mentor, I have been so fortunate to be a part of supportive lab environment. Every person, past and present, was always willing to lend a helping hand. The Goldenring lab and all of the members of the Epithelial Biology Center were instrumental in my education. Special thanks to Dr. Amy Engevik and Dr. Eunyoung Choi for being my support system, both of you have served as role models throughout my doctoral training.

I would also like to acknowledge my committee members: Dr. Matthew Tyska, Dr. Maureen Gannon, Dr. Vivian Gama, and Dr. Stokes Peebles. Thank you for your wisdom, encouragement, insights, and for always challenging me. Under the mentorship of Dr. Goldenring, my committee members, and my collaborators and with the supportive environment at Vanderbilt University I have built a solid foundation of research skills, knowledge, and life experience to become a successful independent investigator in biomedical sciences.

I would like to acknowledge the funding sources that made these studies possible. These studies were supported by grants from Department of Veterans Affairs Merit Review Awards (IBX000930), National Institute of Diabetes and Digestive and Kidney Diseases Research Project Grant Program (RO1 DK071590 and RO1 DK101332) and

Kirschstein Predoctoral National Service Award (F31 DK117592), and National Institute of General Medicine Predoctoral Training Grant Program (T32 GM008554). This work was also supported by core resources: Vanderbilt Digestive Disease Center (NIH P30 DK058404), Translational Pathology Shared Resource (NCI/NIH Cancer Center Support Grant 2P30 CA068485-14), and imaging supported by the Vanderbilt Digital Histology Shared Resource supported by a VA Shared Instrumentation grant (1IS1BX003097).

Finally, I would like to thank my family, friends, and my dog Jackson for providing unwavering support throughout my doctoral training. I couldn't have done this without you.

TABLE OF CONTENTS

LIST OF FIGURES

Figure Page

LIST OF TABLES

Table Page

CHAPTER I:

INTRODUCTION

The epithelial lining of the stomach is exposed to harsh conditions including ingested food and bacteria, as well as gastric acid and digestive enzymes (Beasley et al., 2015; Yang et al., 2013). The stomach is protected from this extreme environment by the mucosal barrier which is lined with epithelial cells linked by tight junctions and a thick mucus gel to block stomach contents from penetrating to the underlying tissue layers. Severe injury to the lining of the stomach leads to reprogramming of differentiated cells to metaplastic cell lineages in order to recruit reparative cells to sites of mucosal injury (Goldenring, 2018). Metaplasia refers to the presence of a normal cell lineage in a tissue where it is not normally found. In most cases, metaplastic lineages are characterized by the expression of mucins, adding further protection to the mucosa. In fact, metaplastic lineages often acquire the characteristics of mucin-secreting cells found in the distal stomach: antral/pyloric glands or Brunner's glands (Goldenring, 2018; Hoffmann, 2015; Schmidt et al., 1999). In addition to metaplastic cell lineages, other reparative cells are recruited to sites of mucosal injury including normal mucin-secreting cells, sensory cells, and immune cells (Choi et al., 2016; Choi et al., 2015; Nomura et al., 2005; Petersen et al., 2017; Petersen et al., 2014). Reparative lineages work to maintain redox balance, boost mucin-secretion, and activate an immune response.

Recent studies have sought to understand the mechanisms used by mature, post-mitotic cells to change their differentiation state. Zymogenic chief cells in the oxyntic

region of the stomach produce enzymes required for digestion, such as pepsinogen and lipases (Ramsey et al., 2007). Following acute or chronic injury, mature chief cells are capable of reprogramming into mucin-secreting spasmolytic polypeptide-expressing metaplasia (SPEM) (Engevik et al., 2016; Leushacke et al., 2017; Meyer et al., 2019; Nam et al., 2010a; Radyk et al., 2017; Willet et al., 2018). Previous studies have shown that SPEM cells have morphological and gene expression profiles intermediate between digestive enzyme-secreting chief cells and mucin-secreting cells found in deep antral glands (Weis et al., 2013).

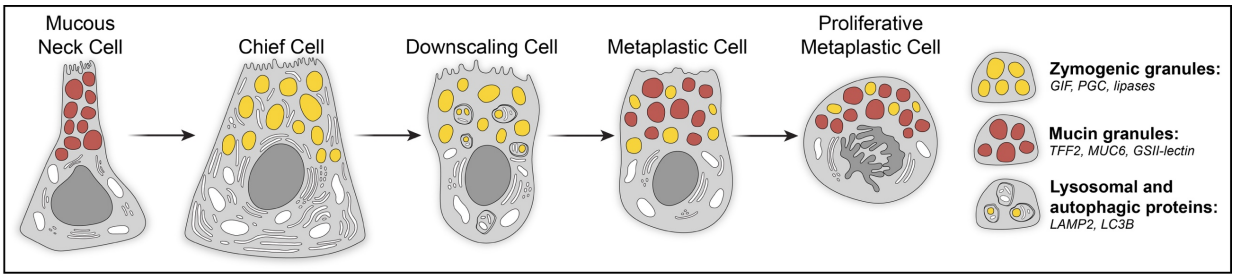

Figure 1. Diagram of chief cell differentiation and reprogramming to a mucin-secreting metaplastic cell lineage.
Mucous neck cells act as the precursor to digestive enzyme-secreting chief cells. Upon damage to the gastric epithelium chief cells undergo a highly regulated reprogramming process. The first step is to downscale mature chief cell characteristics. Autophagic and lysosomal pathways are acutely up-regulated in order to target rough endoplasmic reticulum, mitochondria, and secretory granules for degradation. Next, there are distinct transcriptional changes that include the up-regulation of MUC6 and TFF2 to promote mucin granule formation. Finally, if injury and chronic inflammation persist metaplastic cells are capable of re-entering into the cell cycle and proliferating.

Similar reparative lineages have been described in a number of mucosal contexts including esophagus, stomach, small bowel, colon, and pancreas (Goldenring, 2018). While such processes are programmed to recede following the resolution of injury, chronic damage and inflammation promote the evolution of these reparative metaplastic lineages into dysplastic or pre-neoplastic lineages that are a risk factor for developing cancer (Saenz and Mills, 2018; Schmidt et al., 1999). The most common type of gastric

cancer, intestinal-type adenocarcinoma, almost always evolves in a field of pre-existing parietal cell loss (oxyntic atrophy) and metaplasia (Correa, 1988; de Martel et al., 2012). Two types of metaplasia are observed in the atrophic stomach: intestinal metaplasia (IM) and spasmolytic polypeptide-expressing metaplasia (SPEM). Dr. Pelayo Correa was the first to describe the association of IM (the presence of Mucin2 and TFF3 expressing intestinal-type goblet cells in the stomach) with the development of intestinal-type gastric cancer (Correa et al., 2010). In 1999, Dr. Jim Goldenring described a second metaplastic process associated with intestinal-type gastric cancer designated SPEM, which displayed Mucin6 and TFF2 (also known as spasmolytic polypeptide) expressing cells at the base of oxyntic glands (Schmidt et al., 1999). Globally, gastric cancer is a major health concern and remains one of the leading causes of cancer-related death (Burkitt et al., 2017). Therefore, a more comprehensive understanding of the response to damage in the stomach, development of metaplasia, and progression to intestinal-type gastric cancer is needed.

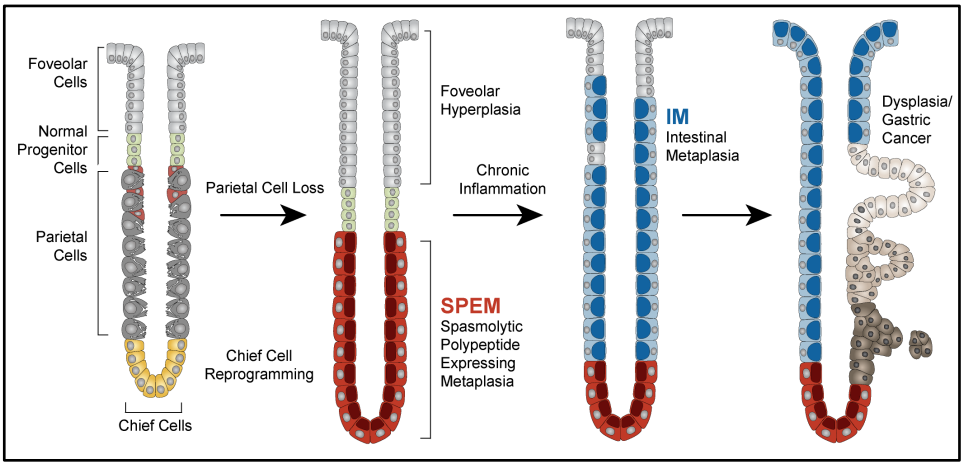

Figure 2. Diagram depicting the evolution of metaplasia and cancer in the stomach. *Evidence indicates that parietal cell loss is the initiating event that leads to the development of SPEM via the reprogramming of chief cells. In the presence of continued inflammation, intestinal metaplasia (IM) develops. SPEM and IM are precancerous lesions and are considered precursors to dysplasia and gastric adenocarcinoma.*

The most common cause of chronic damage to the stomach occurs as a result of infection with the bacterium *Helicobacter pylori*, which leads to the loss of acid-secreting parietal cells (Roth et al., 1999). Gastric pathology can take months to develop in *Helicobacter* infected mice, and years in humans. To facilitate an accelerated model for induction of oxyntic atrophy, our laboratory has developed two acute models of parietal cell loss through the administration of the parietal cell toxic drugs L635 and DMP-777 (Goldenring et al., 2000). Up-regulation of proteins required for the metaplastic transition are visualized within hours of the administration of a parietal cell toxic drug (Meyer et al., 2019; Weis et al., 2013; Willet et al., 2018).

CHARACTERIZATION OF GASTRIC PATHOLOGY

Gastric cancer develops as a result of a multistep process that is influenced by the genetic susceptibility of the host, infection, diet, as well as other environmental factors. Understanding the molecular mechanisms that drive gastric cancer development is important to identify novel targets for gastric cancer prevention and treatment. However, there is often variability in the nomenclature used to describe pathological changes in the gastric mucosa. Therefore, it is necessary to characterize the cellular changes that occur at key stages of gastric carcinogenesis. This has resulted in a set of pivotal biomarkers that correspond to the specific mucosal changes that occur in the multistep process proceeding gastric cancer development.

Gastritis

Gastritis is a general term used to describe inflammation in the lining of the stomach. In humans, chronic gastritis arises as a consequence of *Helicobacter pylori*

infection, environmental factors, or in the context of gastric autoimmunity (Annibale et al., 2020; Sipponen and Maaroos, 2015). Gastritis can be diagnosed on hematoxylin-eosin (H&E) stained tissues. However, biomarkers can also be used to detect specific immune cell lineages including: T cells (CD3), macrophages (F4/80), eosinophils (MBP), mast cells (mast cell chymase), and NK cells (CD161). Chronic inflammation in the stomach can set off destruction of the gastric mucosa, also known as atrophic gastritis.

Oxyntic atrophy

The loss of acid-secreting parietal cells, also known as oxyntic atrophy, initiates a cascade of epithelial changes and metaplastic events in the stomach. (Goldenring and Nam, 2010). The most common cause of oxyntic atrophy in humans is *Helicobacter*-induced chronic inflammation. However, oxyntic atrophy can be modeled in rodents via pharmacological obliteration of parietal cells. Oxyntic atrophy is often diagnosed based on the loss of eosinophilic parietal cells on H&E stained tissue sections. More definitive analysis of parietal cell loss is performed through staining of parietal cell-specific biomarkers such as H^+K^+ ATPase. Oxyntic atrophy triggers mucosal transformation that leads to hyperplastic and metaplastic lesions in the gastric mucosa.

Foveolar hyperplasia

Foveolar hyperplasia is a term used to describe the expansion of the foveolar cell compartment that makes up the luminal section of the gastric gland. Foveolar cells secrete a gel-forming mucin, MUC5AC, that contributes to protection of the epithelium. Foveolar hyperplasia is associated with increased proliferation in the normal gastric stem/progenitor cells (Nomura et al., 2005). Foveolar hyperplasia has been connected

with elevations in gastrin (a hormone that stimulates the secretion of gastric acid) and TGFα (as seen in Menetrier's disease) (Coffey et al., 1992; Poynter et al., 1986). Foveolar hyperplasia is also a common lesion observed in the atrophic mammalian stomach (Goldenring et al., 2000).

Spasmolytic polypeptide-expressing metaplasia

Injury to the epithelial layer and inflammation in the stomach, including *Helicobacter pylori*-induced oxyntic atrophy (Schmidt et al., 1999) or ulceration (Engevik et al., 2016) initiates the reprogramming and proliferation of a differentiated zymogen secretory cell type known as the chief cell (Leushacke et al., 2017; Nam et al., 2010b; Radyk et al., 2017). Chief cells are mature, post-mitotic cells located at the base of the gland that are responsible for secreting digestive enzymes. Chief cells are capable of reprogramming into a mucin-secreting metaplastic cell lineage known as SPEM. Metaplasia refers to the presence of a normal cell lineage in a tissue where it is not normally found. The reprogramming of chief cells into SPEM occurs through a highly regulated process that involves dismantling the chief cell secretory architecture and distinct transcriptional changes that include the up-regulation of MUC6, TFF2, and CD44v9. SPEM cells are reactive to Periodic acid-Schiff (PAS) stain, a stain used to detect polysaccharides and glycoproteins such as mucins within tissues (Fu and Campbell-Thompson, 2017). In the setting of persistent injury and inflammation, SPEM lineages are capable of re-entering the cell cycle and are positive for proliferation markers such as Ki67 and PCNA.

SPEM is a common metaplastic phenotype observed in the atrophic human (Halldorsdottir et al., 2003; Yamaguchi et al., 2002) and rodent (Goldenring et al., 2000;

Weis et al., 2013) stomach that is highly correlated with gastric repair and the development of intestinal-type gastric cancer (Goldenring et al., 2010; Zhang et al., 2017). Indeed, recent investigations have noted that SPEM lineages are present at the edges of healing ulcers in the body of the stomach, and these lineages directly contribute to the mucosal response to injury. Thus, in the stomach where injury may be compounded by the caustic nature of acidic gastric secretions, the presence of increased mucin secretion at the site of damage represents a critical physiological response to local injury. Nevertheless, increasing evidence indicates that maintenance of metaplasia in the presence of chronic inflammation, and perhaps progression of SPEM to intestinal metaplasia, can predispose an individual to develop dysplasia in the gastric mucosa.

Intestinal metaplasia

Intestinal metaplasia (IM) is a term used to describe the presence of mucin-secreting intestinal-type goblet cells in the stomach. Like SPEM, IM is associated with the development of dysplasia and intestinal-type gastric cancer (Correa, 1988; Correa et al., 2010). IM is reactive to Alcian blue stain, however labeling with goblet cell biomarkers such as MUC2 or TFF3 provides the most definitive indication of IM in the stomach.

Dysplasia

The term dysplasia (also referred to as intraepithelial neoplasia) is used to describe an abnormal mass of non-invasive cells. Dysplasia in the gastrointestinal tract is considered a precursor to cancer and a marker of high cancer risk (Sharma and Montgomery, 2013). While biomarkers of metaplasia and cancer in the stomach have been described, the definition of dysplastic transition has not been identified. Generally,

pathologists diagnose dysplasia by a set of cytological and architectural criteria. Recently, a putative marker (TROP2) of the transition from metaplasia to dysplasia has been proposed (Riera et al., 2020). TROP2 is up-regulated in gastric dysplasia and promotes dysplastic cell behaviors.

Intestinal-type gastric adenocarcinoma

Gastric cancer can be divided into two main types: intestinal and diffuse. Intestinal-type gastric adenocarcinoma is the end result of an inflammatory process that progresses from gastritis and oxyntic atrophy to metaplasia and dysplasia in the gastric mucosa (Goldenring and Nam, 2010). Adenocarcinoma cells have aberrant, invasive, and metastatic characteristics. Intestinal-type gastric cancer is detected in H&E stained tissue sections by patterns of irregular structures such as multilayered cell configuration, altered nuclear morphology and positioning, and submucosal invasion. Specific genes/ proteins exhibit high levels of expression in intestinal-type gastric cancer including CDH1, CDX2. and HER2, however, the specific role of these biomarkers in cancer development remains to be determined (Ma et al., 2016).

The response to injury or infection in the stomach is a balancing act between repair mechanisms and the processes that drive carcinogenesis. Recruitment of reparative lineages such as foveolar hyperplasia, SPEM, and IM are integral to the protection and restoration of the stomach after damage. However, maintenance of these lineages in the presence of persistent inflammation and injury can drive cancer development. Identifying the factors required for repair and progression to cancer in the stomach remain a priority.

The following chapters are centered on the early repair mechanisms in the gastric mucosa after acute injury.

PROJECT SUMMARY

Globally, gastric cancer is a major health burden and remains one of the leading causes of cancer-related death. As is true of several cancer types, gastric cancer development is often preceded by the emergence of preneoplastic lesions. In gastric carcinogenesis, *Helicobacter pylori*-induced oxyntic atrophy causes chronic inflammation and histopathologic changes that lead to metaplasia and then cancer in the gastric mucosa. Identifying the events involved in wound repair and metaplasia development in the stomach remain a priority, as identification of any of these factors could lead to better surveillance methods and therapies. Our previous work in mouse models of acute gastric injury have indicated that repair mechanisms and metaplasia development in the stomach require oxidative stress and innate immune responses. The present studies seek to identify the role of antioxidant responses in chief cell reprogramming to mucin-secreting SPEM after gastric injury. Furthermore, the research presented here will interrogate the role of the innate immune system and ILC2s in gastric epithelial repair. The following chapters will provide data suggesting that oxidative stress and innate immune responses are required for recruiting reparative cells to sites of gastric injury.

CHAPTER II:

OXIDATIVE STRESS RESPONSE

Adapted from: **Meyer AR**, Engevik AC, Willet SG, Williams JA, Zou Y, Massion PP, Mills JC, Choi E, Goldenring JR. Cystine/glutamate antiporter (xCT) is required for chief cell plasticity after gastric injury. *Cellular and Molecular Gastroenterology and Hepatology*, 2019

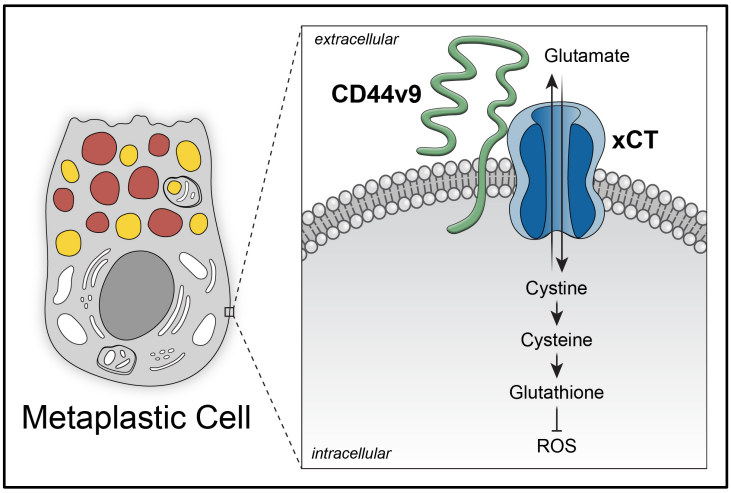

Figure 3. Diagram of the CD44v9-xCT system expressed by metaplastic cells. *CD44v9 stabilizes xCT on the membrane of metaplastic cells. CD44v9 and xCT work together to increases intracellular cystine uptake. Through a multi-step process cystine is converted to glutathione, a potent antioxidant that combats ROS.*

INTRODUCTION

Cluster-of-differentiation (CD)44 is widely known as the receptor for hyaluronic acid that influences cell motility, survival, and proliferation (Isacke and Yarwood, 2002). CD44 regulates proliferation of normal progenitors and metaplastic cells in the stomach (Bertaux-Skeirik et al., 2015; Khurana et al., 2013). Alternative splicing can produce variant isoforms of CD44 with unique functions (Prochazka et al., 2014). CD44 variant isoform 9 (CD44v9) is a cell surface glycoprotein not normally expressed in the stomach.

However, it was recently discovered that CD44v9 is up-regulated early in the transition to SPEM and CD44v9 is now considered a SPEM marker (Wada et al., 2013). One of the functions of CD44v9 is to interact with and stabilize xCT (SLC7A11), a subunit of the heterodimeric cystine-glutamate antiporter (Ishimoto et al., 2011). CD44v9 stabilization of xCT on the cell membrane increases cystine uptake into the cell. Increased intracellular cystine promotes glutathione synthesis, an important molecule for the defense against reactive oxygen species (ROS) (Nagano et al., 2013). The oxidative stress response, including up-regulation of nutrient transporters, plays an important role in many biological processes and the pathogenesis of a variety of diseases. In the stomach, an oxidative stress response in cells at sites of mucosal injury is critical for tissue repair and perturbations to the CD44v9-xCT system often result in redox imbalance and cell death (Sato et al., 2005).

Sulfasalazine is a drug that was first synthesized in the 1940s from a combination of sulfapyridine (an antibiotic) and mesalazine (an anti-inflammatory agent) linked by an azo bridge (Peppercorn, 1984). Recently, it was discovered that the parent compound, sulfasalazine, is a specific and potent inhibitor of xCT-mediated cystine transport (Gout et al., 2001). Several studies have used sulfasalazine treatment to target xCT activity on cancer stem cells (Chung et al., 2005; Nagane et al., 2018; Wada et al., 2013; Zavros, 2017). Here, we utilized sulfasalazine as a tool to inhibit xCT-mediated cystine transport, an event that is required for chief cell reprogramming after gastric injury. We determined that xCT activity is required for cystine uptake and ROS detoxification by SPEM cells and metaplasia proliferation. Inhibition of xCT prevented zymogenic chief cell reprogramming *in vivo*. xCT-deficient mice exhibited increased levels of ROS and apoptosis and did not

develop SPEM after acute parietal cell loss. Our results suggest that adaptation to oxidative stress and up-regulation of xCT activity is crucial for reprogramming of chief cells after gastric injury.

MATERIALS AND METHODS

Mouse Models

C57BL/6J mice approximately eight weeks old were purchased from Jackson Labs (Bar Harbor, Maine, USA). xCT knockout (xCTKO) mice were generously donated by Dr. David E. Featherstone, M.S., Ph.D. at University of Illinois at Chicago (De Bundel et al., 2011; McCullagh and Featherstone, 2014; Sato et al., 2005). Genotype was confirmed for the xCTKO mice using PCR as previously described (De Bundel et al., 2011). Each experimental group consisted of at least three to five mice. L635 (synthesized by the Chemical Synthesis Core of the Vanderbilt Institute of Chemical Biology), dissolved in dH_2O was administered by oral gavage (350 mg/kg) once a day for 3 consecutive days. Three-time points were used to analyze chief cell reprogramming: 12, 24, and 72 hours post L635 treatment ± sulfasalazine. DMP-777 (a gift from DuPont-Merck Co.) dissolved in 1% methylcellulose was administered by oral gavage (350 mg/kg) once a day for 10 consecutive days. Intraperitoneal injection of sulfasalazine (10 mg/day) was administered two days prior to and throughout L635 and DMP-777 treatment. Sulfasalazine was freshly prepared each day in 0.1M NaOH adjusted with 1M HCl to pH 8. Intraperitoneal injection of the metabolites of sulfasalazine, sulfapyridine (3 mg/day) and mesalazine (5 mg/day), were administered two days prior to and throughout L635 treatment in the same manner as sulfasalazine (Nashed et al., 2017). Archival sections of stomach from 12 month *H. felis*-infected mice and human clinical specimens were obtained from previous investigations (Nam et al., 2010a; Sousa et al., 2012). The care, maintenance, and treatment of animals in these studies adhere to the protocols approved by the Institutional Animal Care and Use Committee of Vanderbilt University.

Cell Culture

Cell lines were isolated from Immortomice as previously described (Weis et al., 2014). Immortomice are transgenic mice with interferon-γ (IFN-γ) inducible expression of temperature-sensitive T antigen. In cells that are isolated from Immortomice, addition of IFN-γ promotes the expression of immortalizing T antigen. At the permissive temperature (33 ºC), T antigen protein folds properly and immortalizes the cells. At the nonpermissive temperature (39 ºC) in the absence of IFN-γ, remaining T antigen protein misfolds and returns the cells to a differentiated state. Chief and SPEM cell lines were maintained at the permissive temperature in the presence of IFN-γ and were differentiated at 39 ºC for 48 hours with no IFN-γ before experiments were performed. Cells were cultured in ThermoFisher DMEM/F12 (50:50) media supplemented with 10% Omega Scientific FBS, 100 U/mL penicillin and streptomycin (Corning 30-002-Cl), 100 µg/mL MycoZAP Plus-PR (Lonza VZA-2021), 1 ng/mL EGF (Peprotech AF-100-15), 1 ng/mL bFGF (Peprotech 100-18B), 1 µg/mL hydrocortisone (Sigma H0888), 8 µg/mL insulin/transferring/selenium (ITS) solution (ThermoFisher 41400045), and 5 U/mL IFN-γ (Peprotech 315-05). Cells were plated on collagen (PureCol Type 1 Advanced BioMatrix 5005)-coated plates (working solution 0.03 mg/mL in PBS). For staining, cells were fixed in 4% paraformaldehyde (PFA) for 20 minutes. After fixation, cells were blocked and permeabilized in 1x PBS with 10 % donkey serum and 0.3% Triton X-100 for 30 minutes. Cells were incubated in primary antibodies, diluted in 1x PBS with 1% donkey serum and 0.05% Tween-20, for one hour at room temperature. Cells were then incubated in fluorescent secondary antibodies, diluted in 1x PBS, for one hour at room temperature before DAPI nuclear counter stain was added. Zeiss Axio Imager M2 microscope with Axiovision digital imaging system was

used to image fixed cells. For xCT blockade, cells were treated with 0.1 mM sulfasalazine every day after 48 hours of differentiation. The pH level of media was monitored daily. To monitor cystine uptake, cells were treated with Cystine-FITC (a gift from Dr. Jeffrey Rathmell) for two hours (Siska et al., 2016). After two hours, Hoechst nuclear counter stain was added, and cells were washed three times with 1x PBS. EVOS FL Cell Imaging System was used to visualize intracellular Cystine-FITC. To monitor proliferation, cell number was measured by Biorad TC10 Automated Cell Counter. Three replicates were performed for each experiment.

siRNA Transfection

ImSPEM cells were plated on collagen-coated 6 well plates the day before transfection to provide confluency of 60-70% in 24 hours. ImSPEM cells were transfected with Slc7a11 Mouse siRNA Oligo Duplexes or Trilencer-27 Universal Scrambled Negative Control siRNA Duplex (ORIGENE SR416143) according to manufacturer's recommendations using siTran 1.0 siRNA transfection reagent (ORIGENE TT300001).

Quantitative Real-Time PCR Analysis

Total RNA from the stomach (oxyntic region) was extracted from paraformaldehyde-fixed paraffin-embedded tissue of three to five mice per experimental group to examine the expression of mRNA transcripts (*Cd44v9, xCT, Esrp1, Atg4, Atg5, Atg7, Atg12, Atg16L1, Beclin1, Lamp1, Lamp2, Lc3).* Five-micrometer sections were taken for H&E stain to identify oxyntic region in tissue block. A 2-mm biopsy punch was then used to extract tissue. The standard Qiagen RNeasy FFPE Kit (73504) protocol was used for purification of total RNA. ThermoFisher High-Capacity cDNA Reverse Transcription Kit (4368814)

was used for complementary DNA synthesis. Quantitative real-time polymerase chain reaction was performed with Biorad SsoAdvanced Universal SYBR Green Super Mix (172-5270) and specific primers (Table 2) on the Biorad CFX96 Touch Real-Time PCR Detection System. The expression of mRNA transcripts was normalized to *Tbp* expression and displayed as relative expression levels ($2^{\Delta Cq}$). All graphs and statistics were completed in GraphPad Prism using unpaired Student's *t*-test to determine significance.

Immunohistochemical staining

Mouse stomachs were fixed in 4% PFA overnight at 4°C and were then transferred into 70% ethanol for subsequent paraffin embedding. Five-micrometer sections were used for all immunohistochemistry studies. Deparaffinization, rehydration, and antigen retrieval were performed as previously described (Petersen et al., 2014). Tissue sections were blocked in Dako Peroxidase Blocking Solution at room temperature for 20 minutes followed by Dako Protein Block Serum-Free at room temperature for 1.5 hours. The primary antibodies (Table 1) were added overnight at 4°C in Dako Antibody Diluent with Background Reducing Components. HRP-conjugated secondary antibodies were added for 15 minutes at room temperature. DAB chromogen was added for detection. Leica SCN400 Slide Scanner in the Vanderbilt Digital Histology Shared Resource was used to image sections.

Immunofluorescence Staining

Five-micrometer tissue sections were blocked in Dako Protein Block Serum-Free at room temperature for 1.5 hours. For mouse primary antibodies, Mouse on Mouse (M.O.M.)

blocking reagent was added to slides for 20 minutes at room temperature. The primary antibodies (Table 1) were added overnight at 4°C in Dako Antibody Diluent with Background Reducing Components. Fluorescent donkey secondary antibodies were added in Dako Antibody Diluent at room temperature for one hour. Zeiss Axio Imager M2 microscope with Axiovision digital imaging system, Zeiss LSM 710, or the Leica Aperio Versa 200 Fluorescent Slide Scanner in the Vanderbilt Digital Histology Shared Resource was used to image sections. Immunostaining for LC3 was done at Washington University as previously described (Willet et al., 2018).

Immunofluorescence Quantitation

Experimental groups contained three to five mice. Images were analyzed using CellProfiler to quantify objects and verified manually (nuclei, cells) (Jones et al., 2008). At least five representative images (>150 glands) of proximal stomach corpus were taken from each mouse at 20X objective for quantification. Relative fluorescence intensity was determined using ImageJ and was normalized to cell number (Schneider et al., 2012). Relative fluorescence intensity for greater than 250 cells per replicate was measured. To quantify autophagy of zymogenic granules, GIF-positive cells were selected. Images were analyzed using CellProfiler to quantify objects (puncta). Greater than 250 cells per mouse were measured. All graphs and statistics were completed in GraphPad Prism using unpaired Student's *t*-test or one-way ANOVA with Bonferroni's post-hoc multiple comparisons test to determine significance.

Electron Microscopy

For transmission electron microscopy (TEM), freshly excised stomach (oxyntic region) tissue was washed briefly in 0.1 mol/L cacodylate buffer. Samples were then fixed in 2.5% glutaraldehyde (in 0.1 mol/L sodium phosphate buffer, pH 7.4, 0.1 mol/L cacodylate buffer) for 1 hour at room temperature, followed by overnight fixation at 4°C. Subsequent tissue preparation and imaging for TEM was done as previously described (Weis et al., 2016).

ROS Detection

Fresh stomach tissue was trimmed, embedded in Tissue-Tek optimal cutting temperature (OCT) compound, and snap frozen in an acetone bath on dry ice. Five-micrometer cryosections were obtained on glass slides. Dihydroethidium (DHE Invitrogen D1168) was diluted to a final concentration of 10 μM in 1x PBS with Phalloidin-iFluor 488. DHE/phalloidin solution was applied to slides in a light-protected humidified chamber at 37°C for 30 minutes. Slides were washed with 1x PBS and imaged immediately using the Zeiss Axio Imager M2 microscope with Axiovision digital imaging system. Relative fluorescence intensity (red) of oxidized Dihydroethidium (DHE-ox) was determined using ImageJ and was normalized to area. CellROX Green Reagent (Invitrogen C10444) was diluted to a final concentration of 5 μM in 1x PBS. CellROX solution was applied to slides in a light-protected humidified chamber at 37°C for 30 minutes. Slides were washed with 1X PBS and fixed in 4% PFA for 15 minutes. After fixation, to block/extract the tissue was incubated in 1X PBS with 10% donkey serum and 0.3% Triton X-100 for 30 minutes. Gastric intrinsic factor (GIF) primary antibody was diluted in 1x PBS with 1% donkey serum and 0.05% Tween-20 and incubated for one hour at room temperature.

Fluorescent donkey anti-goat secondary antibody was diluted in 1x PBS and incubated for one hour at room temperature and Hoechst nuclear counter stain was added. Zeiss Axio Imager M2 microscope with Axiovision digital imaging system was used to image fixed tissue within 24 hours. 10 μM DHE or 5 μM Cell ROX Green Reagent was added to ImSPEM cells plated on glass coverslips and incubated at 39°C for 30 minutes. Zeiss Axio Imager M2 microscope with Axiovision digital imaging system was used to image cells immediately. Relative fluorescence intensity (green) of CellROX in GIF-positive cells was determined using ImageJ and was normalized to cell number.

Table 1. *Catalog of antibodies in Chapter II.*		
xCT (1:500)	Abcam	ab37185
CD44v9 (1:25,000)	Cosmo Bio	CAC-LKG-M002
ESRP1 (1:200)	Novus Biologicals	NBP1-82201
Glutathione	Abcam	ab19534
Ki67 (1:1000)	Cell Signaling Technology	#9129
H^+K^+ATPase (1:10,000)	A gift from Dr. Adam Smolka	N/A
Griffonia simplicifolia lectin II (GSII-lectin) (1:2000)	Invitrogen	L32451
Gastric Intrinsic Factor (GIF) (1:2000)	A gift from Dr. David Alpers	N/A
Mist1 (1:1000)	A gift from Dr. Jason Mills	N/A
LC3/MAP1LC3B (1:500)	Novus Biologicals	NB100-2220
LAMP2 (GL2A7) (1:500)	Abcam	ab13524
Lectin from Ulex Europaeus (UEA1-lectin) (1:2000)	Sigma	L9006
Cleaved Caspase-3 (Asp175) (1:200)	Cell Signaling Technology	#9661
Clusterin-α Antibody (M-18) (1:2000)	Santa Cruz Biotechnology	sc-6420
TFF2 (1:500)	A gift from Dr. Nicholas Wright	N/A

Table 2. *Catalog of qPCR primer sequences in Chapter II.*
mCd44v (Cd44v9) primers F 5' GGAGATCAGGATGACTCCTTCT 3' R 5' AGTCCTTGGATGAGTCTCGATC 3'
mSlc7a11(xCT) primers F 5' GGGGGTCTCCATCATCATCGGCA 3' R 5' TCTGCATAGGACAGGGCTCCAAA 3'
mEsrp1 (Esrp1) primers F 5' GCTTCACATTAGGCAGAT 3' R 5' CAGCACTTCTTGAACTCT 3'
mAtg4 (Atg4) primers F 5' GGGAACTGGCCCTACTTCAGA 3' R 5' TCCACCTCCAATCTCGACCTA 3'
mAtg5 (Atg5) primers F 5' GGACAGCTGCACACACTTGG 3' R 5' TGGCTCTATCCCGTGAATCAT 3'
mAtg7 (Atg7) primers F 5' GGCCTTTGAGGAATTTTTTGG 3' R 5' ACGTCTCTAGCTCCCTGCATG 3'
mAtg12 (Atg12) primers F 5' TGAATCAGTCCTTTGCCCCT 3' R 5' CATGCCTGGGATTTGCAGT 3'
mAtg16l1(Atg16l1) primers F 5' GCCCAGTTGAGGATCAAACAC 3' R 5' CTGCTGCATTTGGTTGTTCAG 3'
mBeclin1 (Beclin1) primers F 5' GGCCAATAAGATGGGTCTGA 3' R 5' GCTGCACACAGTCCAGAAAA 3'
mLamp1 (Lamp1) primers F 5' ACCTGTCGAGTGGCAACTTCA 3' R 5' GGGCACAAGTGGTGGTGAG 3'
mLamp2 (Lamp2) primers F 5' TAGGAGCCGTTCAGTCCAAT 3' R 5' GTGTGTCGCCTTGTCAGGTA 3'
mMap1lc3b (Lc3) primers F 5' ACTGCTCTGTCTTGTGTAGGTT 3' R 5' TCGTTGTGTGCCTTTATTAGTGCATC 3'

RESULTS

Parietal cell loss promotes SPEM and up-regulation of CD44v9-xCT system.

L635 is a parietal cell toxic drug that causes acute parietal cell necrosis (Nam et al., 2010a). We utilized L635 treatment to elucidate the role of xCT in epithelial repair and chief cell reprogramming. Chief cell reprogramming can be visualized within hours of administering L635, and proliferative metaplasia subsequently develops within 3 days. Immunohistochemical analysis of tissue sections from wild-type C57Bl/6J mice treated with 3 days of L635 revealed basolateral membrane expression of the metaplastic marker CD44v9 on chief cells at the base of glands. No CD44v9 staining was visualized in the stomach of untreated mice (Figure 4A).

CD44v9 is known to interact and stabilize xCT, a subunit of a cystine-glutamate antiporter, at the plasma membrane (Ishimoto et al., 2011; Nagano et al., 2013). Increased xCT expression on the membrane was observed in L635-treated mice, corresponding to CD44v9 expression on SPEM cells (Figure 4A). Alternative splicing of CD44 is regulated by epithelial splicing regulatory protein 1 (ESRP1) (Warzecha et al., 2009; Yae et al., 2012). Immunostaining showed increased nuclear expression of ESRP1 in GIF-positive chief cells from L635-treated mice (Figure 4C-D). Additionally, we observed increased mRNA expression of *Cd44v9*, *xCT*, and *Esrp1* after 3 days of L635-treatment (Figure 4B). These results suggest that alternative splicing of CD44 is up-regulated by ESRP1 after L635-induced injury to the stomach. Furthermore, increased CD44v9 stabilizes xCT on the plasma membrane of chief cells reprogramming to SPEM.

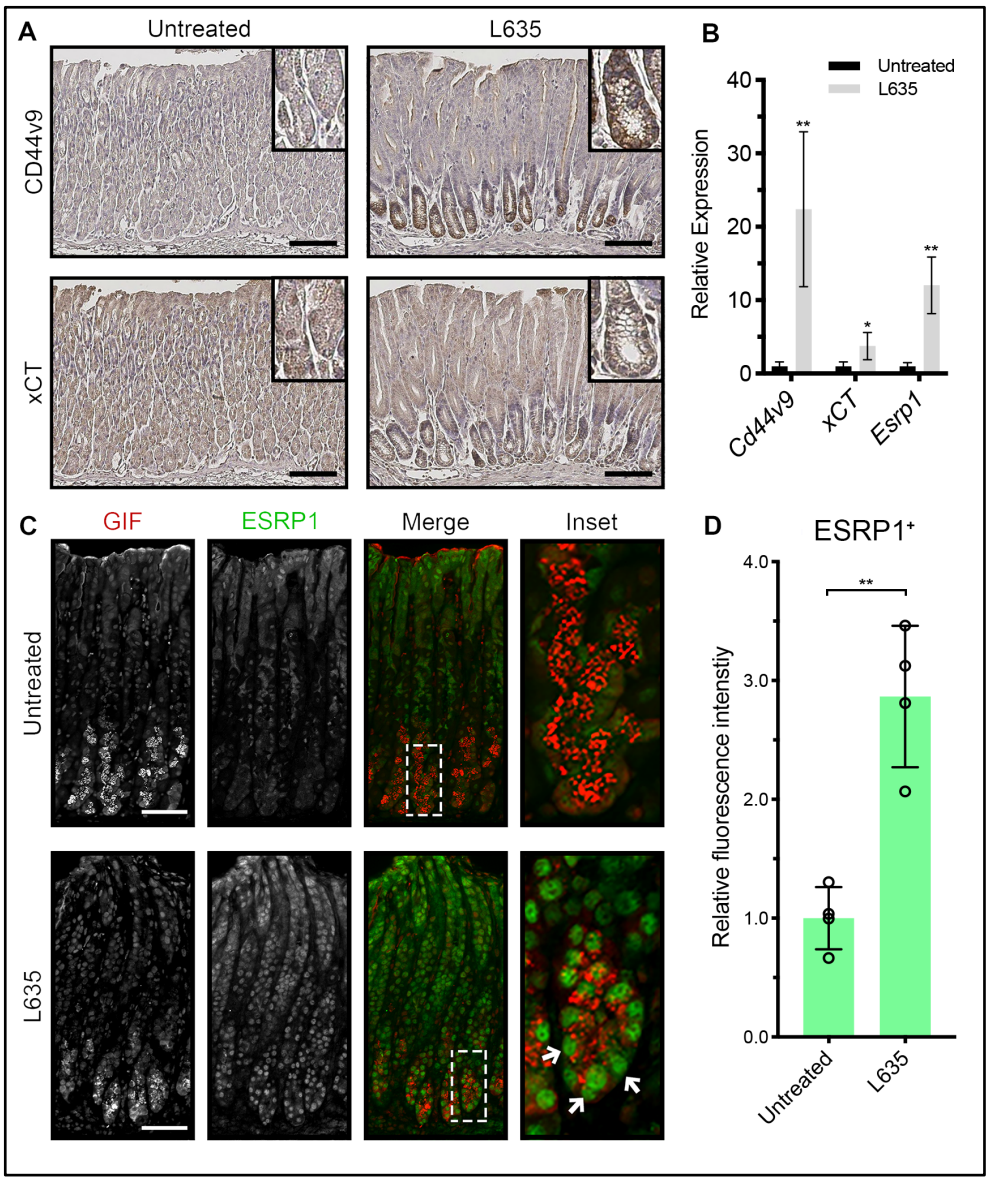

Figure 4. Increased expression of CD44v9, xCT, and ESRP1 in L635-treated mice. ***A.*** *Immunohistochemical staining of serial sections from the body of the stomach for CD44v9 (top) and xCT (bottom) in untreated and L635-treated (3 days) C57Bl/6J mice (scale bar = 100 μm). Magnified inset from corresponding chief cell regions in top right corner.* ***B.*** *Relative mRNA expression of Cd44v9, xCT, and Esrp1 in untreated and L635-treated (3 days) C57Bl/6J mice determined by RT-qPCR (p=0.006, 0.03, 0.001 respectively). Statistical significance determined by unpaired student's t-test (n=4 per group).* ***C.*** *Immunofluorescent staining for the zymogenic granule marker GIF (red) and ESRP1 (green) in untreated and L635-treated (3 days) C57Bl/6J mice (scale bar = 100 μm). Magnified inset of chief cell region with arrows indicating ESRP1 and GIF dual-positive cells (right).* ***D.*** *Relative fluorescence intensity of nuclear ESRP1 in GIF-positive chief cells (p=0.001). Statistical significance determined by unpaired student's t-test (n=4 per group).*

Metaplastic cells are dependent on xCT for cystine uptake, ROS detoxification, proliferation and survival *in vitro.*

To target xCT activity on the plasma membranes of metaplastic (SPEM) cells, we utilized sulfasalazine, an inhibitor of xCT-mediated cystine transport, to treat previously characterized cell lines for chief cells (ImChief) and SPEM cells (ImSPEM) isolated from Immortomice (Weis et al., 2014). The relative expression of *Cd44v9 and xCT* were measured in ImChief and ImSPEM cells. ImSPEM cells exhibited increased expression of *CD44v9* and *xCT* compared to ImChief cells (Figure 5A). ImChief and ImSPEM cells were immunostained for CD44v9. No CD44v9 staining was visualized in ImChief cells, but CD44v9 was observed on the plasma membranes of ImSPEM cells, recapitulating what is observed in chief and SPEM cells in the stomach (Figure 5B-D).

To monitor xCT activity and cystine uptake into ImSPEM cells, we added fluorescently labeled cystine (Cystine-FITC) to cultures (Siska et al., 2016). Abundant intracellular fluorescent signal was observed in ImSPEM cells 2 hours after the addition of Cystine-FITC to culture. xCT blockade with sulfasalazine treatment significantly reduced the uptake of Cystine-FITC by ImSPEM cells (Figure 5E-F). Through a multi-step process, intracellular cystine can be converted to glutathione, a critical antioxidant for protection against ROS. We utilized an antibody that recognizes glutathione and ROS indicators (DHE and CellROX) to measure glutathione production and ROS levels. Inhibition of xCT with sulfasalazine decreased glutathione in ImSPEM cells (Figure 5E-F). Similarly, sulfasalazine increased ROS in ImSPEM cells as demonstrated by increased accumulation of oxidized DHE and CellROX (Figure 5E-F).

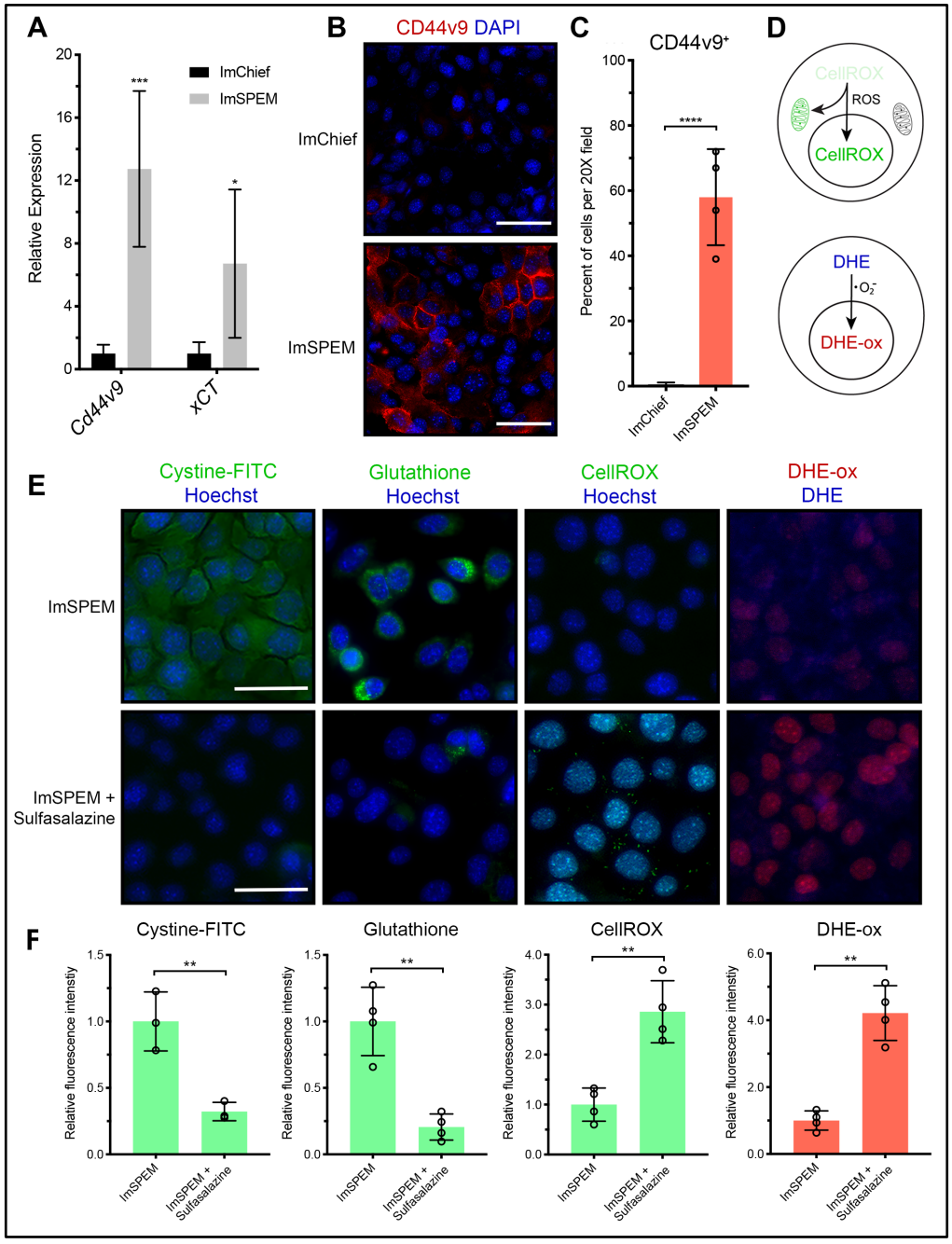

Figure 5. Inhibition of xCT with sulfasalazine blocks cystine uptake and ROS detoxification by metaplastic cells.

A. *Relative mRNA expression of Cd44v9 and xCT in ImChief and ImSPEM cells determined by RT-qPCR.* ***B.*** *ImChief and ImSPEM were immunostained for CD44v9 (red) with nuclear counter stain DAPI (blue) (scale bar = 100 µm).* ***C.*** *Percent of cells per 20X field that are CD44v9-positive ($p < 0.0001$).* ***D.*** *Diagram of ROS indicators CellROX green reagent and Dihydroethidium (DHE).* ***E.*** *Representative fluorescence images of Cystine-FITC (green), Glutathione (green), CellROX (green), and DHE-ox (red) in ImSPEM cells ± sulfasalazine with nuclear counter stain Hoechst (blue) (scale bar = 100 µm).* ***F.*** *Relative*

fluorescence intensity of Cystine-FITC (p=0.007), Glutathione (p=0.001), CellROX (p=0.002), and DHE-ox (p=0.0003) in ImSPEM cells ± sulfasalazine. Statistical significance determined by unpaired student's t-test (n=4 per condition).

Additionally, we observed that sulfasalazine treatment decreased the proliferation of ImSPEM cells by staining for the proliferation marker Ki67, a protein present in all active phases of the cell cycle, and monitoring cell number (Figure 6A-C). Sulfasalazine treatment also increased apoptosis of ImSPEM cells, as assessed by staining for the apoptosis marker, cleaved caspase-3 (CC3) (Figure 6E-F). Caspase-3 is activated when it is cleaved by an initiator caspase and mediates cell death by apoptosis. These results indicate our *in vitro* culture system mimics the expression pattern observed in the stomach and that sulfasalazine inhibits cystine uptake, ROS detoxification, and proliferation of metaplastic cells in culture. Likewise, increased ROS levels led to SPEM cell death.

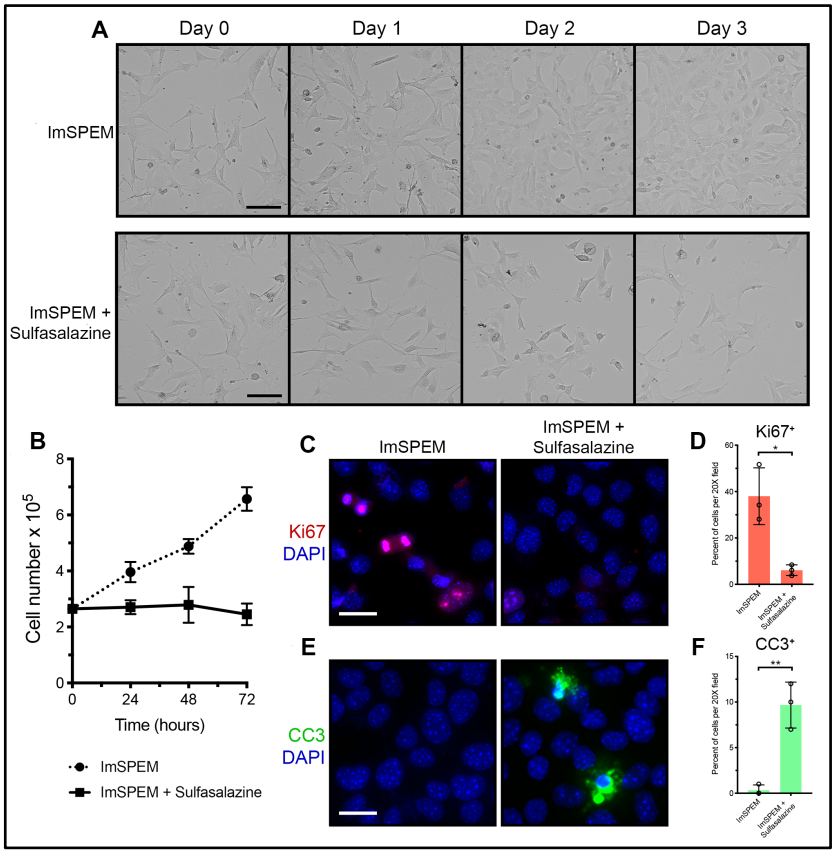

Figure 6. Inhibition of xCT with sulfasalazine decreases proliferation and increases apoptosis of SPEM cells.
A. *ImSPEM cells were seeded at the same density ± sulfasalazine for three days. Representative transmitted light images monitoring cell density over three days (scale bar = 100 μm).* ***B.*** *ImSPEM cell number ± sulfasalazine at 24, 48, and 72 hours (p=0.001, 0.006, 0.0002 respectively).* ***C.*** *ImSPEM cells were treated with sulfasalazine for 48 hours and immunostained for proliferation marker Ki67 (red) with nuclear counter stain DAPI (blue) (scale bar = 100 μm).* ***D.*** *Percent of cells per 20X field that are Ki67-positive (p=0.01).* ***E.*** *ImSPEM cells were treated with sulfasalazine for 72 hours and immunostained for apoptosis marker cleaved caspase-3 (CC3) (green) with nuclear counter stain DAPI (blue) (scale bar = 100 μm).* **F.** *Percent of cells per 20X field that are CC3-positive (p=0.003). Statistical significance determined by unpaired student's t-test (n=3 per condition).*

Sulfasalazine is broken down to sulfapyridine and mesalazine through azo cleavage (Figure 7A). Therefore, we sought to confirm that the outcomes observed were due to the specific inhibition of xCT by sulfasalazine, and not the anti-inflammatory properties of sulfasalazine metabolites. In contrast with sulfasalazine treatment, sulfapyridine or mesalazine treatment of ImSPEM cells in culture did not inhibit cystine uptake or proliferation (Figure 7B-E).

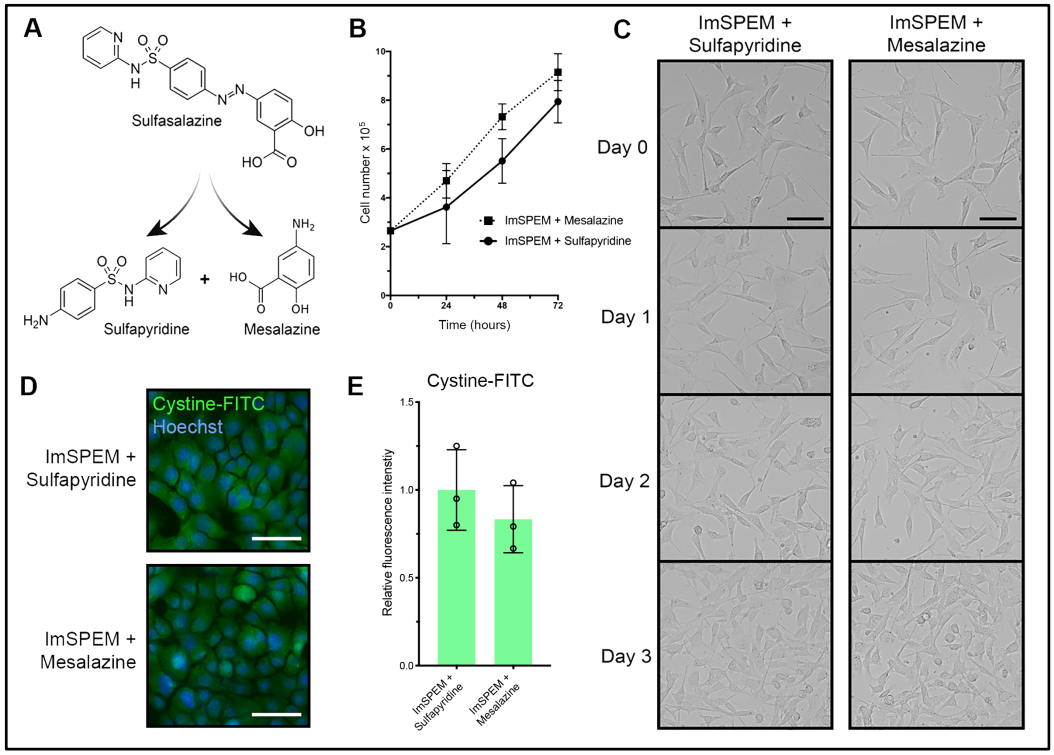

Figure 7. Metabolites of sulfasalazine do not prevent cystine uptake, ROS detoxification and proliferation of metaplastic cells.
A. *Diagram of sulfasalazine metabolism. Sulfasalazine is broken down to sulfapyridine (an antibiotic) and mesalazine (an anti-inflammatory agent) through azo cleavage.* ***B.*** *ImSPEM cells were seeded at the same density plus sulfapyridine or mesalazine for three days. ImSPEM cell number with sulfapyridine or mesalazine at 24, 48, and 72 hours.* ***C.*** *Representative transmitted light images monitoring cell density over three days (scale bar = 100 μm).* ***D.*** *ImSPEM cells were treated with sulfapyridine or mesalazine and then treated with Cystine-FITC. Live cell imaging of intracellular Cystine-FITC (green) in ImSPEM cells treated with sulfapyridine or mesalazine with nuclear counter stain Hoechst (blue) (scale bar = 100 μm).* ***E.*** *Relative fluorescence intensity of intracellular Cystine-FITC in ImSPEM cells treated with sulfapyridine or mesalazine (n=3 per condition).*

To examine further if the effects of sulfasalazine are mediated by inhibition of xCT, we transfected ImSPEM cells with control or xCT siRNAs. Similar to sulfasalazine treatment, ImSPEM cells transfected with xCT siRNA displayed decreased cystine uptake and increased ROS compared to ImSPEM cells transfected with control siRNA (Figure 8). Taken together, these results suggest that sulfasalazine effectively blocks xCT activity on SPEM cells and SPEM cells are dependent on xCT for control of ROS.

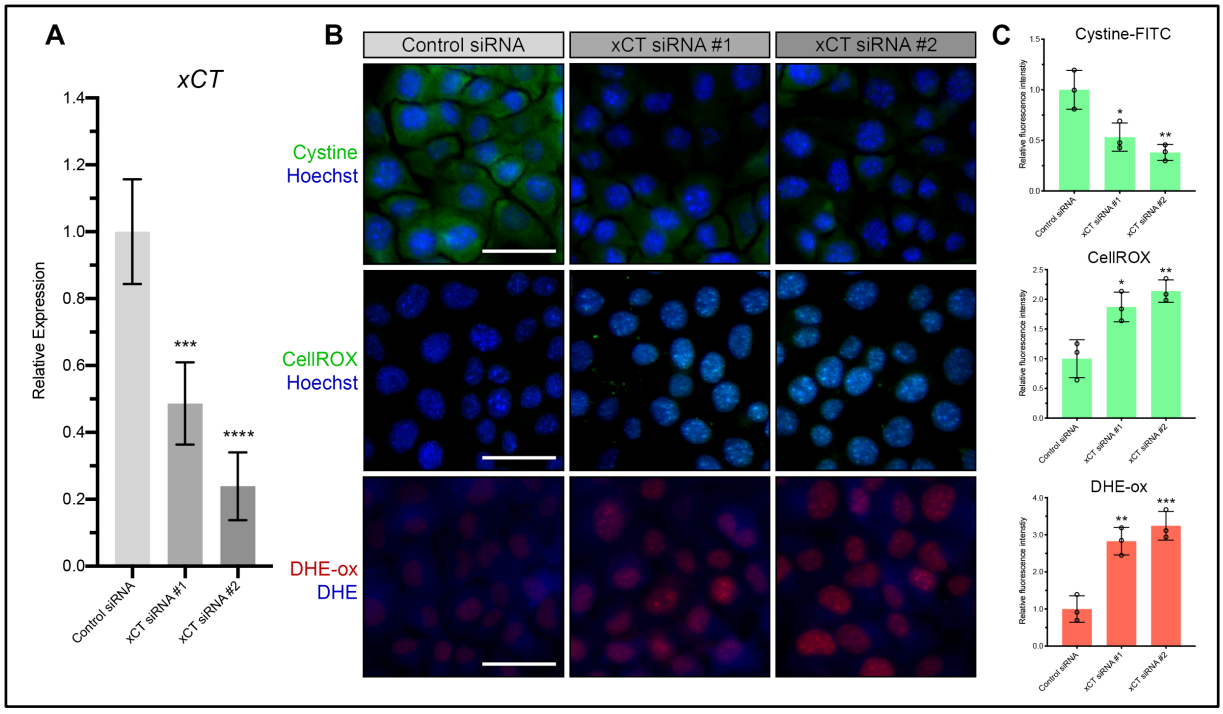

Figure 8. xCT is required for cystine uptake and ROS detoxification in SPEM cells. ***A.*** *Relative mRNA expression of xCT in ImSPEM cells transfected with control or xCT siRNAs determined by RT-qPCR.* ***B.*** *Representative fluorescence images of Cystine-FITC (green), CellROX (green), and DHE-ox (red) in ImSPEM cells transfected with control or xCT siRNAs with nuclear counter stain Hoechst (blue) (scale bar = 100 μm).* ***F.*** *Relative fluorescence intensity of Cystine-FITC (p=0.02 and 0.005), CellROX (p=0.01 and 0.005), and DHE-ox (p=0.002 and 0.0009) in ImSPEM cells transfected with control or xCT siRNAs. Statistical significance determined by one-way ANOVA with Bonferroni's post-hoc multiple comparisons test. (n=3 per condition).*

Inhibition of xCT blocks chief cell reprogramming into SPEM.

To elucidate the role of xCT in chief cell reprogramming *in vivo*, we combined sulfasalazine treatment with the parietal cell toxic drug, L635. Chief cell reprogramming into SPEM occurs through a coordinated process that involves disassembly of the chief cell protein secretory apparatus and transcriptional changes including the up-regulation of mucin granule proteins Muc6 and TFF2 (Nozaki et al., 2008b; Willet et al., 2018). We treated wild-type C57Bl/6J mice with sulfasalazine two days prior to and throughout three days of L635 treatment (Figure 9A). Stomachs were harvested from four experimental groups: 1) untreated, 2) sulfasalazine-treated, 3) L635-treated, and 4) L635 + sulfasalazine-treated mice for histological analysis. Treatment with sulfasalazine by itself did not alter the gastric mucosa (Figure 10A-B). To visualize L635-induced parietal cell loss, we performed immunostaining for the proton pump, H^+K^+ ATPase, an integral membrane protein responsible for gastric acid secretion by parietal cells (Figure 9B). In untreated mice, a large number of H^+K^+ ATPase-positive parietal cells were detected throughout the corpus glands. Treatment with L635 reduced the number of parietal cells by almost eighty-percent. Sulfasalazine treatment did not affect L635-induced parietal cell loss (Figure 9C). To detect chief cell reprogramming, we immunostained for the zymogenic granule marker gastric intrinsic factor (GIF) and the mucin granule marker

Griffonia simplicifolia (GSII)-lectin, which binds to a sugar modification on Muc6 (Figure 9B). Chief cells reprogram to mucin-secreting metaplastic cells to protect and fuel repair of the stomach when there is injury or cell loss in the gastric mucosa. During this process, SPEM cells contain both zymogenic (GIF-positive) granules and mucin (GSII-lectin-positive) granules. Sulfasalazine treatment decreased the number of GIF and GSII-lectin dual-positive SPEM cells by greater than eighty-percent after L635-induced parietal cell loss (Figure 9D).

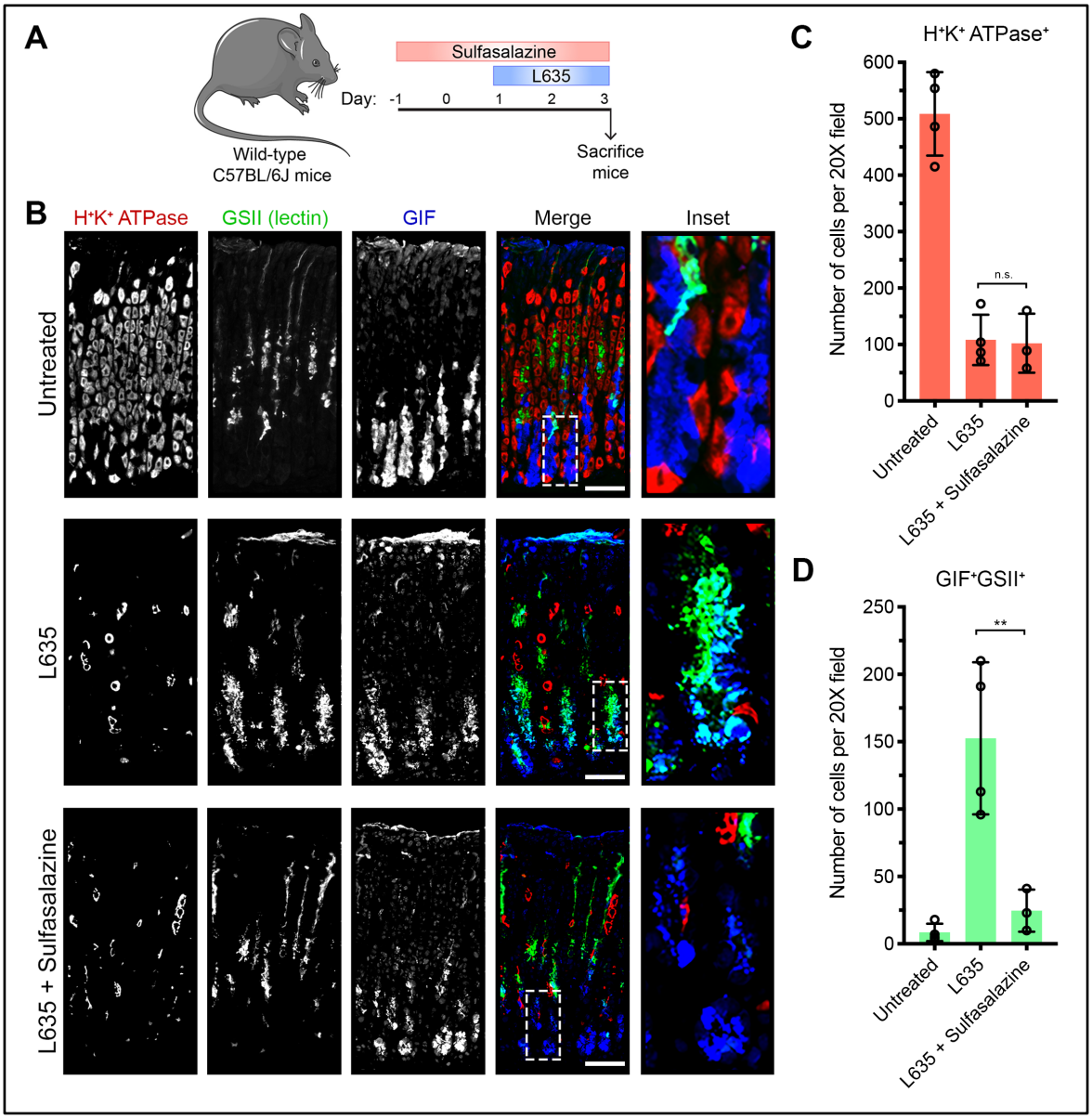

Figure 9. Inhibition of xCT blocks chief cell reprogramming in mouse models of acute gastric damage.
A. *Diagram of drug treatments. L635 was administered to C57BL/6J mice for three days to induce acute gastric damage. Mice were treated with 10 mg of sulfasalazine per day, 2 days prior to and throughout L635 administration. Mice were sacrificed 2 hours after final dose of L635, and stomach tissue from untreated mice (n=4), L635-treated mice (n=4), and L635 + sulfasalazine-treated mice (n=3) were harvested for histological analysis.* ***B.*** *Immunofluorescence staining for parietal cell marker H+K+ ATPase (red), mucin granule marker GSII-lectin (green), zymogenic granule marker GIF (blue) (scale bars = 100 μm). Magnified inset of chief cell region (right).* ***C.*** *Quantification of parietal cells as determined by number of H+K+ ATPase-positive (red) cells per 20X objective field (n.s. = not significant).* ***D.*** *Quantification of GSII (green) and GIF (blue) dual-positive (SPEM) cells per 20X objective field (p=0.004). Statistical significance determined by one-way ANOVA with Bonferroni's post-hoc multiple comparisons test.*

Similarly, PAS staining, a stain that detects mucins, revealed decreased mucin at the base of glands in L635 + sulfasalazine-treated mice (Figure 10B). Collectively, these results suggest that xCT blockade prevents chief cell reprogramming after acute parietal cell loss.

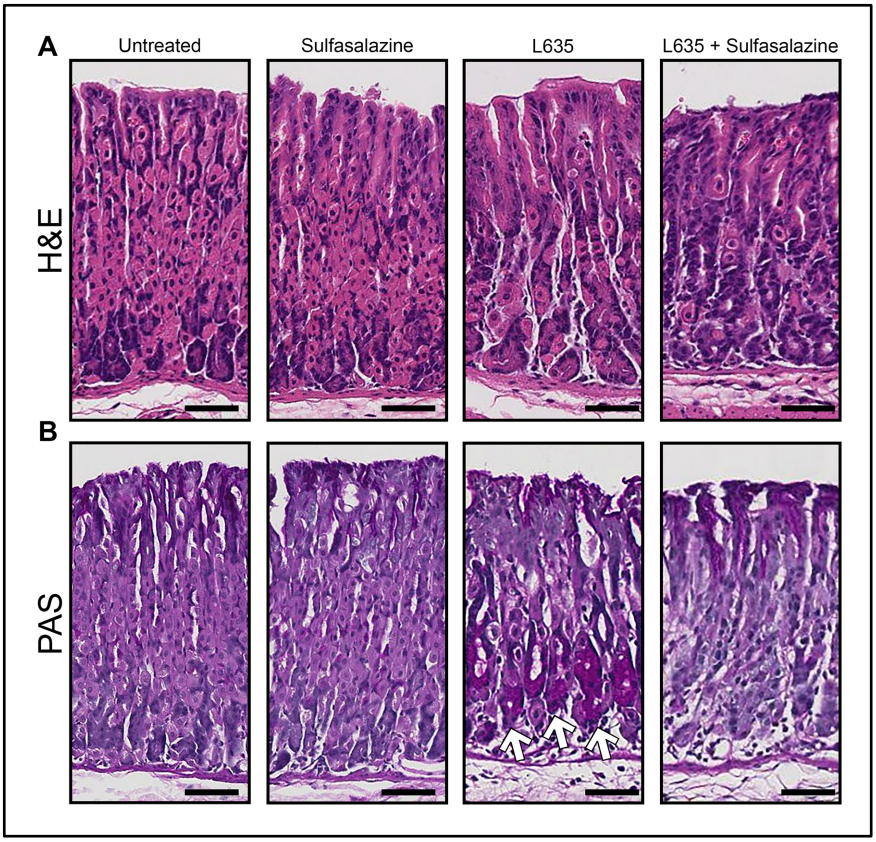

Figure 10. Histological analysis of sulfasalazine treated mice.
A. *Hematoxylin and eosin (H&E) and* ***B.*** *Periodic acid-Schiff (PAS) stained sections from untreated (n=4), sulfasalazine-treated (n=4), L635-treated (n=4), and L635 + sulfasalazine-treated (n=3) mice (scale bars = 100 μm). Dark magenta color represents PAS-positive mucin-producing cells. Glands containing PAS-positive cells at the base are indicated with arrows.*

xCT activity is required for autophagy in reprogramming chief cells.

The process of reprogramming requires chief cells to downscale their mature characteristics. The basic helix-loop-helix transcription factor Mist1 (Bhlha15) governs the secretory architecture of chief cells including production of large protein-containing zymogen granules and cellular organization (Ramsey et al., 2007). Loss of Mist1 is a distinct feature of chief cell reprogramming into SPEM (Lennerz et al., 2010). Dual immunofluorescence staining for GIF and Mist1 allows for monitoring of Mist1 loss in zymogenic granule-containing chief cells (Figure 11A). In untreated mice, GIF-positive chief cells were positive for the transcription factor Mist1. L635 treatment resulted in almost complete loss of Mist1 expression in GIF-positive cells. Interestingly, treatment with L635 + sulfasalazine did not rescue Mist1 loss by chief cells (Figure 11B). This suggests that xCT inhibition with sulfasalazine does not influence the initiating step of Mist1 loss in reprogramming chief cells.

In addition to loss of Mist1, autophagic and lysosomal pathways in chief cells are up-regulated acutely following injury to the stomach. In particular, rough endoplasmic reticulum, mitochondria, and secretory granules are targeted for degradation during early stages of SPEM development. Furthermore, mice with defects in autodegradative function (*Gnptab*$^{-/-}$ mice) are unable to develop SPEM following gastric injury (Willet et al., 2018). To investigate autophagic and lysosomal pathways, L635-treated mice were

sacrificed 12 or 24 hours after L635 treatment. We performed immunostaining for the autophagosome marker LC3B and the lysosome marker LAMP2 (Figure 11C and E). Very few LC3B or LAMP2-positive puncta were observed in GIF-positive chief cells from untreated mice. As expected, however, gastric injury induced by L635 treatment resulted in increased LC3B and LAMP2-positive puncta in close proximity to GIF-positive zymogenic granules. By contrast, L635 + sulfasalazine-treated mice showed fewer LC3B and LAMP2-positive puncta in GIF-positive cells compared to L635 treatment only (Figure 11D and F). Notably, large/dense zymogen granules were maintained in L635 + sulfasalazine-treated mice compared to the L635-treated mice. Similarly, transmission electron microscopy (TEM) of tissue from L635-treated mice revealed abundant double membrane-bound (autophagic) structures engulfing granules and other cytosolic components in chief cells. While similar double membrane-bound structures were observed in L635 + sulfasalazine-treated mice, they were significantly less frequent (Figure 11G). Real-time qPCR analysis for several autophagy-related genes revealed a significant decrease in the relative expression of *Atg4*, *Atg7*, *Atg16L1*, *Lamp1*, and *Lc3* in sulfasalazine-treated mice (Figure 11H). Although there was Mist1 loss in L635 + sulfasalazine-treated mice, these findings suggest that xCT blockade decreases downscaling by autophagic and lysosomal pathways in reprogramming chief cells.

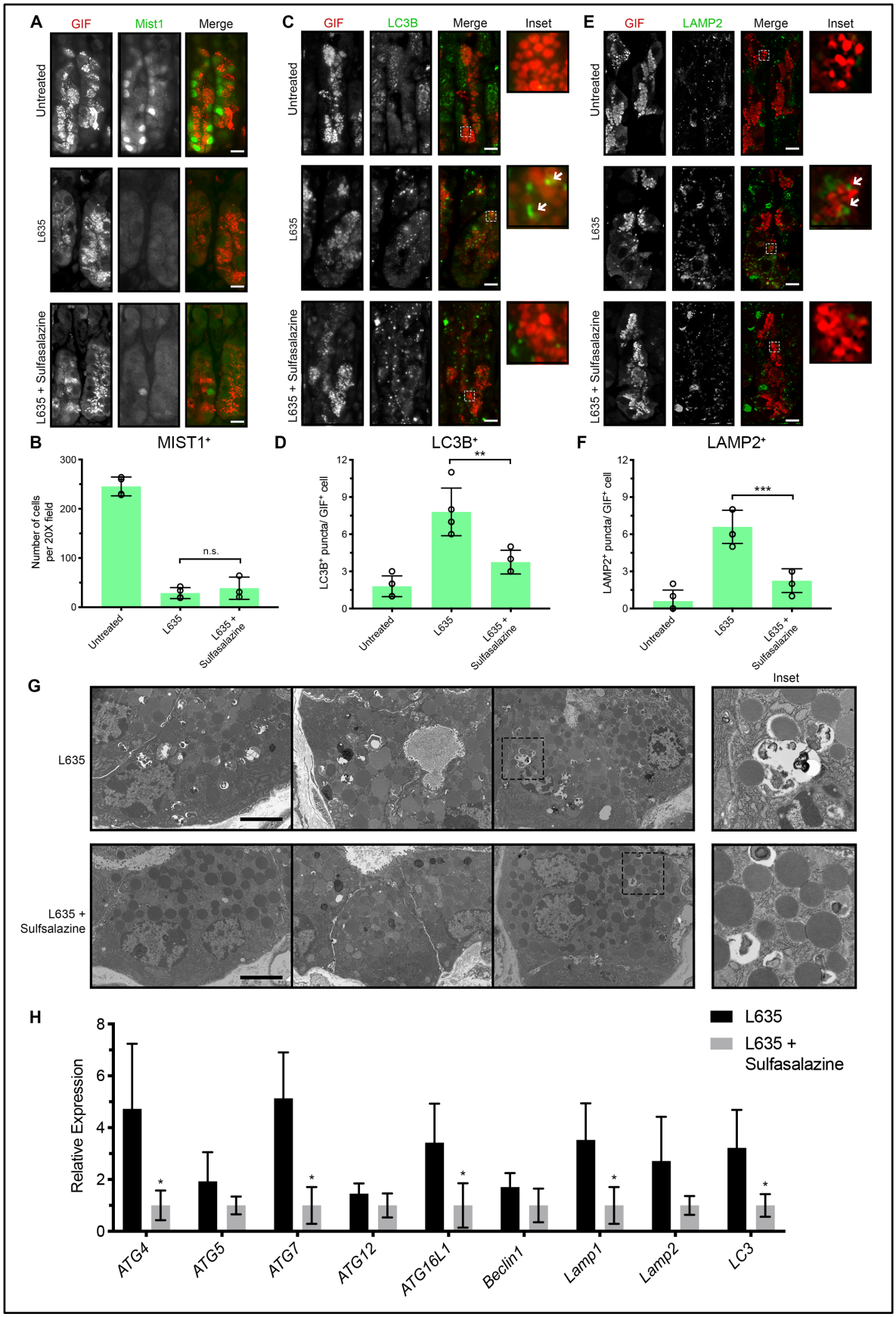
A
GIF
Mist1
Merge
Untreated
L635
L635 + Sulfasalazine
C
GIF
LC3B
Merge
Inset
E
GIF
LAMP2
Merge
Inset
B
MIST1+
Number of cells per 20X field
n.s.
D
LC3B+
LC3B+ puncta/ GIF+ cell
**
F
LAMP2+
LAMP2+ puncta/ GIF+ cell
***
Untreated
L635
L635 + Sulfasalazine
G
Inset
H
Relative Expression
L635
L635 + Sulfasalazine
ATG4
ATG5
ATG7
ATG12
ATG16L1
Beclin1
Lamp1
Lamp2
LC3

Figure 11. xCT blockade inhibits autophagy of zymogenic granules in downscaling chief cells.
A. *Immunostained sections from untreated (n=4), L635-treated (n=4), and L635 + sulfasalazine-treated (n=3) C57Bl/6J mice sacrificed after 3 days of L635 treatment for zymogenic granule marker GIF (red) and chief cell transcription factor Mist1 (green) (scale bars = 50 μm).* ***B.*** *Quantification of Mist1-positive cells per 20X field (n.s. = not significant).* ***C.*** *Immunostained sections from untreated (n=5), L635-treated (n=5), and L635 + sulfasalazine-treated (n=4) C57Bl/6J mice sacrificed after 24 hours of L635 treatment for GIF (red) and autophagosome marker LC3B (green) (scale bars = 50 μm). Magnified inset of GIF-positive cell with arrows indicating puncta (right).* ***D.*** *Average number of LC3B puncta per GIF-positive cell (p=0.003).* ***E.*** *Immunostained sections from untreated (n=5), L635-treated (n=5), and L635 + sulfasalazine-treated (n=4) C57Bl/6J mice sacrificed after 24 hours of L635 treatment for GIF (red) and lysosome marker LAMP2 (green) (scale bars = 50 μm). Magnified inset of GIF-positive cell with arrows indicating puncta (right).* ***F.*** *Average number of LAMP2 puncta per GIF-positive cell (p=0.0003). Statistical significance determined by one-way ANOVA with Bonferroni's post-hoc multiple comparisons test.* ***G.*** *Transmission electron micrographs of zymogenic chief cells 12 hours after L635 treatment ± sulfasalazine (scale bars = 2 μm). Magnified inset of double membrane autophagic structures (right).* ***H.*** *Relative mRNA expression of autophagy related proteins in L635-treated and L635 + sulfasalazine treated mice. (Atg4, Atg5, Atg7, Atg12, Atg16L1, Beclin1, Lamp1, Lamp2, Lc3) (p=0.02, 0.005, 0.03, 0.01, 0.02 respectively). Statistical significance determined by unpaired student's t-test.*

xCT blockade suppresses proliferation of reprogramming chief cells.

Sulfasalazine treatment inhibited proliferation of ImSPEM cells in culture, so we sought to determine the effect of sulfasalazine treatment on proliferation after gastric injury *in vivo.* To do this, we immunostained for the proliferation marker Ki67. In the normal oxyntic mucosa, Ki67 labelled stem/progenitor cells about a third of the way down the gland in the gland isthmus. Upon gastric injury, chief cells reprogram and are capable of re-entering into the cell cycle and proliferating. Additionally, surface mucin-producing (foveolar) cells located near the lumen also expand in response to injury and increases in gastrin. This gastric lesion is referred to as foveolar hyperplasia. Foveolar cells produce Muc5ac, a mucin recognized by *Ulex Europaeus Agglutinin I* (UEA1)-lectin. Unlike reprogramming chief cells, foveolar cells do not express xCT. To classify the identity of

the proliferating cells in each of our experimental groups we immunostained for Ki67, UEA1-lectin, and GIF (Figure 12A). To evaluate foveolar hyperplasia after L635 treatment, we measured the average thickness of the UEA1-positive foveolar region. L635-treated mice and L635 + sulfasalazine-treated mice showed similar levels of foveolar hyperplasia (Figure 12B). We also quantified the total number of Ki67-positive cells in the oxyntic mucosa of each experimental group. While the total number of Ki67-positive proliferating cells was not significantly different between L635-treated mice and L635 + sulfasalazine-treated mice, the percent of Ki67-positive cells that were dual-positive for GIF was significantly decreased in the sulfasalazine-treated group (Figure 12C-D). Together, these results show that proliferation of xCT-negative foveolar cells is not affected by xCT blockade. However, chief cells that express high levels of xCT as they reprogram, do not proliferate after xCT blockade with sulfasalazine.

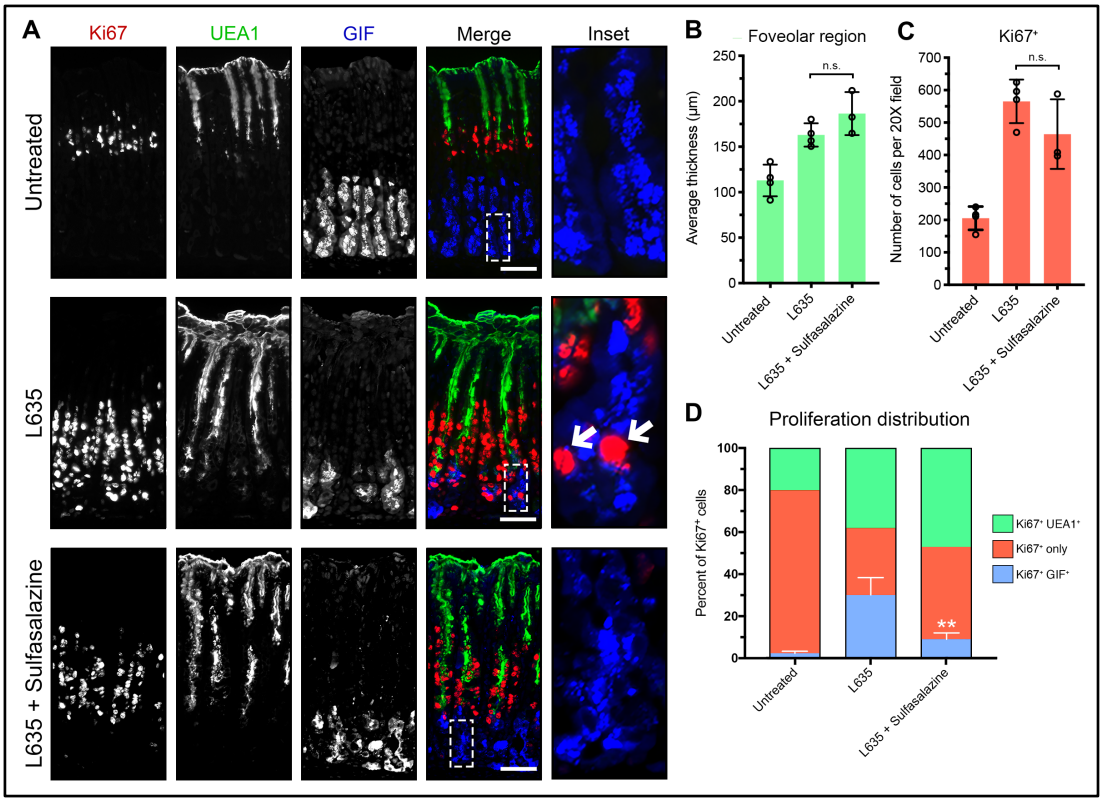

Figure 12. Inhibition of xCT suppresses SPEM proliferation.
A. *Immunostained sections from untreated (n=4), L635-treated (n=4), and L635 + sulfasalazine-treated (n=3) C57Bl/6J mice sacrificed after 3 days of L635 treatment for proliferation marker Ki67 (red), mucin-producing foveolar cell marker Ulex Europaeus Agglutinin I (UEA1)-lectin (green), and zymogen granule marker GIF (blue) (scale bars = 100 μm). Magnified inset of chief cell region with arrows indicating proliferative metaplasia (right).* ***B.*** *Average thickness (μm) of UEA1-positive foveolar region (n.s. = not significant).* ***C.*** *Quantification of Ki67-positive (red) proliferating cells per 20X field (n.s. = not significant).* ***D.*** *Percent of Ki67 only-positive cells or Ki67-positive cells dual-positive for UEA1 or GIF to determine distribution of proliferative cells (p=0.002). Statistical significance determined by one-way ANOVA with Bonferroni's post-hoc multiple comparisons test.*

Inhibition of xCT leads to oxidative stress and chief cell death after gastric injury.

Next, we examined evidence of cell stress or cell death. Clusterin (Clu) is a heterodimeric protein up-regulated in many diseases related to oxidative stress and is associated with clearance of cellular debris and apoptosis (Zhang et al., 2014). Previous studies revealed clusterin expression in SPEM lineages through gene microarray analysis. Clu protein expression in SPEM was validated in DMP-777, L635, and *Helicobacter* infection mouse models (Weis et al., 2013). In the normal oxyntic mucosa, clusterin is expressed in some mucous neck cells along with the spasmolytic polypeptide, TFF2. In L635-treated mice, clusterin and TFF2 are up-regulated in chief cells at the base of oxyntic glands as they reprogram into SPEM. Interestingly, while sulfasalazine inhibited TFF2 up-regulation, chief cells at the gland base still exhibited clusterin expression after L635 treatment (Figure 13 A-C). Thus, it is likely that Clu is not up-regulated as a part of the metaplastic process, but rather as a result of increased oxidative stress.

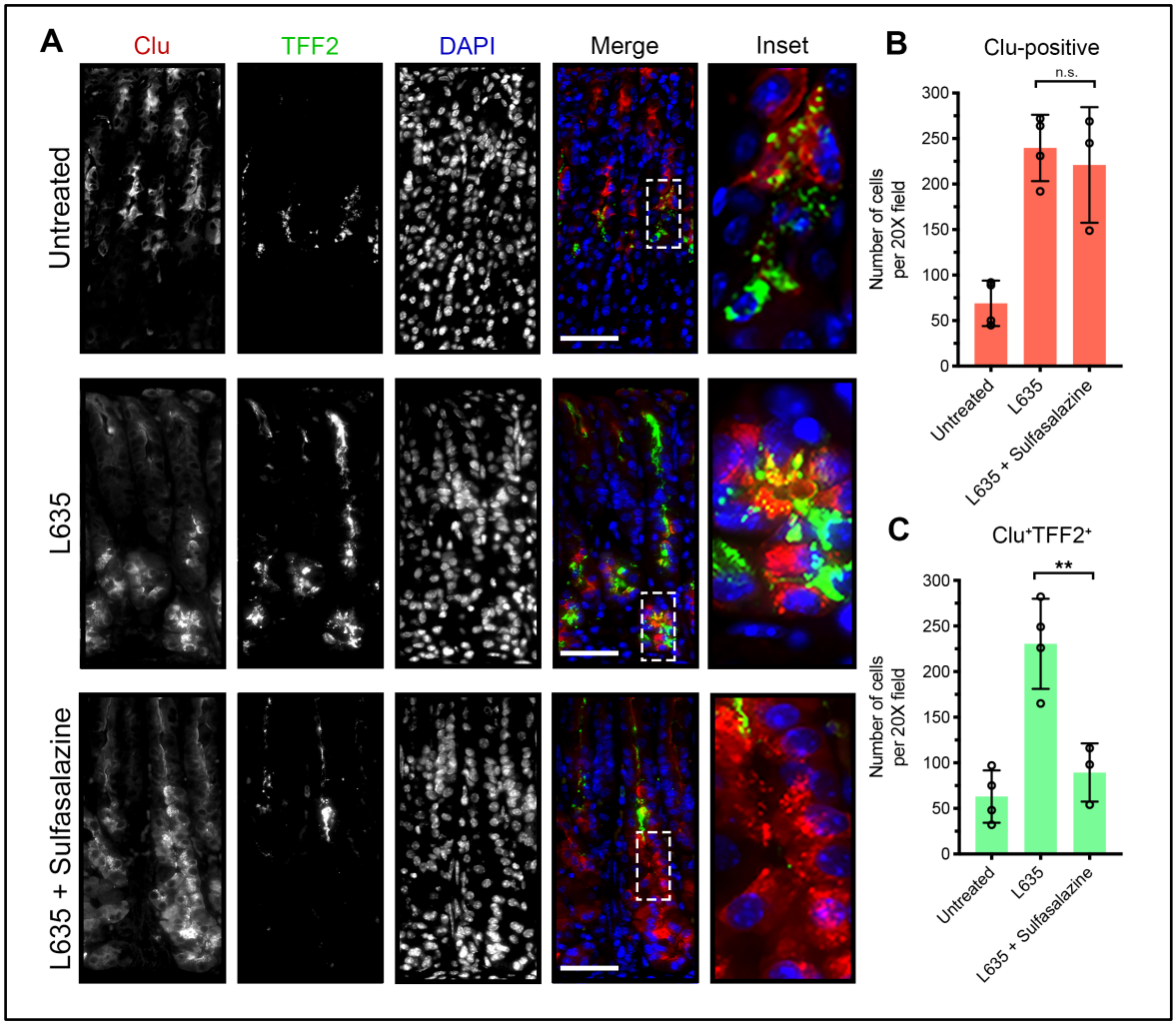

Figure 13. Inhibition of xCT blocks reprogramming of chief cells and results in cellular stress.
A. Representative immunostained sections from untreated (n=4), L635-treated (n=4), and L635 + sulfasalazine-treated (n=3) C57Bl/6J mice sacrificed after 3 days of L635 treatment for cellular stress marker Clusterin (red) and TFF2 (green), with nuclear counter stain DAPI (blue) (scale bars = 100 μm). Magnified inset of chief cell region (right). B. Quantification of Clu-positive (red) cells per 20X field (n.s. = not significant). C. Quantification of Clu (red) and TFF2 (green) dual-positive cells per 20X field (p=0.004). Statistical significance determined by one-way ANOVA with Bonferroni's post-hoc multiple comparisons test.

Similarly, staining with ROS indicators (DHE and CellROX) revealed increased levels of ROS in L635 + sulfasalazine-treated mice compared to L635-treated mice, especially in GIF-positive chief cells (Figure 14 A-D).

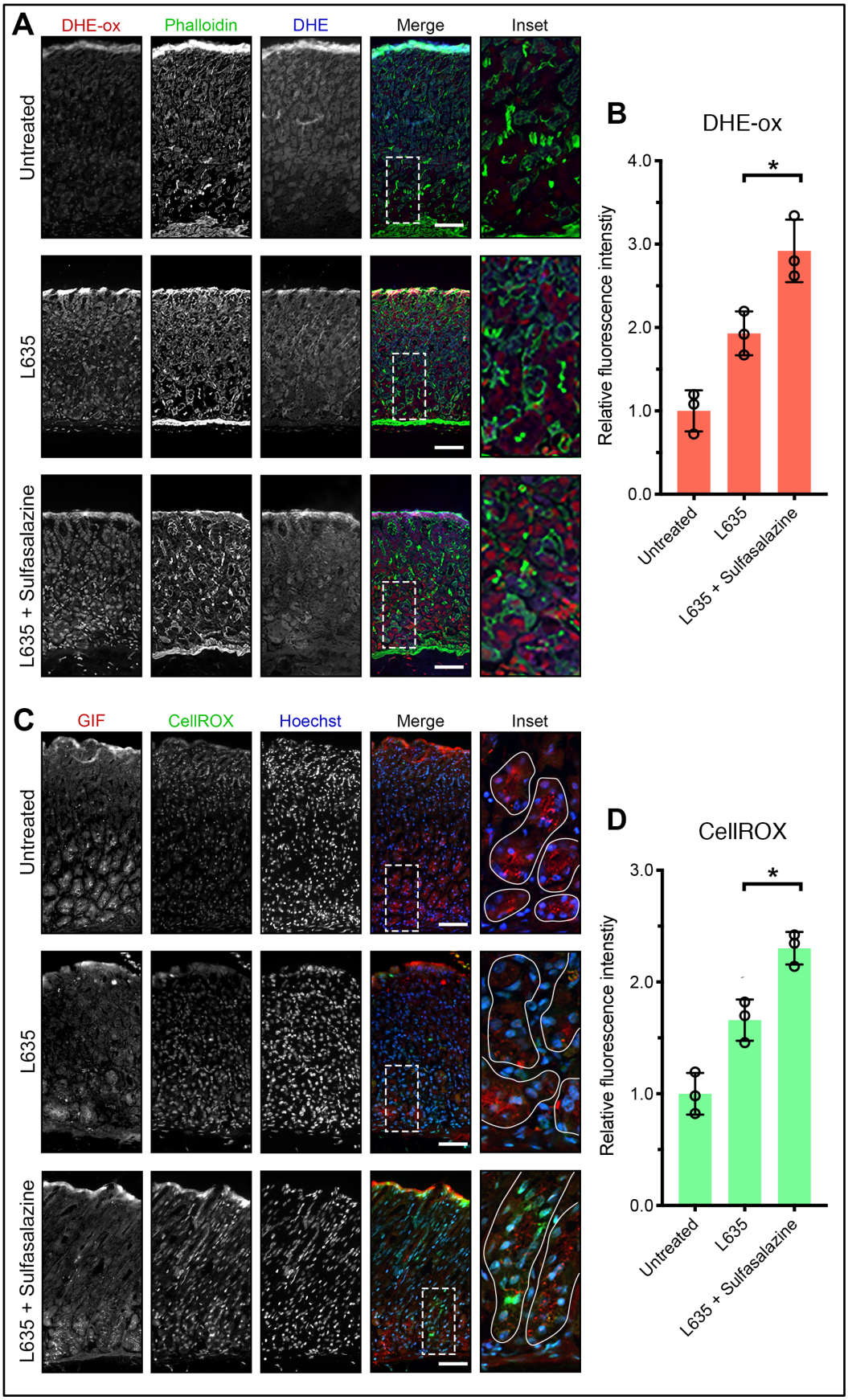
A
DHE-ox
Phalloidin
DHE
Merge
Inset
Untreated
L635
L635 + Sulfasalazine
B
DHE-ox
Relative fluorescence intenstiy
4.0
3.0
2.0
1.0
0.0
*
Untreated
L635
L635 + Sulfasalazine
C
GIF
CellROX
Hoechst
Merge
Inset
Untreated
L635
L635 + Sulfasalazine
D
CellROX
Relative fluorescence intenstiy
3.0
2.0
1.0
0.0
*
Untreated
L635
L635 + Sulfasalazine

Figure 14. xCT blockade leads to elevated ROS after acute gastric damage. *Sections from untreated (n=3), L635-treated (n=3), and L635 + sulfasalazine-treated (n=3) C57Bl/6J mice sacrificed after 3 days of L635 treatment were treated with ROS indicators Dihydroethidium (DHE) and CellROX.* ***A.*** *Representative images of DHE staining with oxidized DHE (DHE-ox) (red), f-actin marker Phalloidin (green), and unoxidized DHE (blue) (scale bars =100 μm). Magnified inset of chief cell region (right).* ***B.*** *Relative fluorescence intensity of nuclear DHE-ox (p= 0.02).* ***C.*** *Representative images of CellROX green staining with zymogenic granule marker GIF (red), CellROX Green Reagent (green), with nuclear counter stain Hoechst (blue) (scale bars =100 μm). Magnified inset of chief cell region right).* ***D.*** *Relative fluorescence intensity of CellROX in GIF-positive cells (p= 0.01). Statistical significance determined by one-way ANOVA with Bonferroni's post-hoc multiple comparisons test.*

Furthermore, L635 + sulfasalazine-treated mice exhibited a few GIF-positive chief cells that were dual-positive for the apoptosis marker cleaved caspase-3 (Figure 15A). Taken together, these findings indicate that inhibition of xCT prevents chief cell reprogramming, but chief cells still initiate a stress response due to increased ROS and, in some cases, undergo apoptosis.

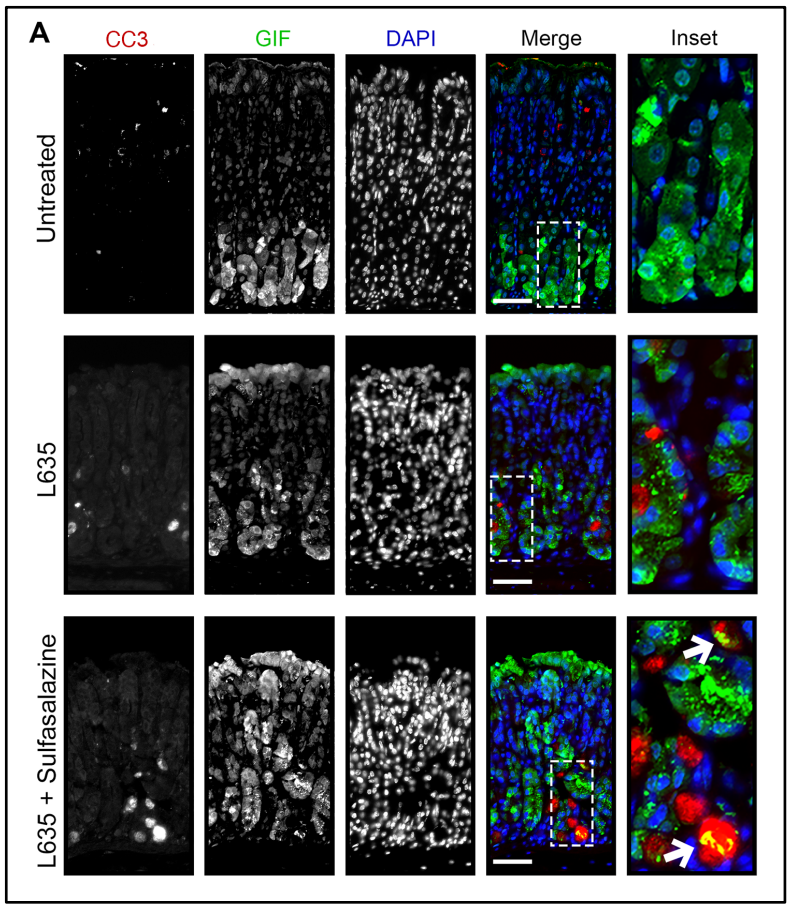

Figure 15. Inhibition of xCT in reprogramming chief cells results in apoptosis.
A. *Immunostained sections from untreated (n=4), L635-treated (n=4), and L635 + sulfasalazine-treated (n=3) C57Bl/6J mice sacrificed after 3 days of L635 treatment for apoptosis marker cleaved caspase-3 (red), zymogenic granule marker GIF (green), with nuclear counterstain DAPI (blue) (scale bars = 100 μm). Magnified inset of chief cell region with arrows indicating cleaved caspase-3 and GIF dual-positive apoptotic chief cells.*

Next, we examined in each of our experimental groups the expression of CD44v9, a metaplastic cell marker protein that interacts and stabilizes xCT (Figure 16A). Immunostaining for CD44v9 confirmed no expression in untreated mice. Similarly, no CD44v9 staining was observed in the sulfasalazine only treatment group. In contrast, mice treated with L635 exhibited high expression of CD44v9 on the basolateral membranes of cells at the base of oxyntic glands. The majority of these cells were dual-positive for the mucin granule marker GSII-lectin. Interestingly, reduced expression of CD44v9 was observed in L635 + sulfasalazine-treated mice (Figure 16B). The remaining CD44v9 staining in mice treated with L635 and sulfasalazine appeared to be intracellular and not on the basolateral membrane. We utilized real-time PCR to measure the relative expression of *Cd44v9* mRNA transcript in each of the experimental groups (Figure 16C). No significant difference in *Cd44v9* mRNA was observed between L635-treated mice ± sulfasalazine treatment. Therefore, these results indicate that sulfasalazine may disrupt the interaction of CD44v9 and xCT on the membrane and may result in mislocalization and possible degradation of CD44v9 protein. On the other hand, it is also possible that maintenance of redox balance is required for up-regulation of CD44v9 protein.

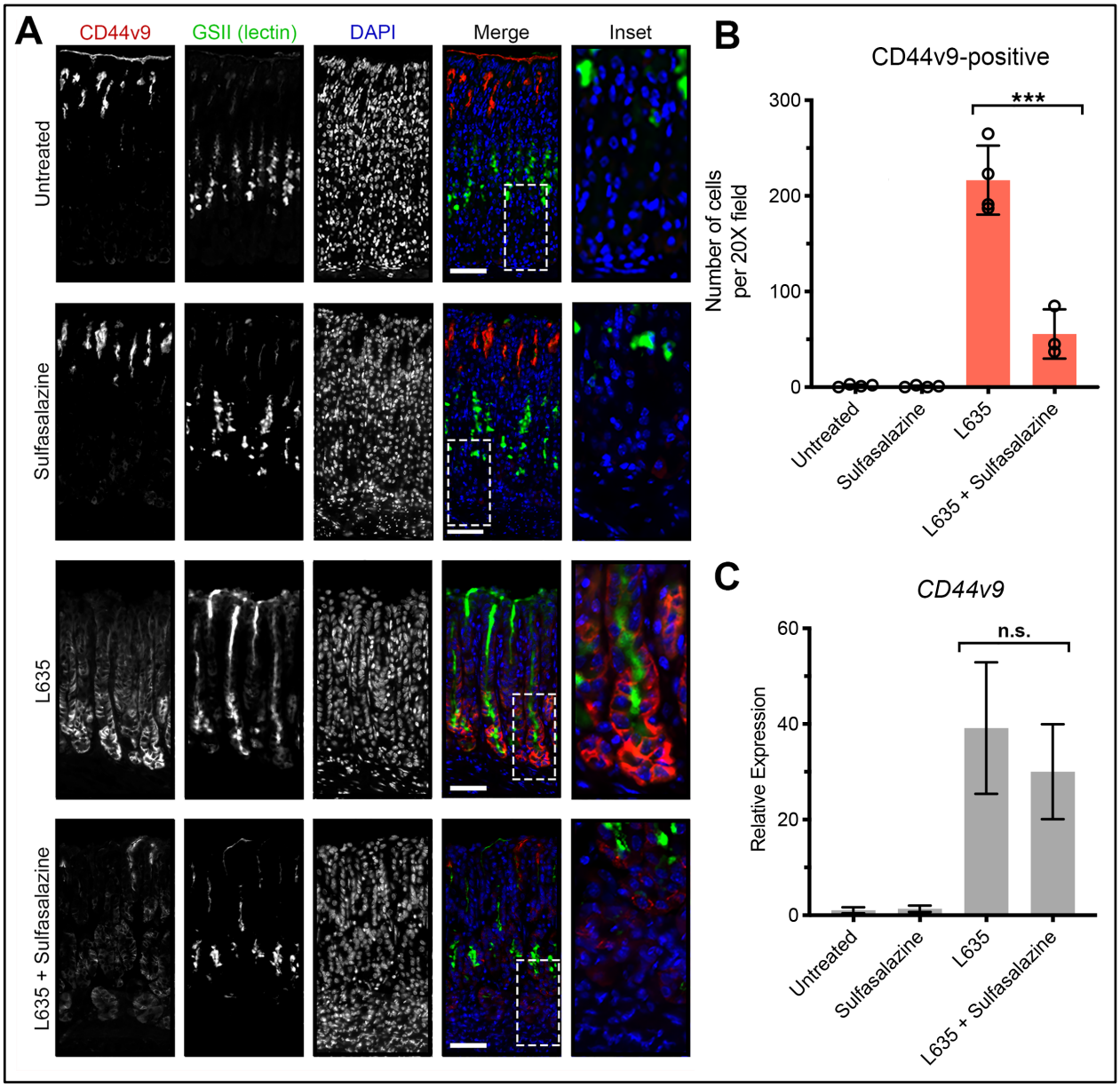

Figure 16. Basolateral membrane expression of CD44v9 is decreased after xCT inhibition with sulfasalazine.

A. *Immunostained sections from untreated (n=4), sulfasalazine-treated (n=4), L635-treated (n=4), and L635 + sulfasalazine-treated (n=3) C57Bl/6J mice sacrificed after 3 days of L635 treatment for CD44v9 (red), mucin granule marker GSII-lectin (green), with nuclear counter stain DAPI (blue) (scale bars = 100 μm). Magnified inset of chief cell region (right).* ***B.*** *Number of cells per 20X field with basolateral membrane expression of CD44v9 ($p<0.0001$).* ***C.*** *Relative mRNA expression of Cd44v9 (n.s. = not significant). Statistical significance determined by one-way ANOVA with Bonferroni's post-hoc multiple comparisons test.*

Metabolites of sulfasalazine do not alter metaplasia development.

To validate further that our observations were due to specific xCT blockade by sulfasalazine and not the anti-inflammatory properties of sulfasalazine metabolites, we treated mice with sulfapyridine or mesalazine two days prior to and throughout three days of L635 treatment (Figure 14A) (Nashed et al., 2017). Immunostaining for CD44v9, mucin granule marker GSII-lectin, and zymogenic granule marker GIF showed similar high numbers of triple-positive cells in both sulfapyridine + L635-treated mice and mesalazine + L635-treated mice (Figure 17B-C). These results indicate that metabolites of sulfasalazine are not sufficient to block chief cell reprogramming to SPEM.

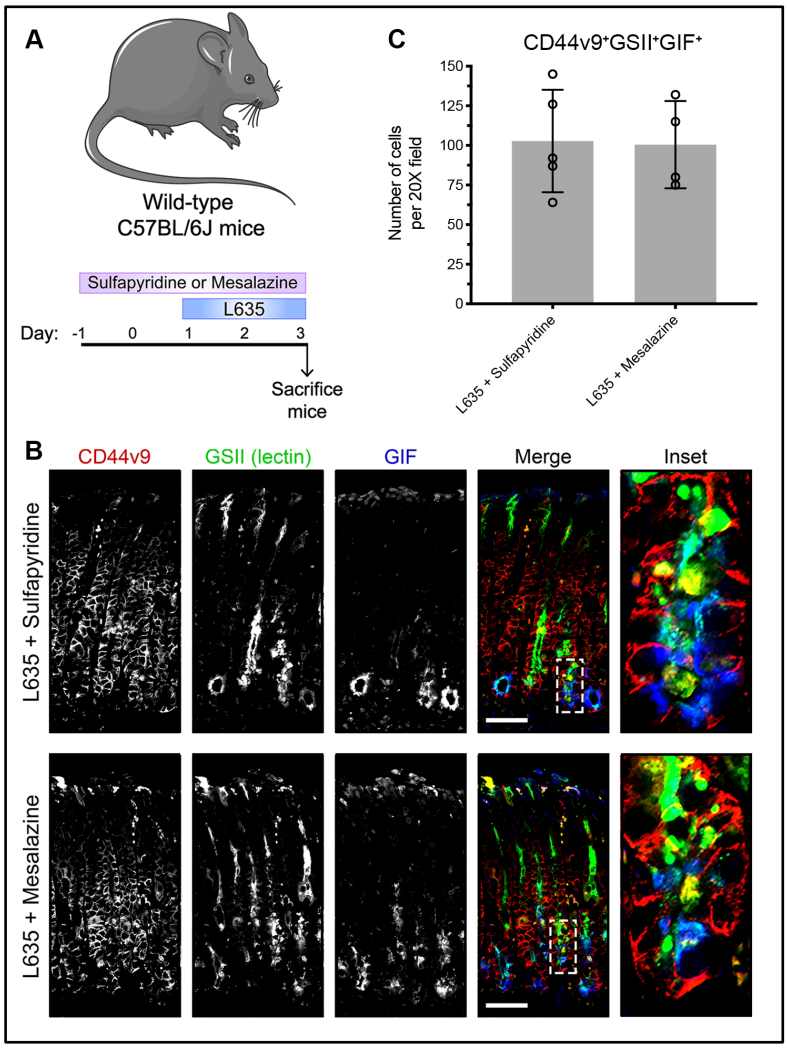

Figure 17. Metabolites of sulfasalazine do not prevent metaplasia development after acute gastric damage.
A. *Diagram of drug treatments. L635 was administered to C57BL/6J mice for three days to induce acute gastric damage. Mice were treated with sulfapyridine or mesalazine daily, 2 days prior to and throughout L635 administration. Mice were sacrificed 2 hours after final dose, and stomachs from sulfapyridine + L635-treated (n=4) and mesalazine + L635-treated (n=4) C57Bl/6J mice were harvested for histological analysis.* ***B.*** *Immunofluorescence staining for metaplastic cell marker CD44v9 (red), mucin granule marker GSII-lectin (green), zymogenic granule marker GIF (blue) (scale bars = 100 μm). Magnified inset of chief cell region (right).* ***C.*** *Quantification of CD44v9, GIF, GSII-lectin triple-positive cells per 20X field.*

xCT knockout mice recapitulate the phenotype of sulfasalazine-treated mice.

To examine further if the effects of sulfasalazine are mediated by inhibition of xCT we treated xCT knockout (xCTKO) mice with the parietal cell toxic drug, L635. Stomachs were harvested from two experimental groups: 1) untreated xCTKO mice and 2) L635-treated xCTKO mice for histological analysis (Figure 18A). H&E or PAS staining revealed normal gastric histology in xCTKO mice (Figure 18B). To visualize L635-induced parietal cell loss, we performed immunostaining for the proton pump H^+K^+ ATPase (Figure 18C). In untreated xCTKO mice, a large number of H^+K^+ ATPase-positive parietal cells were detected throughout the corpus glands. Treatment with L635 in xCTKO mice reduced the number of parietal cells by more than seventy percent (Figure 18D). To detect chief cell reprogramming, we immunostained for the zymogenic granule marker GIF and the mucin granule marker GSII-lectin (Figure 18C). L635-treated xCTKO mice did not display reprogramming chief cells, dual-positive for GIF and GSII (Figure 18E). Similarly, PAS staining revealed no mucin staining at the bases of glands in L635-treated xCTKO mice (Figure 18B). Collectively, these results suggest that chief cells from xCT-deficient mice are unable to reprogram after acute parietal cell loss.

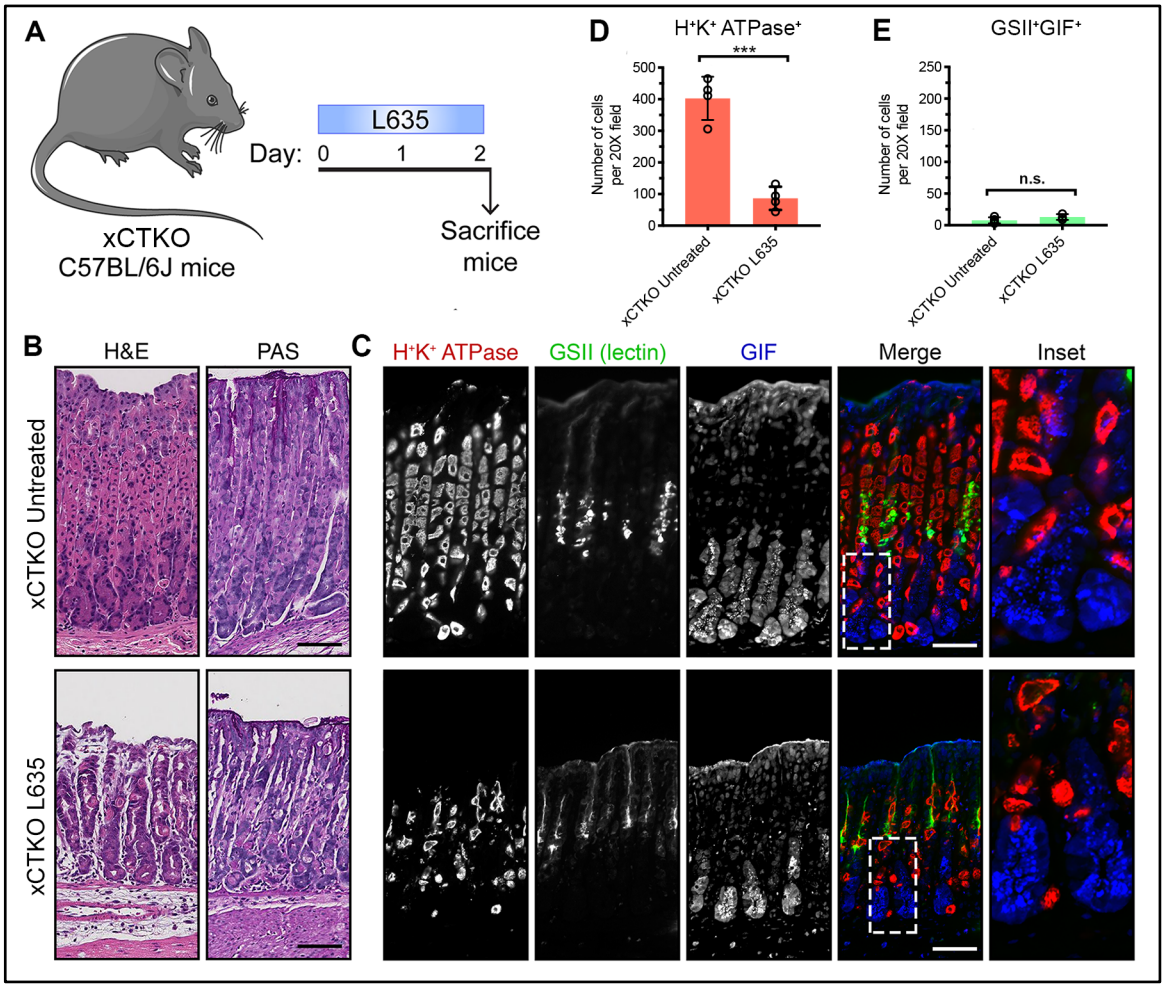

Figure 18. Loss of xCT prevents the development of metaplasia after acute gastric damage.

A. *Diagram of drug treatments. L635 was administered to xCTKO C57BL/6J mice for three days to induce acute gastric damage. Mice were sacrificed 2 hours after final dose of L635, and stomach tissue from untreated xCTKO mice (n=4), L635-treated xCTKO mice (n=4), were harvested for histological analysis.* ***B.*** *Hematoxylin and eosin (H&E) and Periodic acid-Schiff (PAS) stained sections.* ***C.*** *Immunostained sections for parietal cell marker H+K+ ATPase (red), mucin granule marker GSII-lectin (green), zymogenic granule marker GIF (blue) (scale bars = 100 μm). Magnified inset of chief cell region (right).* ***D.*** *Quantification of parietal cells as determined by number of H+K+ ATPase-positive (red) cells per 20X objective field (p=0.0002).* ***E.*** *Quantification of GSII (green) and GIF (blue) dual-positive (SPEM) cells per 20X objective field (n.s. = not significant). Statistical significance determined by unpaired student's t-test.*

Additionally, we examined xCTKO mice to determine ROS levels using the ROS indicators, DHE and CellROX. While untreated xCTKO mice had low levels of ROS, after L635-treatment xCTKO mice exhibited high levels of ROS (Figure 19A-D). Similar to L635 + sulfasalazine-treated mice, GIF-positive chief cells from L635-treated xCTKO mice had elevated ROS determined by CellROX Green Reagent staining (Figure 19D).

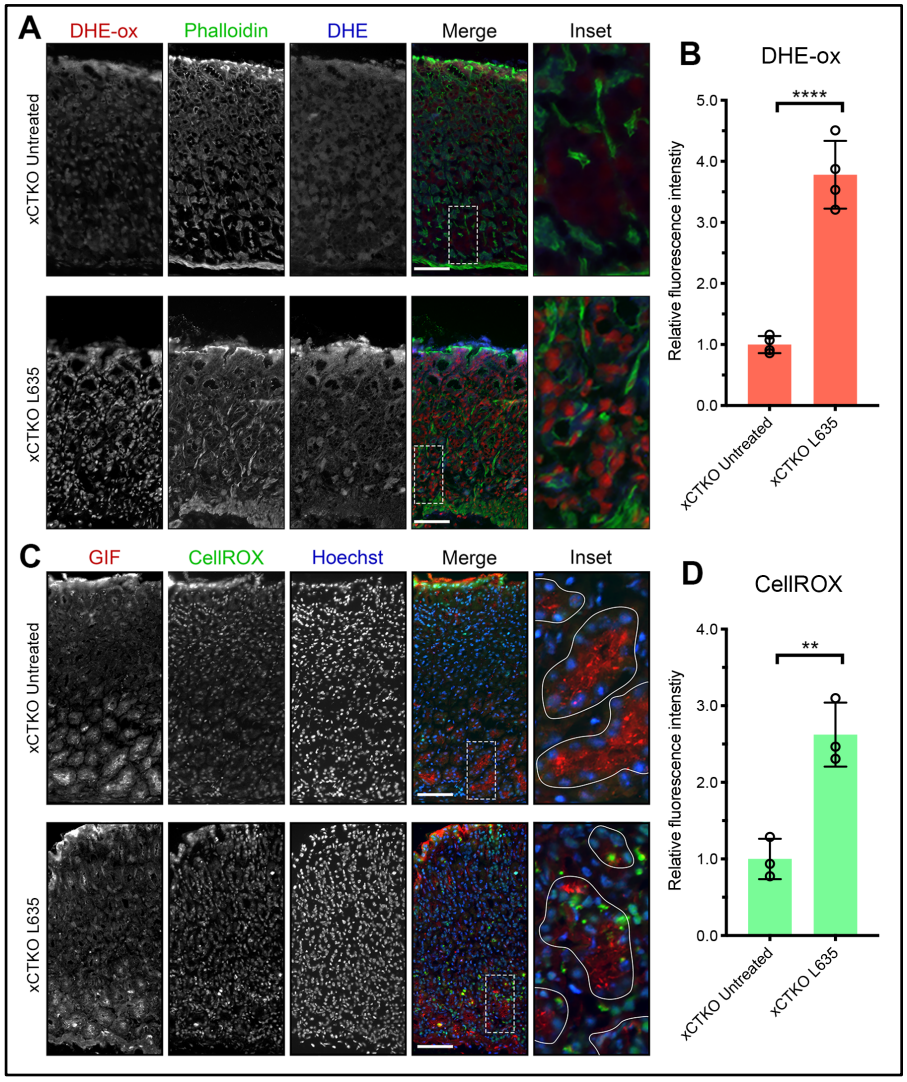

Figure 19. xCT is required for ROS detoxification.
Sections from untreated xCTKO (n=4) and L635-treated xCTKO (n=4) C57Bl/6J mice sacrificed after 3 days of L635 treatment were incubated with ROS indicators Dihydroethidium (DHE) and CellROX. ***A.*** *Representative images of DHE staining with oxidized DHE (DHE-ox) (red), f-actin marker Phalloidin (green), and unoxidized DHE*

(blue) (scale bars =100 μm). Magnified inset of chief cell region (right). ***B.*** *Relative fluorescence intensity of nuclear DHE-ox (p<0.0001).* ***C.*** *Representative images of CellROX green staining with zymogenic granule marker GIF (red), CellROX Green Reagent (green), with nuclear counter stain Hoechst (blue) (scale bars =100 μm). Magnified inset of chief cell region right).* ***D.*** *Relative fluorescence intensity of CellROX in GIF-positive cells (p= 0.004). Statistical significance determined by unpaired student's t-test.*

Likewise, several GIF-positive chief cells from L635-treated xCTKO mice were dual-positive for cleaved caspase-3 (Figure 20A). Taken together, our results indicate that chief cells from xCT-deficient mice are unable to reprogram and experience oxidative stress that leads to apoptotic cell death.

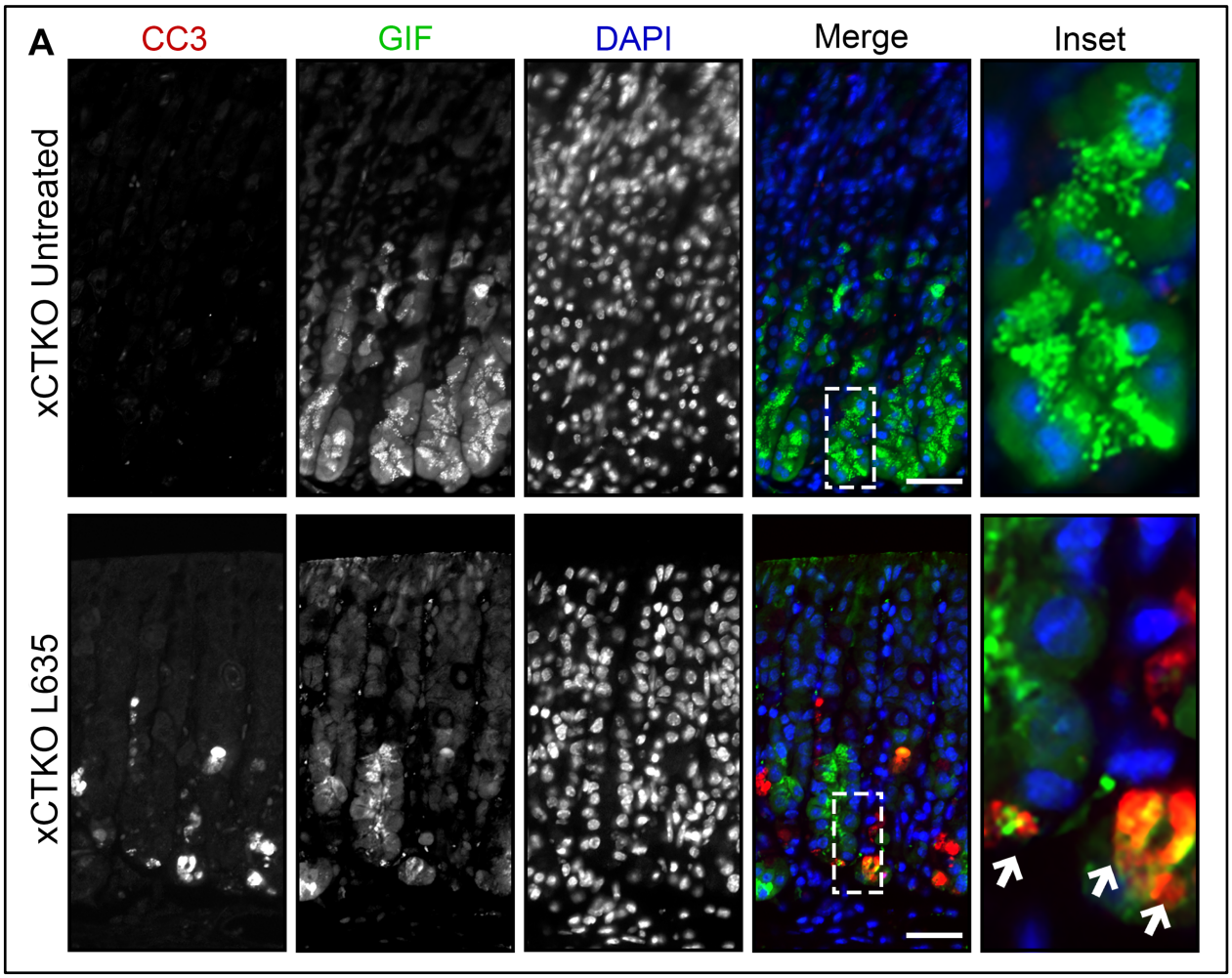

Figure 20. Chief cells from xCT knockout mice apoptose after acute gastric damage.
A. *Immunostained sections from untreated xCTKO (n=4) and L635-treated xCTKO (n=4) C57Bl/6J mice sacrificed after 3 days of L635 treatment for apoptosis marker CC3 (red), zymogenic granule marker GIF (green), with nuclear counterstain DAPI (blue) (scale bars = 100 μm). Magnified inset of chief cell region with arrows indicating CC3 and GIF dual-positive apoptotic chief cells.*

Inhibition of xCT prevents DMP-777 induced SPEM.

To test the efficacy of xCT blockade on chief cell reprogramming in a different mouse model of acute parietal loss, we utilized another parietal toxic drug, DMP-777. Similar to L635, DMP-777 induces parietal cell necrosis. However, DMP-777 also functions as an elastase inhibitor and prevents inflammatory infiltration (Goldenring et al., 2000). With DMP-777 treatment, chief cell reprogramming and metaplasia development occur in the absence of inflammation. We treated mice with sulfasalazine two days prior to and throughout ten days of DMP-777 treatment. Stomachs were harvested from two experimental groups, 1) DMP-777-treated and 2) DMP-777 + sulfasalazine-treated mice, for histological analysis (Figure 21A). H^+K^+ ATPase staining demonstrated similar levels of parietal cell loss in both groups (Figure 21B-C). We also performed immunostaining for the zymogenic granule marker GIF and mucin granule marker GSII-lectin to detect chief cell reprogramming. Sulfasalazine treatment decreased the number of GIF and GSII-lectin dual-positive SPEM cells by greater than seventy-five-percent after DMP-777-induced parietal cell loss (Figure 21B and D). Therefore, xCT inhibition with sulfasalazine prevents metaplasia development even in the absence of inflammation.

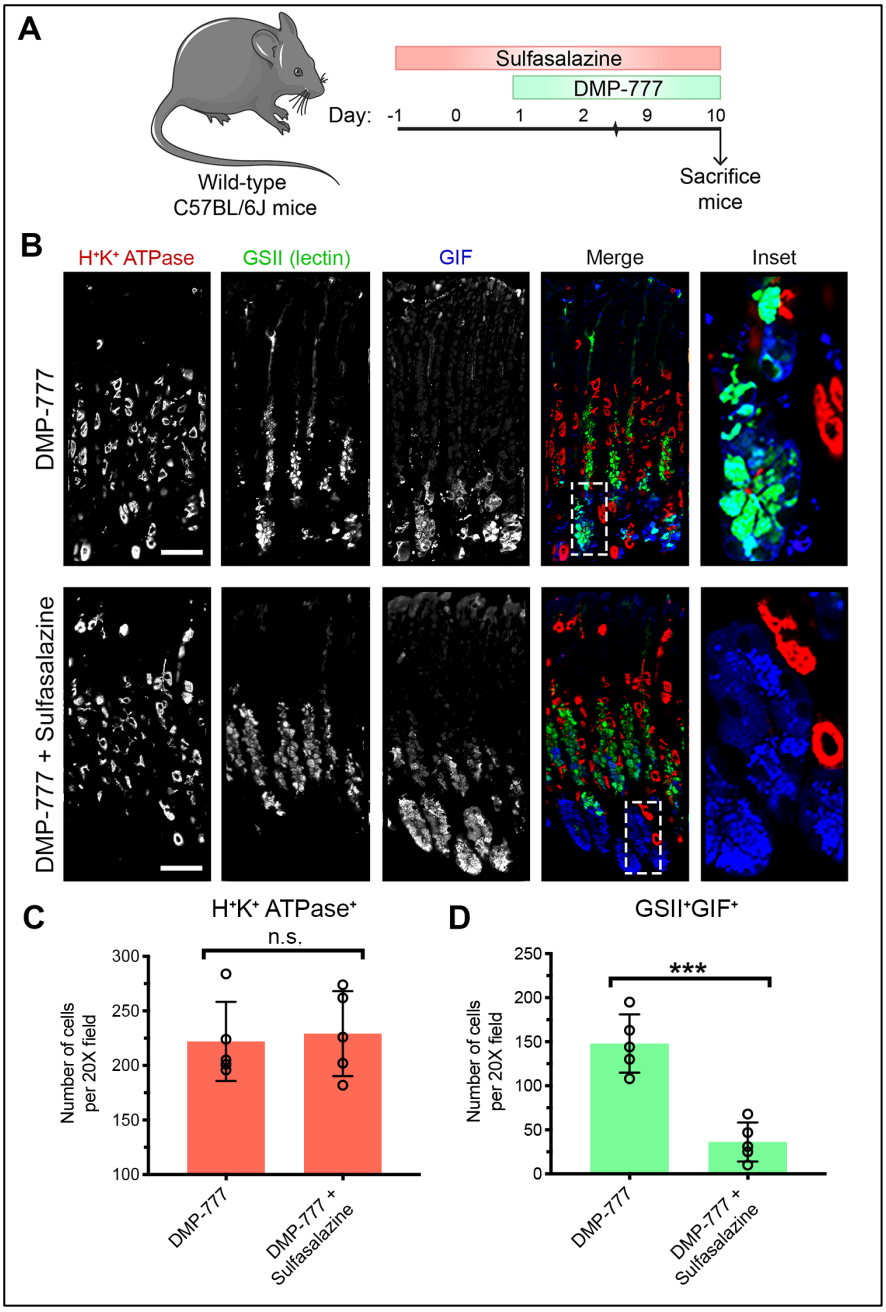

Figure 21. Sulfasalazine inhibits metaplasia development in the absence of inflammation.

A. *Diagram of drug treatments. A parietal cell toxic drug (DMP-777) was administered to C57BL/6J mice for ten days to induce acute gastric damage. Mice were treated with 10 mg of sulfasalazine per day, 2 days prior to and throughout DMP-777 administration. Mice were sacrificed 2 hours after final dose of DMP-777, and stomachs from DMP-777-treated (n=5) and DMP-777 + sulfasalazine-treated (n=5) mice were harvested for histological analysis.* ***B.*** *Immunofluorescence staining for parietal cell marker H+K+ ATPase (red), mucin granule marker GSII-lectin (green), zymogenic granule marker GIF (blue) (scale*

bars = 100 µm). Magnified inset of chief cell region (right). ***C.*** *Quantification of parietal cells as determined by number of H+K+ ATPase-positive (red) cells per 20X objective field (n.s. = not significant).* ***D.*** *Quantification of GSII (green) and GIF (blue) dual-positive (SPEM) cells per 20X objective field (p=0.0002). Statistical significance determined by unpaired student's t-test.*

We further examined DMP-777-treated mice with the ROS indicators (DHE and CellROX) and apoptosis markers. DMP-777 + sulfasalazine-treated mice exhibited slightly elevated levels of ROS compared to DMP-777-treated mice (Figure 22A-D).

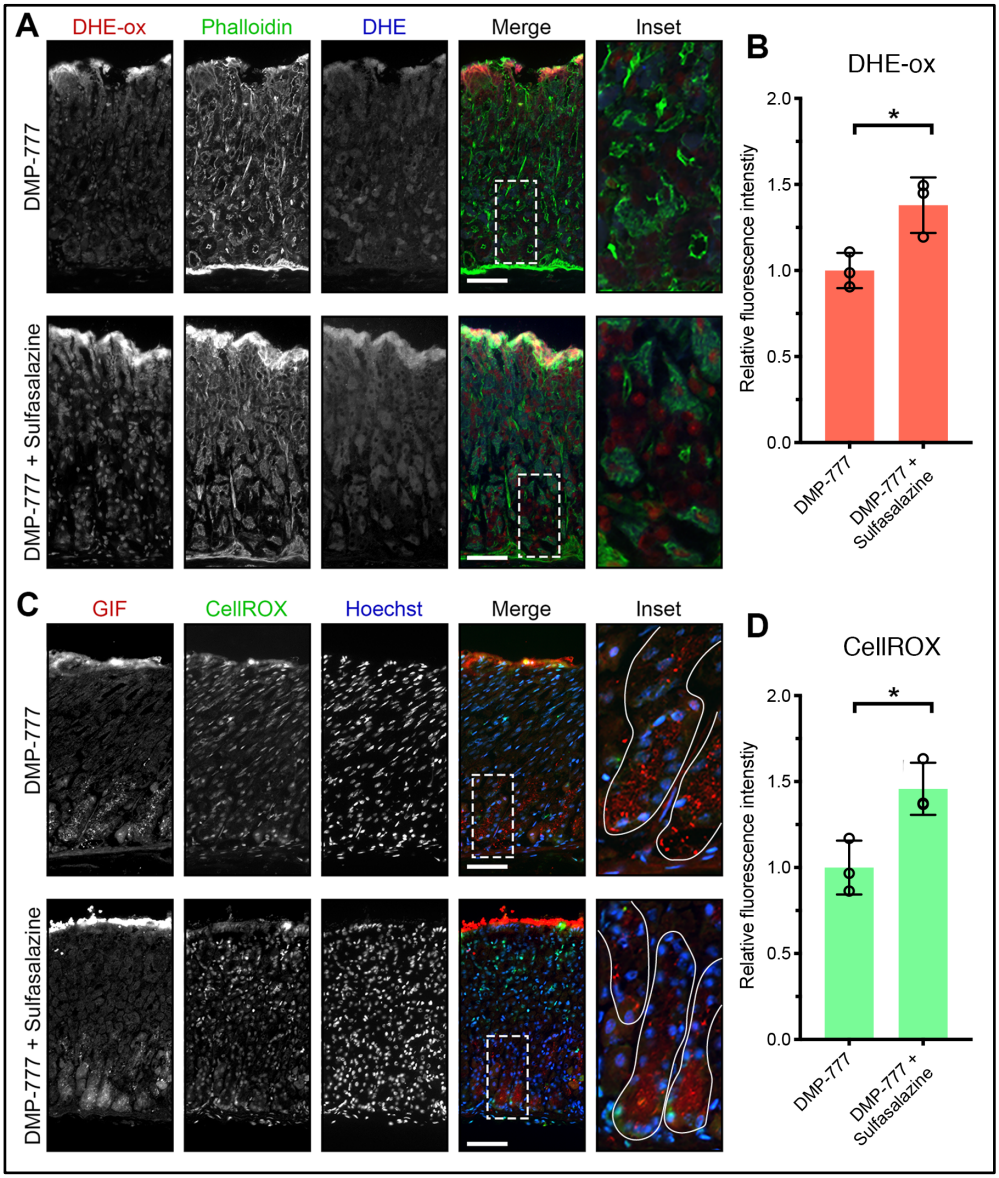

Figure 22. xCT blockade with sulfasalazine leads to elevated ROS in chief cells without inflammation.
Sections from DMP-777-treated (n=3) and DMP-777 + sulfasalazine-treated (n=3) C57Bl/6J mice sacrificed after 3 days of L635 treatment were incubated with ROS indicators Dihydroethidium (DHE) and CellROX. ***A.*** *Representative images of DHE staining with oxidized DHE (DHE-ox) (red), F-actin marker Phalloidin (green), and unoxidized DHE (blue) (scale bars = 100 μm). Magnified inset of chief cell region (right).* ***B.*** *Relative fluorescence intensity of nuclear DHE-ox (p=0.02).* ***C.*** *Representative images of CellROX green staining with zymogenic granule marker GIF (red), CellROX Green Reagent (green), with nuclear counter stain Hoechst (blue) (scale bars = 100 μm). Magnified inset of chief cell region right).* ***D.*** *Relative fluorescence intensity of CellROX in GIF-positive cells (p=0.02). Statistical significance determined by unpaired student's t-test.*

Furthermore, very few GIF-positive chief cells were dual-positive for the apoptosis marker cleaved caspase-3 (Figure 23A). It is likely that the generation of ROS intrinsic to the reprogramming process account for the increased ROS observed in DMP-777 + sulfasalazine-treated mice. However, in the absence of inflammatory ROS, chief cells are able to endure the oxidative stress, at least over the 10-day time course.

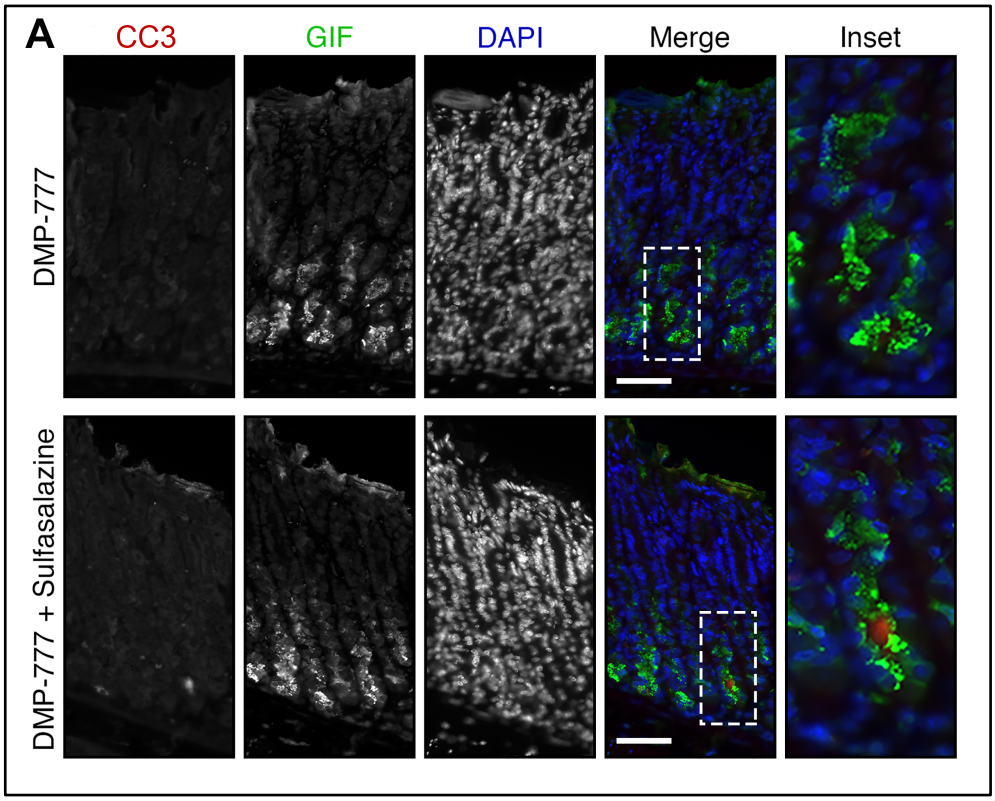

Figure 23. Reprogramming chief cells survive oxidative stress without inflammatory ROS.
A. *Immunostained sections from DMP-777-treated (n=5) and DMP-777 + sulfasalazine-treated (n=5) C57Bl/6J mice sacrificed after 10 days of DMP-777 treatment for apoptosis marker CC3 (red), zymogenic granule marker GIF (green), with nuclear counterstain DAPI (blue) (scale bars = 100 μm). Magnified inset of chief cell region with arrows indicating CC3 and GIF dual-positive apoptotic chief cells.*

CD44v9 and xCT are up-regulated in SPEM in *Helicobacter*-infected mice and humans.

Given the prominent changes observed in the acute models of parietal cell loss, we sought to examine whether CD44v9 and xCT were also up-regulated following chronic SPEM induction in *Helicobacter felis*-infected mice or in human patients. Figure 24A demonstrates that staining for both CD44v9 and xCT is observed in SPEM from the stomach of mice infected with *H. felis* for 12 months. Similarly, Figure 24B displays that both CD44v9 and xCT staining is observed in SPEM from human patients. These studies confirm the up-regulation of ROS detoxification mechanisms in chronic induction of SPEM in addition to SPEM associated with acute gastric damage.

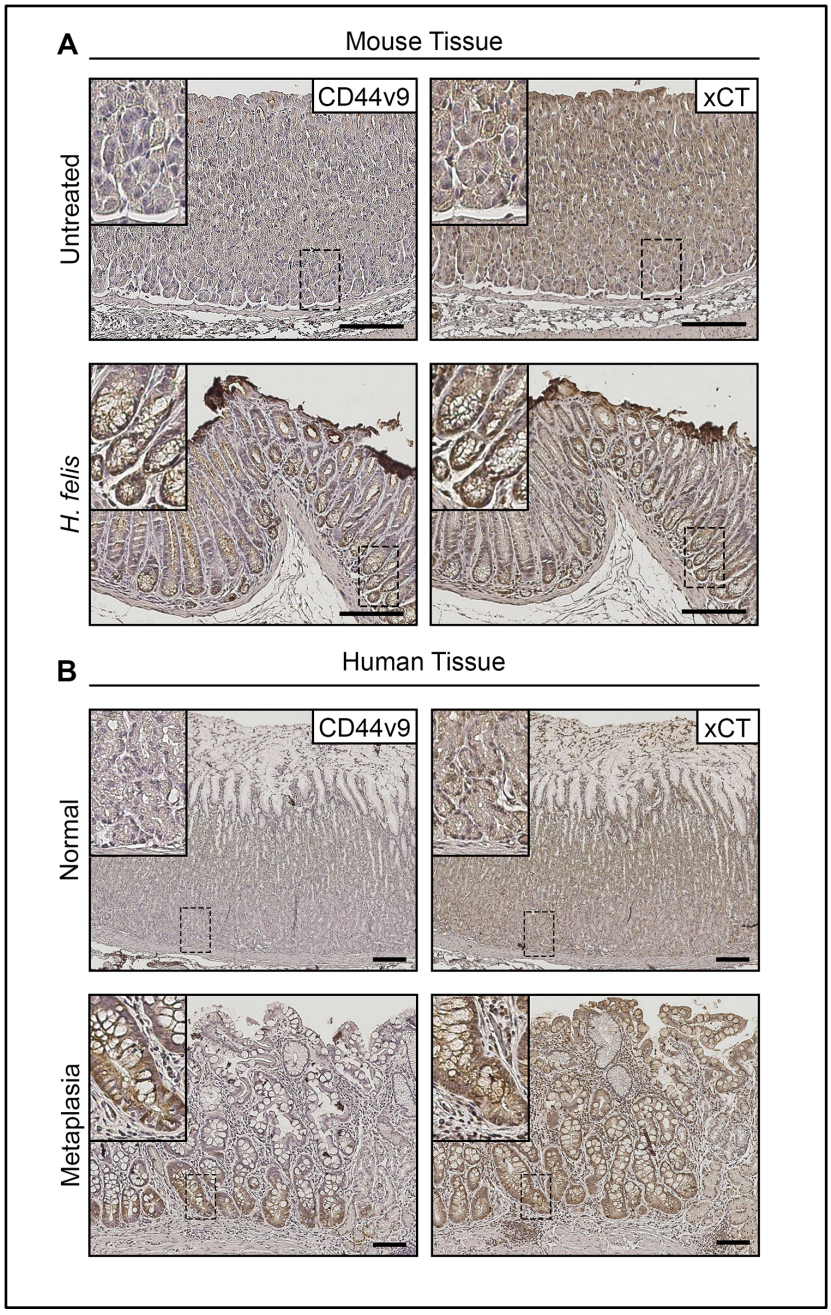

Figure 24. CD44v9 and xCT are expressed in Helicobacter-infected mice and human metaplasia.

A. *Representative immunohistochemical stained serial sections from the body of the stomach for CD44v9 (left) and xCT (right) in untreated (n=3) and 12 months Helicobacter felis-infected (n=3) C57Bl/6J mice (scale bar = 100 μm).* ***B.*** *Representative immunohistochemical stained serial sections from the body of the stomach for CD44v9 (left) and xCT (right) in normal (n=6) and metaplastic (n=3) human stomach (scale bar = 100 μm).*

DISCUSSION

Following significant gastric injury, chief cells reprogram to mucin-secreting metaplasia or SPEM. The present study identifies that xCT is required for the reprogramming of digestive enzyme-secreting chief cells following gastric injury. Increased membrane expression of xCT is observed in reprogramming chief cells expressing CD44v9 after gastric damage with parietal cell toxic drugs. Inhibition of xCT, through sulfasalazine treatment, or xCT siRNA knockdown blocks cystine uptake, ROS detoxification, proliferation and survival of metaplastic cells in culture. In addition, chief cells from sulfasalazine-treated mice or xCT knockout mice were unable to reprogram after acute gastric injury. Importantly, we confirm that our findings were due to specific inhibition of xCT by sulfasalazine, and not the anti-inflammatory characteristics of sulfasalazine metabolites. While loss of xCT activity inhibited chief cell reprogramming, chief cells endured oxidative stress and in some cases apoptosis. Interestingly, the transcription factor Mist1 was downregulated in chief cells after acute parietal cell loss, even with xCT blockade. In contrast, inhibition of xCT restricted the up-regulation of autosomal and lysosomal degradation machinery, a distinct step in the reprogramming process. Thus, while xCT inhibition does not alter initiation of reprogramming, it arrests the completion of the process. These results demonstrate that the process of reprogramming involves multiple discrete steps leading to metaplasia.

Reprogramming promotes the regenerative capacity of differentiated cells. This is a critical process used to repair damage in tissues that lack an active adult stem cell compartment such as the pancreas (Jensen et al., 2005). Still, in tissues with active adult stem cells such as the stomach and intestine, reprogramming differentiated cells can

enable repair after tissue damage (Mills and Sansom, 2015). It is evident that reprogramming of differentiated cells occurs through a stepwise process. First, differentiated cells must undergo autodegradation to downscale mature characteristics. Next, metaplastic genes are up-regulated, and mucin-containing granules are formed. Finally, metaplastic cells have the capability of re-entering into the cell cycle and proliferating. Progression through this stepwise process can be blocked at intervening checkpoints. The results presented here suggest that maintaining redox balance is crucial for progression through the reprogramming process in gastric chief cells and may represent a checkpoint for this process. It is likely that the downscaling of zymogen granules and up-regulation of mucus granule formation would engender the production of ROS. Furthermore, acute and chronic inflammation can add to elevated ROS levels (Mittal et al., 2014). Indeed, it is likely that decreased ROS levels are important for the undifferentiated status or stemness of reprogramming chief cells. CD44v9 and xCT have also been implicated as key players in malignant transformation in a variety of tissues and are often highly expressed by cancer stem cells (Chung et al., 2005; Nagane et al., 2018; Wada et al., 2013; Zavros, 2017). Thus, up-regulation of xCT activity may be used by reprogramming cells or cancer stem cells to combat increased oxidative stress.

Oxidative stress refers to high levels of intracellular ROS that can cause damage to lipids, proteins, and DNA (Ni et al., 2012). Elevated ROS act as signaling molecules that contribute to both physiological and pathological conditions (Vaahtera et al., 2014). Cells utilize several mechanisms to counteract oxidative stress by producing antioxidants such as glutathione (Rushworth and Megson, 2014). Increased expression of xCT is part of the oxidative stress response (Habib et al., 2015; Ishii and Mann, 2014). In addition,

molecules that work to stabilize and increase the activity of xCT, such as CD44v9, are up-regulated as a consequence of oxidative stress. Increased xCT activity results in a build-up of intracellular cystine, which through a multi-step process can be converted to glutathione (Nagano et al., 2013). Disruption of xCT activity in cases of tissue injury leads to elevated levels of ROS and oxidative damage. Excessive oxidative damage may cause cell death (Navarro-Yepes et al., 2014). The results here suggest that generation of ROS is inherent to the process of injury and reprogramming. Therefore, activation of antioxidant responses is required for the successful reprogramming of differentiated cells and epithelial repair. Although the cell of origin for cancer in the stomach is still under debate, cellular reprogramming to metaplasia in the setting of chronic injury and inflammation may expose these cells to prolonged oxidative stress, which could promote neoplastic transformation (Hardbower et al., 2013).

In summary, our investigations have demonstrated that a response to ROS and up-regulation of xCT activity is crucial for reprogramming of zymogenic chief cells into SPEM. Recruiting reparative lineages that can combat the increased oxidative burden associated with injury is critical for proper tissue repair. Targeting xCT may prove as an effective tool for arresting metaplasia development in the stomach as well as mucous metaplasia in other epithelial tissues for the analysis of cellular plasticity and oxidative stress response.

CHAPTER III:

INNATE IMMUNE RESPONSE

Adapted from: **Meyer AR**, Engevik AC, Madorsky T, Belmont E, Stier MT, Norlander AE, Pilkinton MA, McDonnell WJ, Weis JA, Mallal SA, Peebles RS, Goldenring JR. Group 2 innate lymphoid cells (ILC2s) coordinate damage response in the stomach.

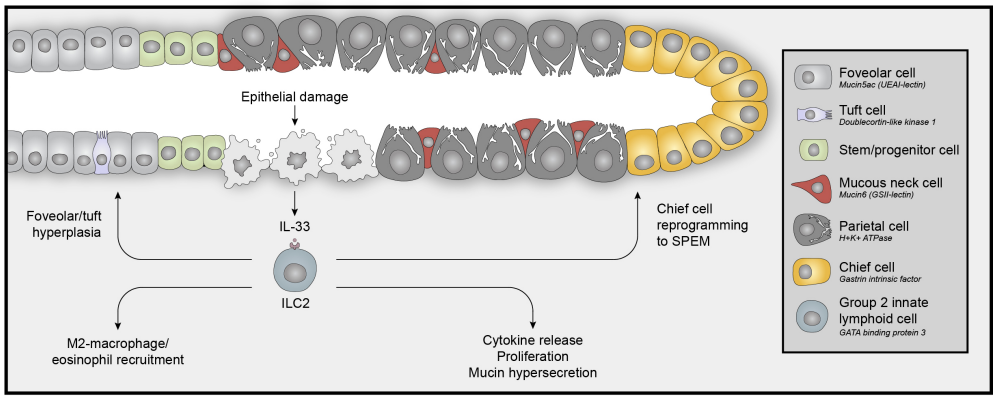

Figure 25. Diagram of ILC2s coordinating damage response in the stomach.
GATA3-positive ILC2s in the stomach are stimulated by IL-33 after epithelial damage to promote cytokine release, proliferation, mucin hypersecretion, chief cell reprogramming to SPEM, expansion of foveolar/tuft cell lineages, and M2 macrophage/ eosinophil recruitment.

INTRODUCTION

Severe damage to the lining of the stomach leads to reprogramming of the epithelium to recruit reparative cells to sites of mucosal injury. In the stomach, reprogramming is characterized by the transdifferentiation of digestive enzyme-secreting chief cells to mucin-secreting metaplasia (spasmolytic polypeptide-expressing metaplasia or SPEM), expansion of the foveolar and tuft cell lineages, and infiltration and activation of immune cells including M2 macrophages and eosinophils. Our previous investigations

have suggested reprogramming is governed by a cytokine signaling cascade (Petersen et al., 2017). The cascade begins with the alarmin interleukin-33 (IL-33) which is released from cells at sites of mucosal injury or infection (Schwartz et al., 2016). Mice lacking IL-33 or the IL-33 receptor (ST2) are blocked from epithelial reprogramming after drug-induced injury (Buzzelli et al., 2015). Similarly, chronic treatment with recombinant IL-33 promotes oxyntic atrophy, metaplasia development, and inflammatory infiltration in the stomach (Buzzelli et al., 2015). Downstream pathway analysis confirmed that IL-33 release in the stomach promotes the induction of type II cytokines, including IL-4, IL-5, IL-9, and IL-13. Mice lacking IL-13, but not other type II cytokines, are inhibited from the development of mucin-secreting metaplasia after gastric damage. Furthermore, recombinant IL-13 treatment to ST2 null mice restored metaplasia development following acute parietal cell loss (Petersen et al., 2017).

Recent advances in our understanding of immune responses to tissue damage or infection have indicated a crucial role for innate lymphoid cells (ILCs) (Neill et al., 2010). Derived from lymphoid progenitors, ILCs generate potent levels of cytokines that were previously thought to be primarily produced by T helper cells, but are negative for conventional lineage markers (Guo et al., 2012). ILCs have no antigen-specific receptors and cause antigen-independent immune responses (Eberl et al., 2015). They are prevalent at mucosal surfaces where they respond to factors derived from the epithelium that indicate damage or infection (Spits and Di Santo, 2011). A subtype of the ILC family, known as group 2 innate lymphoid cells or ILC2s, are regulated by the transcription factors RORα and GATA3 (Klein Wolterink et al., 2013; Serafini et al., 2015). They are stimulated by epithelial cell-derived stress signals such as IL-33, IL-25, and TSLP to provide an

innate source of type 2 cytokines (Li et al., 2014; Salimi et al., 2013; Stier et al., 2016). While ILC2s are commonly studied in tissues such as: lung, intestine, and skin, few investigations have addressed the role of ILC2s in the stomach (Fuchs and Colonna, 2013; Roediger et al., 2014; Satoh-Takayama et al., 2020; Scanlon and McKenzie, 2012). ILC2s are involved in tissue remodeling, mucin-secreting metaplasia, eosinophilia, and alternative macrophage activation through the production of type 2 cytokines in other tissues (Bernink et al., 2014; Roediger and Weninger, 2015). I hypothesized that ILC2s similarly regulate epithelial reprogramming after damage to the stomach.

We have now sought to evaluate the role of ILC2s in the regulation of the gastric mucosal response to significant injury. The present study reveals that there is a sizable accumulation of ILC2s in the stomach after damage, that is blocked in mice lacking IL-33. We have performed single cell RNA sequencing of ILC2s isolated from the normal "healthy" stomach as well as the L635-induced metaplastic stomach of mice and characterized a unique marker signature of gastric mucosal ILC2s, as well as identified a distinct transcriptional profile of metaplasia-associated ILC2s. Sequencing revealed several genes that may inform how ILC2s contribute to gastric pathology including *Il5, Il13, Csf2*, *Pd1,* and *Ramp3*. Depletion of ILC2s blocked the development of metaplasia after drug-induced injury in wild-type and Rag1 knockout mice. Similarly, ILC2 depletion prevented foveolar and tuft cell hyperplasia and the infiltration/activation of macrophages and eosinophils after injury. Understanding the role of type 2 inflammation and ILC2s in the induction of metaplasia may link the damage response in the stomach to other type 2-mediated diseases and could pave the way to better detection methods and therapies for precancerous metaplasia in the stomach.

MATERIALS AND METHODS

Mouse Models

Wild-type and Rag1 knockout C57BL/6J mice approximately eight weeks old were purchased from Jackson Labs (Bar Harbor, Maine, USA). Each experimental group consisted of at least three to four mice. L635 (synthesized by the Chemical Synthesis Core of the Vanderbilt Institute of Chemical Biology), dissolved in dH_2O was administered by oral gavage (350 mg/kg) once a day for 3 consecutive days. Rat IgG2b isotype control antibody (BioXCell BP0090) or anti-CD90.2 antibody (BioXCell BP0066) was administered intraperitoneally (300 µg) to wild-type and Rag1 knockout C57BL/6J mice every fourth day for 12 days for a total of four injections. Archival sections of stomach from wild-type, IL-33KO, and IL-13KO mice (n=6 per group) were obtained from previous investigations (Petersen et al., 2017). The care, maintenance, and treatment of animals in these studies adhere to the protocols approved by the Institutional Animal Care and Use Committee of Vanderbilt University.

Single Cell Isolation

Mouse stomachs were harvested, opened along the greater curvature, and washed in ice cold 1X PBS without calcium and magnesium. The antrum was removed with a razor blade and the oxyntic mucosa was harvested with a cell scraper to separate the mucosa from the serosa. The corpus mucosa was then finely minced using a razor blade and collected in ice cold Advanced DMEM/F12 cell culture medium. Tissue was allowed to settle, and the top layer of media was removed leaving a few milliliters of media containing gastric mucosa. The solution with tissue was transferred to 50 mL of pre-warmed (37°C) digestion buffer (Advanced DMEM/F12 + 5% FBS + 1 mg/mL collagenase type 1a + 1/100

DNAse I) in a round bottom flask with stir bar. The flask containing digestion buffer and tissue was placed in a 37°C water bath with stir plate and stirred at low speed for 30 minutes. To stop the reaction, 50 mL of Advanced DMEM/F12 supplemented with Y-27632 (1:1000) and 1mM DTT was added. The mixture was centrifuged at 300 x g for 5 minutes to pellet glands/cells. The supernatant was aspirated, and the pellet was resuspended in 1 mL of Advanced DMEM/F12 supplemented with Y-27632. The solution was drawn up into a 1 mL syringe with 25-gauge needle attached. The solution was pushed through needle and strained through 70 µm cell strainer to disrupt the glandular structures and achieve a single cell suspension. The cell strainer was washed with 9 mL of Advanced DMEM/F12 supplemented with Y-27632. Cells were centrifuged at 300 x g for 5 minutes. Supernatant was removed and cells were resuspended in 1 mL of Advanced DMEM/F12 supplemented with Y-27632 and stored on ice.

Flow Cytometry

Three million cells per sample were added to BD Falcon 5 mL polypropylene round-bottom tubes. Cells were washed with 2 mL of 1X PBS and centrifuged at 1200 rpm for 5 minutes at 4°C. Supernatant was removed and cells were washed in 2 mL of FACS buffer (1X PBS + 3% FBS). Supernatant was removed and 3 µL of Fc Receptor Block (BD) was diluted in 50 µL of FACS buffer per sample and incubated for 15 minutes at 4°C. Cells were washed with 2 mL of FACS buffer and centrifuged at 1200 rpm for 5 minutes at 4°C. Supernatant was removed and antibodies were diluted in 50 µL of FACS buffer and incubated for 30 minutes at 4°C. Cells were washed with 2 mL of FACS buffer and centrifuged at 1200 rpm for 5 minutes at 4°C. If biotinylated antibody was used, streptavidin was diluted in 100 µL FACS buffer per sample and incubated for 30 minutes

at 4°C. Viability staining was performed by adding Tonbo Ghost Dye UV450 (1:500) or DAPI (1:1000). Cells were analyzed on the 5-Laser BD LSR II or sorted on the 5-Laser FACS Aria III in the VUMC Flow Cytometry Shared Resources.

Immunohistochemical Staining

Mouse stomachs were fixed in 4% PFA overnight at 4°C and were transferred into 70% ethanol for subsequent paraffin embedding. Five-micrometer sections were used for all immunohistochemistry studies. Deparaffinization, rehydration, and antigen retrieval were performed as previously described (Petersen et al., 2014). Five-micrometer tissue sections were blocked in Dako Protein Block Serum-Free at room temperature for 1.5 hours. For mouse primary antibodies, Mouse on Mouse (M.O.M.) blocking reagent was added to slides for 20 minutes at room temperature. Primary antibodies (Table 3) were added overnight at 4°C in Dako Antibody Diluent with Background Reducing Components. Fluorescent donkey secondary antibodies were added in Dako Antibody Diluent at room temperature for one hour or HRP-conjugated secondary antibodies were added for 15 minutes at room temperature. DAB chromogen was added for detection of HRP-conjugated secondary antibodies. The Zeiss Axio Imager M2 microscope with Axiovision digital imaging system or the Leica Aperio Versa 200 Fluorescent Slide Scanner in the Vanderbilt Digital Histology Shared Resource was used to image sections.

Cell Culture

Freshly sorted gastric ILC2s were cultured in RPMI culture media supplemented with 10% FBS, 100 U/ml penicillin/streptomycin, 10 mM HEPES buffer solution, 1xMEM nonessential amino acids, 1 mM sodium pyruvate, 50 μM 2-mercaptoethanol and 50

μg/ml gentamycin sulfate in 96-well round bottom plates. Cells were cultured with IL-2 (Peprotech 212-12) or IL-33 (210-33) at 10 ng/ml for 24 hr. IL-13 cytokine levels were measured by ELISA (ThermoFisher BMS6015) and detected on Biotek Synergy 4 instrument.

Quantitative Real-Time PCR

Total RNA from the stomach (oxyntic region) was extracted from paraformaldehyde-fixed paraffin-embedded tissue of three to four mice per experimental group to examine the expression of mRNA transcripts. Five-micrometer sections were taken for H&E stain to identify oxyntic region in tissue block. A 2-mm biopsy punch was then used to extract tissue. The standard Qiagen RNeasy FFPE Kit (73504) protocol was used for purification of total RNA. Alternatively, Qiagen RNeasy Plus Mini Kit was used for purification of total RNA from sorted cells. ThermoFisher High-Capacity cDNA Reverse Transcription Kit (4368814) was used for complementary DNA synthesis. Quantitative real-time polymerase chain reaction was performed with Biorad SsoAdvanced Universal SYBR Green Super Mix (172-5270) and specific primers on the Biorad CFX96 Touch Real-Time PCR Detection System. The expression of mRNA transcripts was normalized to *Tbp* expression and displayed as relative expression levels ($2^{\Delta Cq}$).

Data Analysis

Experimental groups contained three to six mice. Images were analyzed using CellProfiler to quantify objects (nuclei, cells) and verified manually (Jones et al., 2008). At least five representative images (>150 glands) of proximal stomach corpus were taken from each mouse at 20X objective for quantification. Spatial quantification of GATA3-positive cells

was performed as previously described (Weis et al., 2017). All graphs and statistics were completed in GraphPad Prism using unpaired Student's t-test or one-way ANOVA with Bonferroni's post-hoc multiple comparisons test to determine significance.

Table 3. *Catalog of antibodies in Chapter III.*		
CD127 (1:100)	eBioscience	25-1273-82
CD161 (1:500)	Novus Biologicals	NB100-77528SS
CD163 (1:100)	NeoMarkers	163C01
CD3 (1:100)	eBioscience	12-0032-82
CD3 (1:500)	Santa Crus	sc-1127
CD45 (1:200)	Tonbo Biosciences	80-0451
CD90 (1:200)	eBioscience	11-0903-81
DCLK1 (1:2000)	Abcam	ab109029
DGAT2 (1:500)	Abcam	ab96094
F4/80 (1:100)	Life Technologies	MF48000
FcεRI (1:100)	eBioscience	13-5898-81
GATA3 (1:500)	Abcam	ab199428
GATA3 (1:20)	eBioscience	12-9966-42
GATA3 (1:500)	Proteintech	66400-1-Ig
GIF (1:2000)	A gift from Dr. David Alpers	N/A
GSII-lectin (1:2000)	Invitrogen	L32451
H^+K^+ATPase (1:10,000)	A gift from Dr. Adam Smolka	N/A
ICOS (1:50)	eBioscience	25-1273-82

ICOS (1:500)	LSBio	LS-B11916
IL1RL1 (1:500)	Novus Biologicals	NBP1-85252
IL17RB (1:200)	Bioss	bs-2610R
IL2RB (1:500)	Proteintech	13602-1-AP
IL7R (1:1000)	LSBio	LS-B2831
KI67 (1:1000)	Cell Signaling Technology	#9129
Lineage Cocktail (1:12.5)	Miltenyi	120-092-613
MBP (1:100)	Mayo Clinic	Clone MR-14.7
MCC (1:500)	Abcam	ab111239
MIST1 (1:1000)	A gift from Dr. Jason Mills	N/A
PCNA (1:15000)	Cell Signaling Technology	#2586
PD1 (1:500)	Proteintech	18106-1-AP
TFF2 (1:500)	A gift from Dr. Nicholas Wright	N/A
UEA1-lectin (1:2000)	Sigma	L9006

Table 4. *Catalog of qPCR primer sequences in Chapter III.*
mAreg primers F 5' GCAGATACATCGAGAACCTGGAG 3' R 5' CCTTGTCATCCTCGCTGTGAGT 3'
mArpp19 primers F 5' CTCACTTGGGACAAAAGCCTGG 3' R 5' TGCTTTTGCCATGTTGTAGTCCC 3'
mCsf2 primers F 5' AACCTCCTGGATGACATGCCTG 3' R 5' AAATTGCCCCGTAGACCCTGCT 3'
mCxcr4 primers F 5' GACTGGCATAGTCGGCAATGGA 3' R 5' CAAAGAGGAGGTCAGCCACTGA 3'
mDgat2 primers F 5' CTGTGCTCTACTTCACCTGGCT 3' R 5' CTGGATGGGAAAGTAGTCTCGG 3'

mElf1 primers F 5' ACCCAGCTCTTCCGAACTGTTC 3' R 5' AGGAGACACCACTACTGGAACC 3'
mGata3 primers F 5' TTTACCCTCCGGCTTCATCCTCCT 3' R 5' TGCACCTGATACTTGAGGCACTCT 3'
mIcos primers F 5' GCAGCTTTCGTTGTGGTACTCC 3' R 5' TGTGTTGACTGCCGCCATGAAC 3'
mIcam1 primers F 5' AAACCAGACCCTGGAACTGCAC 3' R 5' GCCTGGCATTTCAGAGTCTGCT 3'
mIfrd1 primers F 5' CTGGCGAATCTTTGGCACTTCTG 3' R 5' ACCGCTGCTTTCTCTTGTCCAC 3'
mIl1rl1 primers F 5' GGATTGAGGTTGCTCTGTTCTGG 3' R 5' TCGGGCAGAGTGTGGTGAACAA 3'
mIl17rb primers F 5' CCATCCCTCCAGATGACAAC 3' R 5' TGCTCCTTCCTTGCCTCCAAGTTA 3'
mIl2ra primers F 5' GCGTTGCTTAGGAAACTCCTGG 3' R 5' GCATAGACTGTGTTGGCTTCTGC 3'
mIl2rb primers F 5' CTCAAGTGCCACATCCCAGATC 3' R 5' AGCACTTCCAGCGGAGAGATCT 3'
mIl2rg primers F 5' GGAGCAACAGAGATCGAAGCTG 3' R 5' CCACAGATTGGGTTATAGCGGC 3'
mIl4 primers F 5' ATCATCGGCATTTTGAACGAGGTC 3' R 5' ACCTTGGAAGCCCTACAGACGA 3'
mIl4ra primers F 5' ACCAGATGGAACTGTGGGCTGA 3' R 5' AGCAGCCATTCGTCGGACACAT 3'
mIl5 primers F 5' GATGAGGCTTCCTGTCCCTACT 3' R 5' TGACAGGTTTTGGAATAGCATTTCC 3'
mIl7r primers F 5' CACAGCCAGTTGGAAGTGGATG 3' R 5' GGCATTTCACTCGTAAAAGAGCC 3'
mIl9 primers F 5' TCCACCGTCAAAATGCAGCTGC 3' R 5' CCGATGGAAAACAGGCAAGAGTC 3'
mIl13 primers F 5' AACGGCAGCATGGTATGGAGTG 3' R 5' TGGGTCCTGTAGATGGCATTGC 3'
mLilrb4 primers F 5' CTGGATGCTGTTACTCCCAACC 3' R 5' TGGGTGTAGAGGACTGGTCCTT 3'
mPd1 primers F 5' CGGTTTCAAGGCATGGTCATTGG 3' R 5' TCAGAGTGTCGTCCTTGCTTCC 3'
mPsen1 primers F 5' GAGACTGGAACACAACCATAGCC 3' R 5' AGAACACGAGCCCGAAGGTGAT 3'
mPtgs2 primers F 5' GCGACATACTCAAGCAGGAGCA 3' R 5' AGTGGTAACCGCTCAGGTGTTG 3'

mRamp3 primers F 5’ AGAAGGTGGCTGTCTGGAAGTG 3’ R 5’ GCCAGTAGCAGCCCATGATGTT 3’
mRora primers F 5’ CAGAGCAATGCCACCTACTCCT 3’ R 5’ CTGCTTCTTGGACATCCGACCA 3’
mTnfrsf9 primers F 5’ CCAAGTACCTTCTCCAGCATAGG 3’ R 5’ GCGTTGTGGGTAGAGGAGCAAA 3’

RESULTS

Gastric ILC2s express GATA3.

To evaluate the presence of ILC2s in the gastric mucosa, we performed flow cytometry on isolated single cells from the stomachs of wild-type C57BL6/J mice. Single cells were stained for cell-surface proteins and ILC2s were defined as $CD45^{+}Lin^{-}CD127^{+}CD90^{+}ICOS^{+}$, where Lin included CD3, CD5, CD11b, CD45R, Anti-7-4, FcεRI, Ly6G/C, Anti-Ter-119. The cells were fixed/permeabilized and stained for GATA3, the transcription factor that is critical for the development and maintenance of ILC2s. Greater than 93-percent of ILC2s collected were positive for GATA3 when compared to an isotype control antibody (Figure 26A).

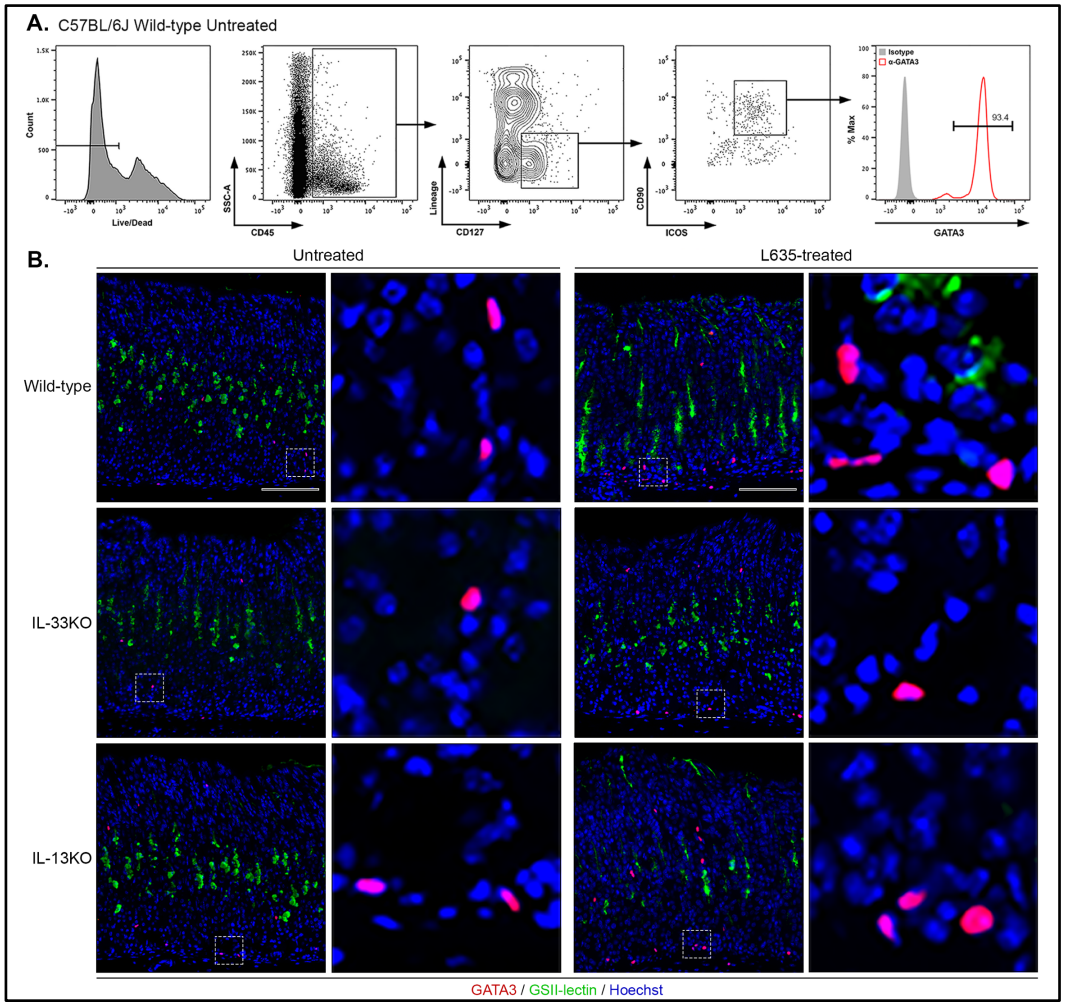

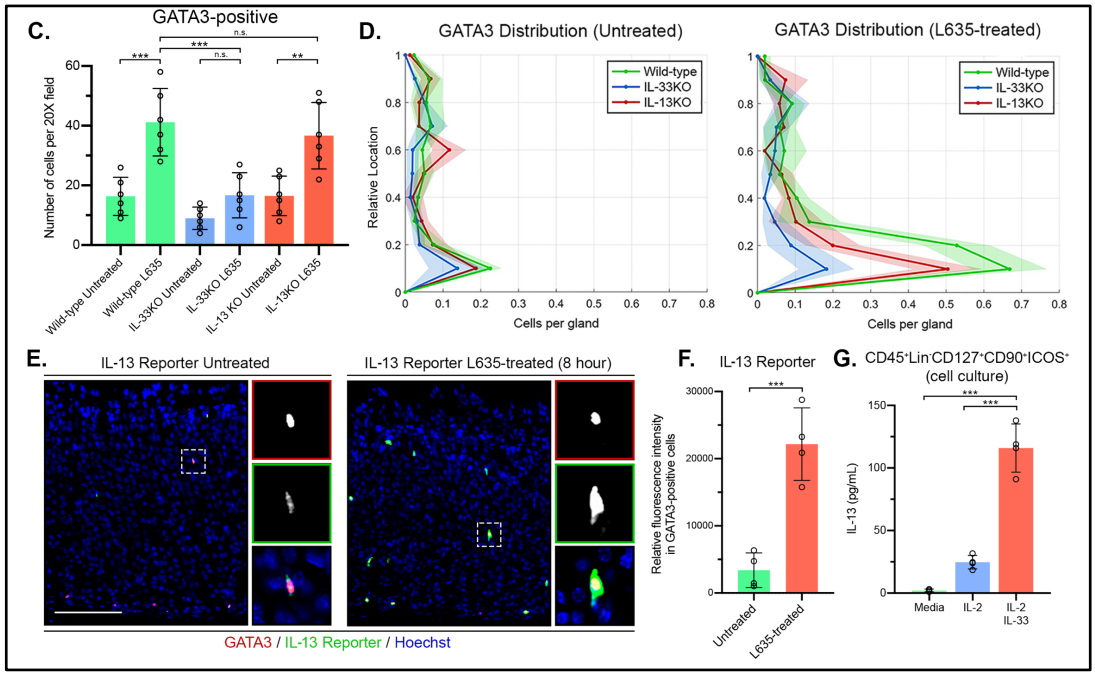

Figure 26. Accumulation of GATA3-positive ILC2s after gastric damage is dependent on IL-33 but not IL-13.

A. *Flow cytometric analysis of isolated fixed cells from wild-type C57BL/6J mice. Greater than 93-percent of CD45$^+$Lin$^-$CD127$^+$CD90$^+$ICOS$^+$ ILC2s are positive for GATA3. Rat IgG2b kappa antibody utilized as isotype control.* ***B.*** *Immunofluorescence staining for GATA3 (red), mucin-6 containing granule marker GSII-lectin (green), with nuclear counter stain Hoechst (blue) in both untreated and L635-treated wild-type, IL-33KO, and IL-13KO mice (scale bars = 100 μm).* ***C.*** *Quantification of GATA3-positive ILC2 per 20X objective field.* ***D.*** *Relative localization of each GATA3-positive cell from panel B is shown in distribution histograms with the y-axis representing the gastric gland divided into 10% increments (1 = lumen and 0 = base) and the x-axis depicting the number of cells per gland.* ***E.*** *Immunofluorescence staining for GATA3 (red), TdTomato and IL13 reporter (green), with nuclear counterstain Hoechst (blue) (scale bars = 100 μm)* ***F.*** *Relative fluorescence intensity of the IL-13 reporter in GATA3-positive ILC2s.* ***G.*** *Effects of IL-2 or IL-2 + IL-33 on IL-13 secretion from sorted primary gastric ILC2s (CD45$^+$Lin$^-$CD127$^+$CD90$^+$ICOS$^+$). IL-13 production assayed by ELISA in media after 24 hours of incubation. Statistical significance determined by one-way ANOVA with Bonferroni's post-hoc multiple comparisons test. N.S. for not significant $p \geq 0.05$, * for $p < 0.05$, ** for $p < 0.01$, and *** for $p < 0.001$. Error bars represent mean ± SD.*

Furthermore, we determined that GATA3-positive cells in the stomach were negative for other immune cell lineage markers by both flow cytometry and immunostaining (Figure 27). These findings verified that GATA3 is an efficient marker for ILC2s in the normal gastric mucosa and following L635-induced acute gastric damage.

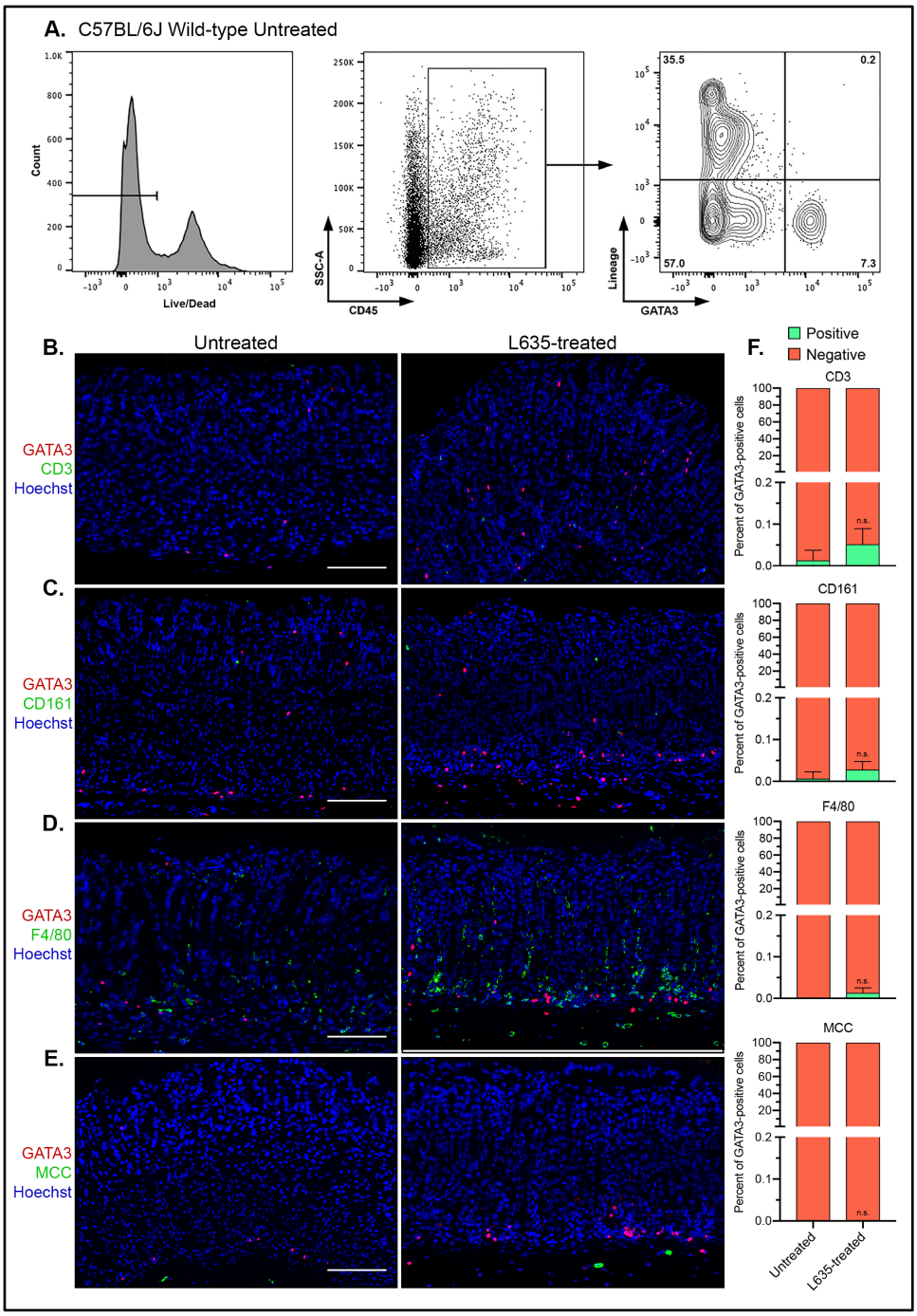

Figure 27. Identification of GATA3-expressing cell populations in the gastric mucosa.
A. *Flow cytometric analysis of isolated fixed CD45-positive cells from wild-type C57BL/6J mice for lineage markers and GATA3. GATA3-positive cells are negative for lineage markers.* ***B.*** *Immunofluorescence staining for GATA3 (red) and T cell marker CD3 (green)* ***C.*** *GATA3 (red) and NK cell marker CD161 (green)* ***D.*** *GATA3 (red) and macrophage marker F4/80 (green)* ***E.*** *GATA3 (red) and mast cell marker MCC (green) in untreated and 3-day L635-treated wild-type C57BL6/J mice (n=6 per group) with nuclear counter stain Hoechst (blue) (scale bars = 100 μm).* ***F.*** *Percent of GATA3-positive cells that are dual positive for each marker. Statistical significance determined by student's t-test (n=6 per group). N.S. for not significant p ≥ 0.05. Error bars represent mean ± SD.*

Gastric injury leads to an IL-33-dependent increase in ILC2s.

To visualize ILC2s *in situ* we performed immunohistochemical analysis for GATA3 in tissue sections from wild-type, IL-33 knockout (IL-33KO), or IL-13 knockout (IL-13KO) mice that were untreated or treated for three days with L635 (Figure 26B). Analysis revealed an accumulation of GATA3-positive ILC2s after damage that is contingent on IL-33, but not IL-13 (Figure 26C). In the untreated mice, rare GATA3-positive ILC2s were observed scattered throughout the glands. After L635 treatment to induce parietal cell loss in wild-type mice, a significant increase in the number of ILC2s was detected specifically located near the base of the glands (Figure 26D). Basal accumulation of ILC2s coincides with the location of chief cell reprogramming to SPEM and macrophage/eosinophil recruitment to the gastric mucosa. The significant increase of GATA3-positive ILC2s after L635 treatment was blocked in IL-33KO mice. However, similar to wild-type mice, immunostaining revealed a significant increase in ILC2s in IL-13KO mice treated with L635 (Figure 26C and D).

To evaluate the responsiveness of gastric ILC2s, IL-13 reporter mice were treated with L635 for 8 hours. In the IL-13 reporter mice one of the copies of IL-13 is replaced with tdTomato, an exceptionally bright red fluorescent protein. In these mice, cells that

express IL-13 are labelled by tdTomato. To visualize IL-13 production in GATA3-positive ILC2s, tissue sections from untreated and L635-treated IL-13 reporter mice were immunostained with an anti-tdTomato antibody and GATA3 (Figure 26E). A significant increase in the relative fluorescence of the IL-13 reporter was observed in GATA3-positive ILC2s after 8 hours of L635-induced injury (Figure 26F). Additionally, flow sorted ILC2s from the stomachs of wild-type C57BL6/J mice were cultured with media supplemented with IL-2 alone or IL-2 and IL-33. IL-13 secretion was detected using an enzyme-linked immunosorbent assay. The ILC2s treated with IL-2 and IL-33 secreted greater than four times the amount of IL-13 compared to ILC2s treated with IL-2 alone (Figure 26G). Thus, gastric ILC2s respond to IL-33 and are likely a source of type II cytokines including IL-13 after acute gastric damage.

Single-cell RNA sequencing of gastric ILC2s.

To characterize ILC2s from the normal and metaplastic gastric mucosa, we performed single cell RNA-sequencing on ILC2s from the stomachs of wild-type C57BL6/J mice that were untreated (ILC2 Control) or treated for one day with L635 (ILC2 L635). Individual ILC2s were sorted by fluorescence activated cell sorting (FACS) directly into a 96-well plate containing lysis buffer and bar-coded primers (Figure 28A). By flow sorting, ILC2s accounted for 0.47% of viable isolated cells from the untreated gastric mucosa. However, ILC2s increased to 0.88% of viable isolated cells after one day of L635 treatment. Single cell RNA sequencing was performed as previously described using Smart-seq2 (Picelli et al., 2014). Both principle component and t-distributed stochastic neighbor embedding (t-SNE) analysis revealed that the L635-treated ILC2s have a

distinct phenotype from the control ILC2s (Figure 28B-C). We have identified a distinctive transcriptional profile of gastric mucosal ILC2s that includes the transcription factors *Gata3* and *Rorα*, the immune checkpoint protein *Icos*, and the cell surface receptors *Il1rl1, Il17rb, Il7r, Il2ra,* and *Il2rg*. Not surprisingly, several secreted factors involved in ILC2 function are increased in ILC2 L635 cells compared to control ILC2s including *Il4, Il5, Il9, Il13,* and *Areg*. Unsupervised analysis identified a unique signature of the L635-treated, metaplasia-associated ILC2s that includes the secreted factor *Csf2 (Gour et al., 2018),* lipid mediator *Dgat2 (Robinette et al., 2015),* adhesion molecule *Icam1 (Lei et al., 2018),* cell surface receptors *Il2rb (Moro et al., 2010)* and *Il4ra (Kim et al., 2014),* immune checkpoint protein *Pd1 (Taylor et al., 2017),* and receptor (calcitonin) activity modifying proteins *Ramp3 (Nagashima et al., 2019; Sui et al., 2018; Wallrapp et al., 2019)* (Figure 2D).

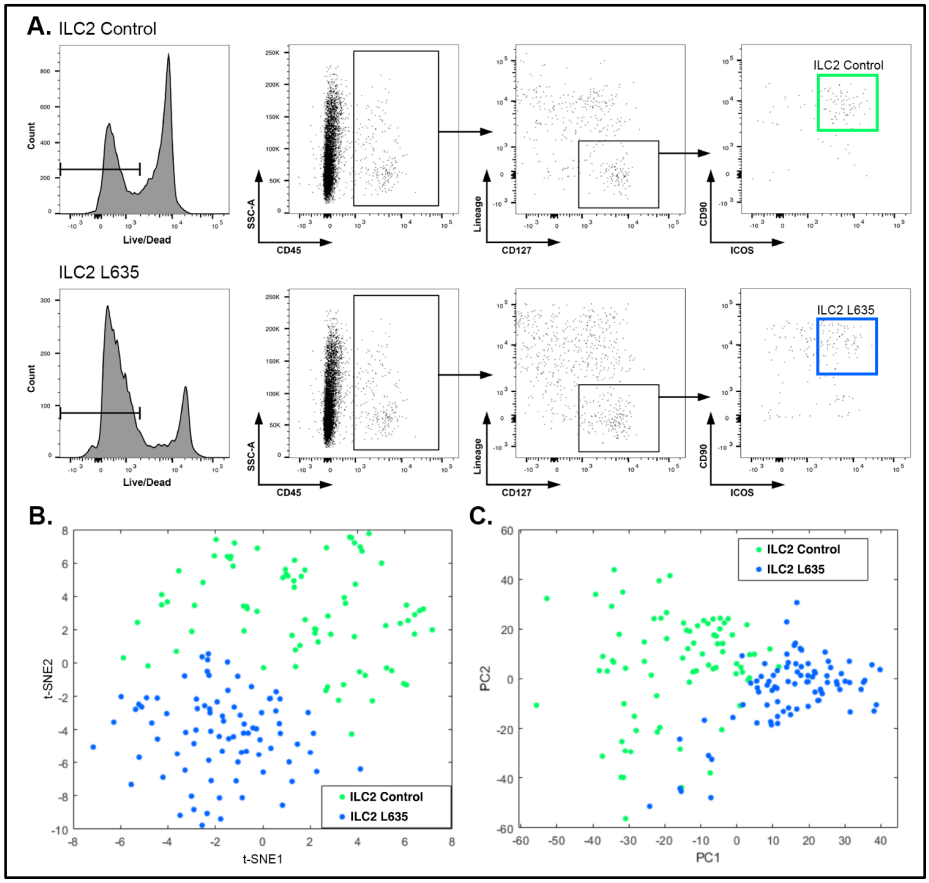

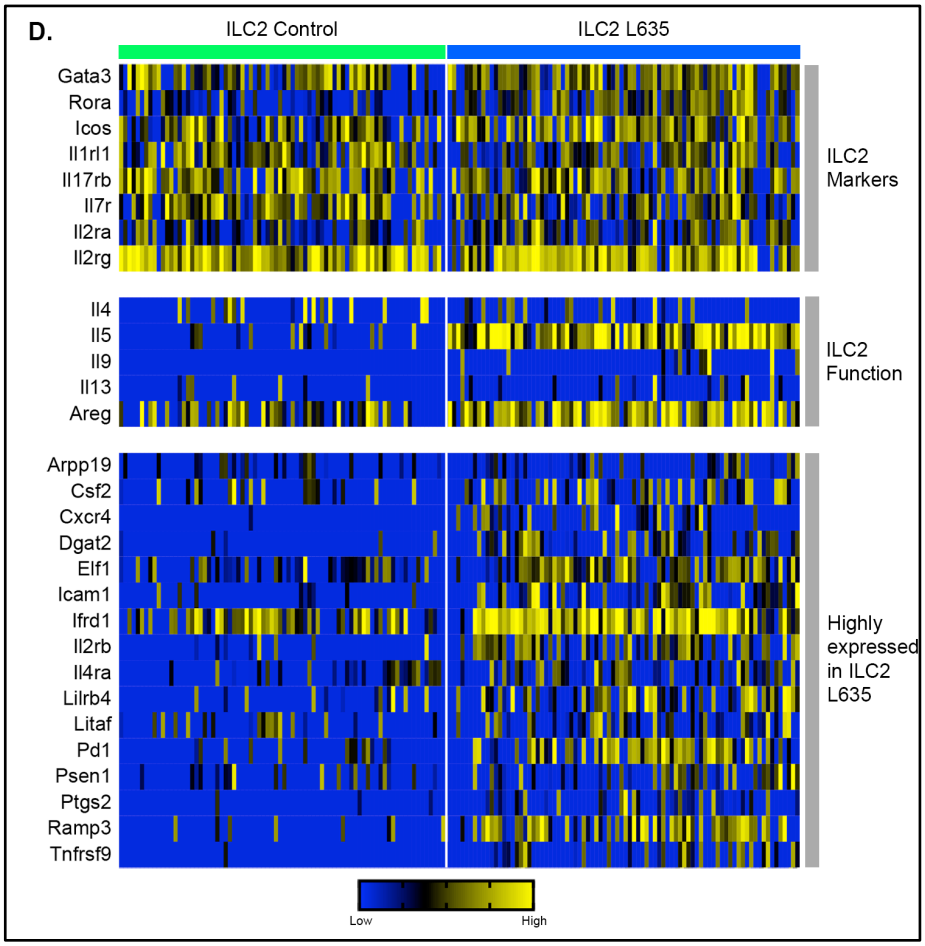

Figure 28. Single cell RNA-sequencing of ILC2s.
A. *Flow cytometric analysis of sorted single cells from wild-type untreated C57BL/6J mice (ILC2 Control) and wild-type C57BL/6J mice treated with one dose of L635 and sacrificed 24 hours after administration (ILC2 L635).* ***B.*** *t-SNE plots of ILC2 Control and ILC2 L635.* ***C.*** *Principle component analysis of ILC2 Control and ILC2 L535.* ***D.*** *A heatmap of single cell RNA-seq data for eight ILC2 marker genes, five genes involved in ILC2 function, and sixteen genes that were identified as being highly expressed in ILC2 L635.*

These single-cell RNA sequencing results were validated by qPCR and by immunostaining when antibodies were available (Figures 29 and 30).

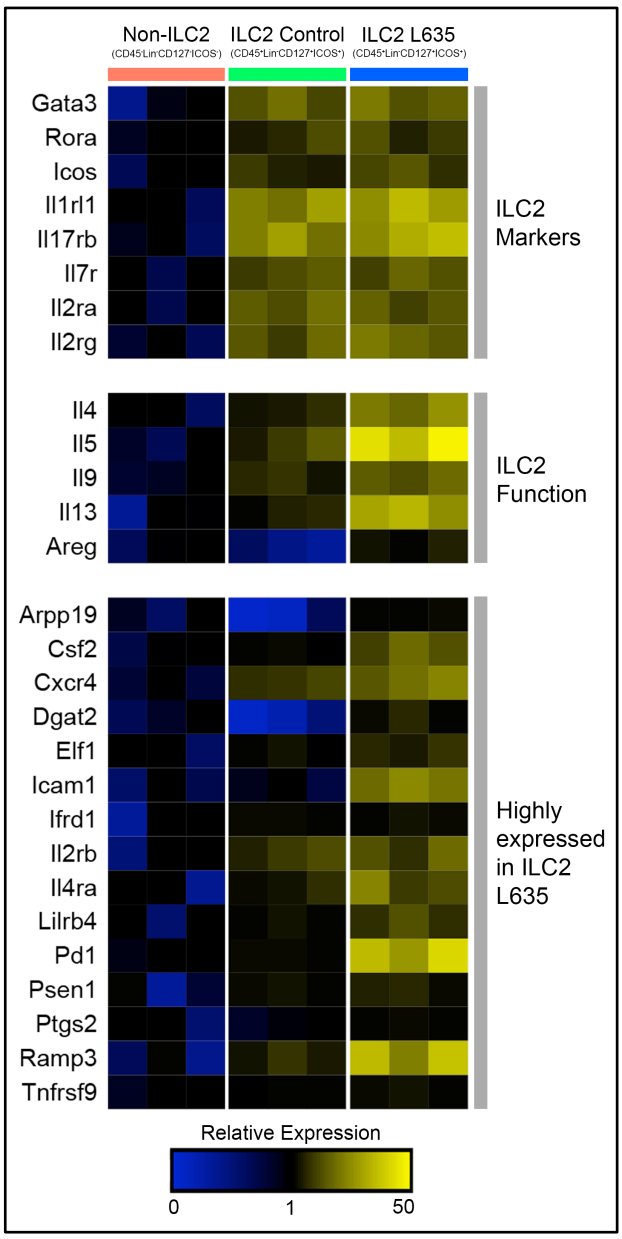

Figure 29. Enrichment of transcripts in ILC2 populations.
A heatmap of quantitative PCR relative expression values for eight ILC2 marker genes, five genes involved in ILC2 function, and sixteen genes that were identified as being highly expressed in ILC2 in the single cell RNA-seq data. Three populations were sorted from the gastric mucosa by fluorescence activated cell sorting: CD45$^-$Lin$^-$CD127$^-$ICOS$^-$ Non-ILC2s (red), CD45$^+$Lin$^-$CD127$^+$ICOS$^+$ ILC2 Control (green), and CD45$^+$Lin$^-$CD127$^+$ICOS$^+$ ILC2 L635 (blue) from mice treated with 1 day of L635. Expression values normalized to Non-ILC2 population.

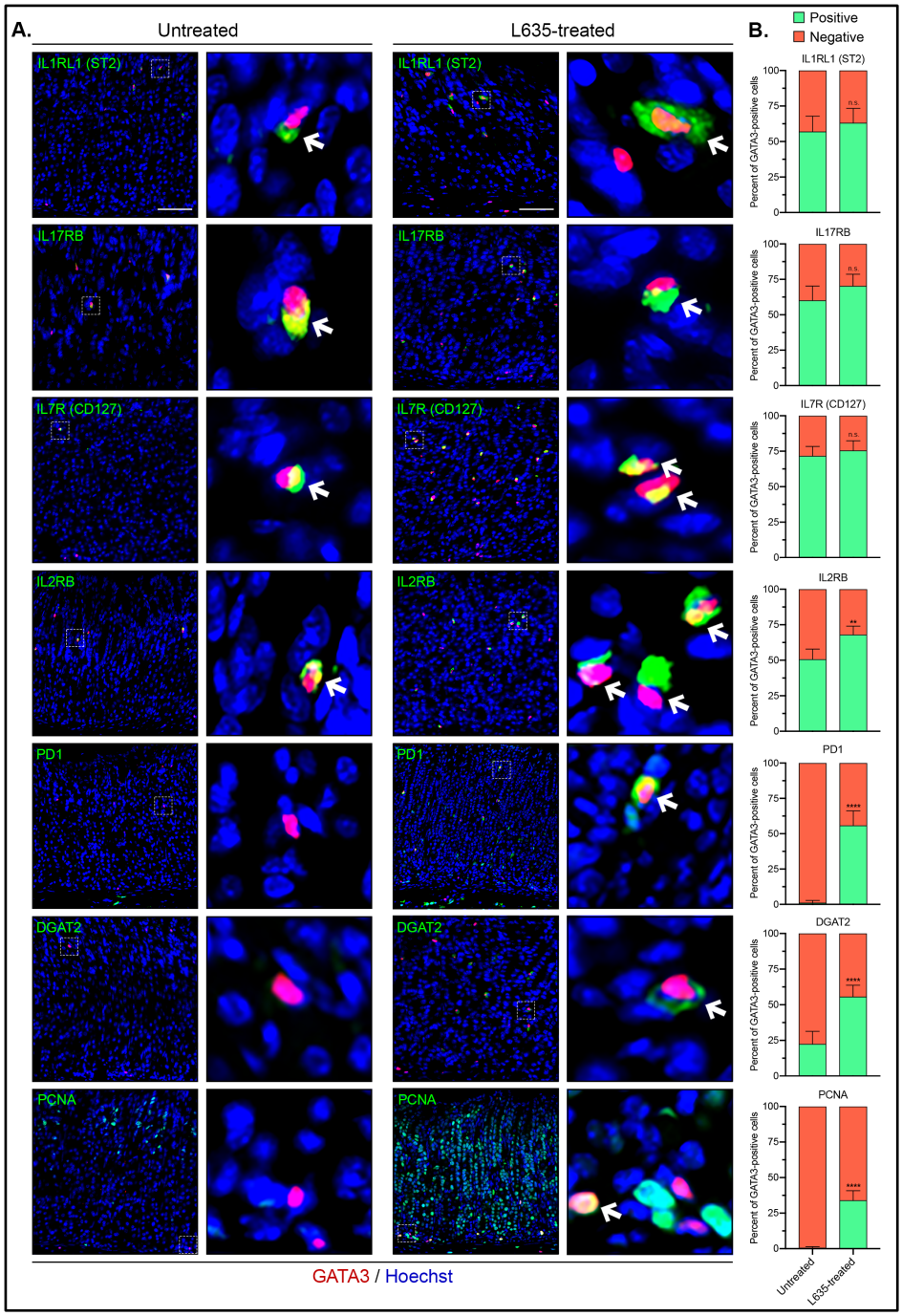

Figure 30. Validation of protein expression in populations of gastric ILC2s. *Untreated mice (n=6) and 3-day L635-treated mice (n=6)* ***A.*** *Immunofluorescence staining for GATA3 (red), IL1RL1 (ST2), IL17RB, IL7R (CD127), IL2RB, PD1, DGAT2, and PCNA (green), with nuclear counter stain Hoechst (blue).* ***B.*** *Percent of GATA3-positive cells that are dual positive for each marker. Statistical significance determined by student's t-test. N.S. for not significant $p \geq 0.05$.** for $p < 0.01$, and **** for $p < 0.0001$. Error bars represent mean ± SD.*

Depletion of ILC2s inhibits development of metaplasia following injury.

To elucidate if ILC2s are essential for epithelial reprogramming, we depleted ILC2s using a previously described antibody depletion method (Engelbertsen et al., 2015; Hayakawa et al., 2015; Monticelli et al., 2011). Treatment with anti-CD90.2 antibody effectively removes ILC2s from peripheral tissues. Mice were treated with Rat IgG2b antibody as an isotype control immunoglobulin. We treated wild-type C57Bl/6J mice with anti-CD90.2 or Rat IgG2b antibody every fourth day for 12 days. Following the final antibody administration, mice were treated with L635 for three days. Stomachs were harvested from four experimental groups: 1) Rat IgG2b only, 2) anti-CD90.2 only, 3) Rat IgG2B + L635-treated, and 4) anti-CD90.2 + L635-treated mice for histological analysis and flow cytometry (Figure 31A). Treatment with either Rat IgG2b only or anti-CD90.2 only did not alter the gastric mucosa. Flow cytometry and immunostaining for GATA3 revealed significant depletion of ILC2s with anti-CD90.2 treatment (Figure 31B-D). To visualize L635-induced parietal cell loss, we performed immunostaining for the proton pump H^+K^+ ATPase, an integral membrane protein responsible for gastric acid secretion by parietal cells (Figure 31E). In the Rat IgG2b only and anti-CD90.2 only groups, a large number of H^+K^+ ATPase-positive parietal cells were detected throughout the oxyntic glands. Both the Rat IgG2b and anti-CD90.2 groups had comparable levels of L635-induced parietal cell loss (Figure 3G). Parietal cell loss promotes zymogenic chief cell reprogramming to mucin-secreting metaplastic cells (SPEM) to protect and fuel repair of the stomach. During this process, SPEM cells contain both zymogenic granules positive for GIF and mucin granules positive for GSII-lectin, which binds to a sugar modification on Mucin 6. To detect chief cell reprogramming in ILC2 depleted mice, we immunostained

with GIF and GSII-lectin (Figure 31E). Anti-CD90.2 treatment decreased the number of GIF and GSII-lectin dual-positive SPEM cells by greater than sixty-percent after L635-induced parietal cell loss (Figure 31H).

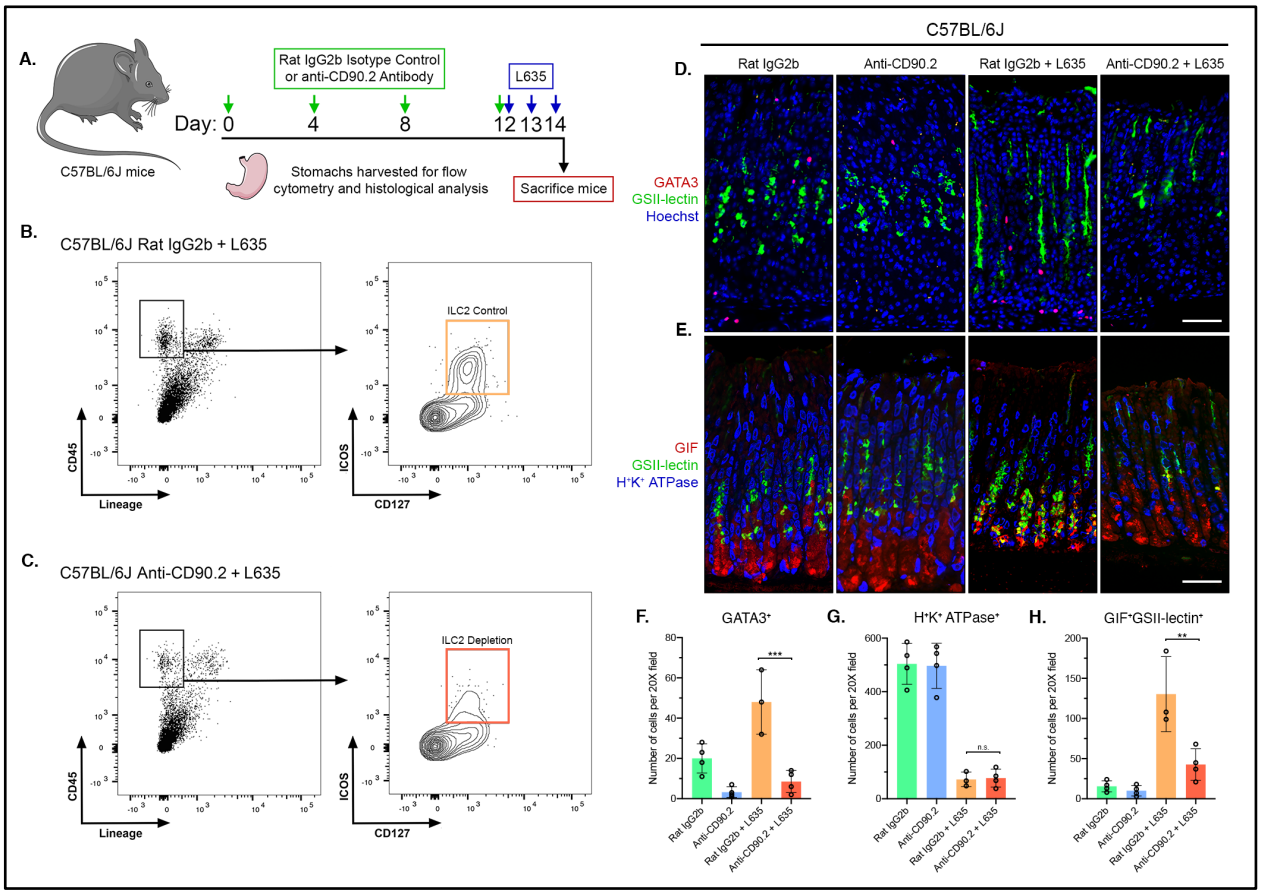

Figure 31. ILC2 depletion blocks development of L635-induced metaplasia.
A. *Diagram of ILC depletion and drug treatments. Rat IgG2b isotype control antibody or Anti-CD90.2 antibody was administered intraperitoneally to wild-type C57BL/6J mice every fourth day for 12 days. Following the final antibody administration, mice were treated with the parietal cell toxic drug L635 by oral gavage daily for three days. Mice were sacrificed 2 hours after final dose of L635, and stomach tissue from Rat IgG2b only mice (n=4), Anti-CD90.2 only mice (n=4), Rat IgG2b + L635 mice (n=3), and Anti-CD90.2 + L635 mice (n=3) was harvested for flow cytometry or histological analysis. Flow cytometric analysis of isolated single cells from* ***B.*** *Rat IgG2b + L635 and* ***C.*** *Anti-CD90.2 + L635 stomach tissue. Depletion of $CD45^{+}Lin^{-}CD127^{+}ICOS^{+}$ ILC2 population with Anti-CD90.2 treatment.* ***D.*** *Immunofluorescence staining for GATA3 (red), Mucin 6 containing granule marker GSII-lectin (green), with nuclear counter stain Hoechst (blue) (scale bars = 100 µm).* ***E.*** *Immunofluorescence staining for zymogenic granule marker GIF (red), Mucin 6 containing granule marker GSII-lectin (green), and parietal cell marker $H^{+}K^{+}$*

*ATPase (blue) (scale bars = 100 μm). Quantification of **F.** GATA3-positive ILC2 **(G)** H^+K^+ ATPase-positive parietal cells and **H.** GIF and GSII-lectin dual-positive (SPEM) cells per 20X objective field. Statistical significance determined by one-way ANOVA with Bonferroni's post-hoc multiple comparisons test. N.S. for not significant $p \geq 0.05$, ** for $p < 0.01$, and *** for $p < 0.001$. Error bars represent mean ± SD.*

We also validated these experiments in Rag1 knockout C57BL/6J mice, which do not produce any mature B or T lymphocytes (Figure 32), and we observed a similar pattern of inhibition of SPEM development with ILC2 depletion. Collectively, these results suggest that anti-CD90.2 treatment effectively depletes ILC2s and ILC2 depletion prevents chief cell reprogramming after acute parietal cell loss.

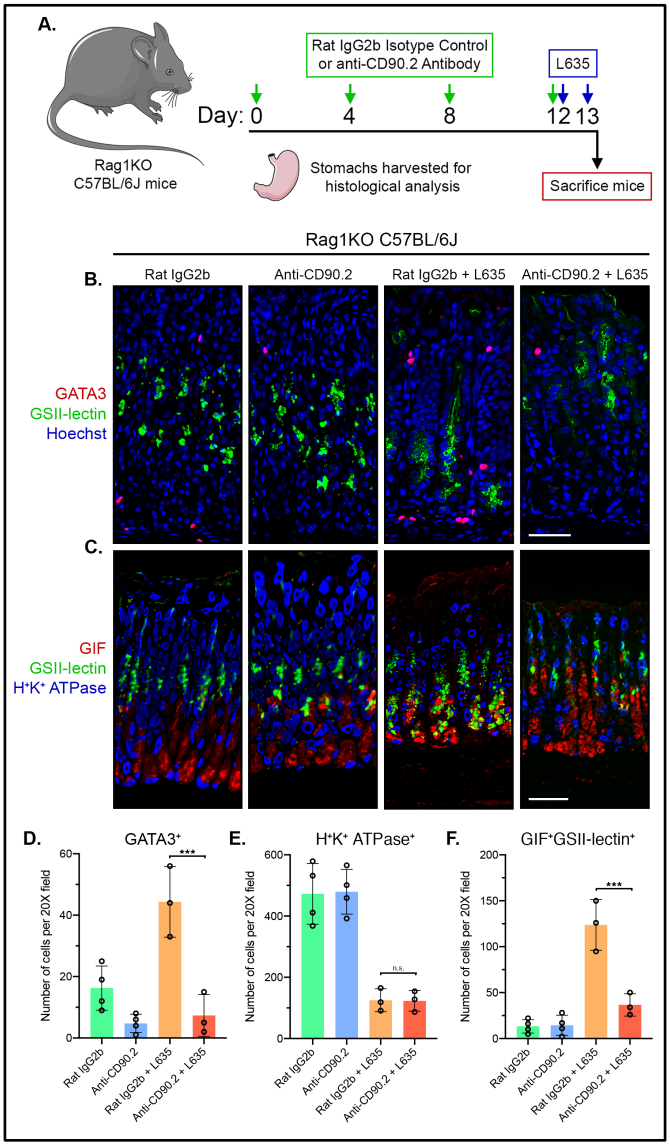

Figure 32. ILC2 depletion blocks development of L635-induced metaplasia in Rag1 knockout mice.
A. *Diagram of ILC depletion and drug treatments. Rat IgG2b isotype control antibody or Anti-CD90.2 antibody was administered intraperitoneally to Rag1KO C57BL/6J mice every fourth day for 12 days. Following the final antibody administration, mice were treated with the parietal cell toxic drug L635 by oral gavage daily for two days. Mice were sacrificed 24 hours after final dose of L635, and stomach tissue from Rat IgG2b only mice (n=4), Anti-CD90.2 only mice (n=4), Rat IgG2b + L635 mice (n=3), and Anti-CD90.2 + L635 mice (n=3) was harvested for histological analysis.* ***B*** *Immunofluorescence staining for GATA3 (red), Mucin 6 containing granule marker GSII-lectin (green), with nuclear counter stain Hoechst (blue) (scale bars = 100 μm).* ***C.*** *Immunofluorescence staining for zymogenic granule marker GIF (red), Mucin 6 containing granule marker GSII-lectin (green), and parietal cell marker H^+K^+-ATPase (blue) (scale bars = 100 μm). Quantification of* ***D.*** *GATA3-positive ILC2,* ***E.*** *H^+K^+ ATPase-positive parietal cells, and* ***F.*** *GIF and GSII-lectin dual-positive (SPEM) cells per 20X objective field. Statistical significance determined by one-way ANOVA with Bonferroni's post-hoc multiple comparisons test. N.S. for not significant $p \geq 0.05$ and *** for $p < 0.001$. Error bars represent mean ± SD.*

Finally, we evaluated the effects of ILC2 depletion on the expression of ILC2-related genes in the gastric mucosa. Figure 33A demonstrates that while PD1 positive cells were present in the gastric mucosa after anti-CD90.2 treatment, none of the cells were GATA3-positive ILC2s. Similarly, we found that anti-CD90.2 depletion of ILC2s led to significant reductions in transcripts elevated in ILC2s following L635 treatment, including *IL4, IL5, IL9, IL13, Areg, Csf2, Pd1* and *Ramp3* (Figure 33B).

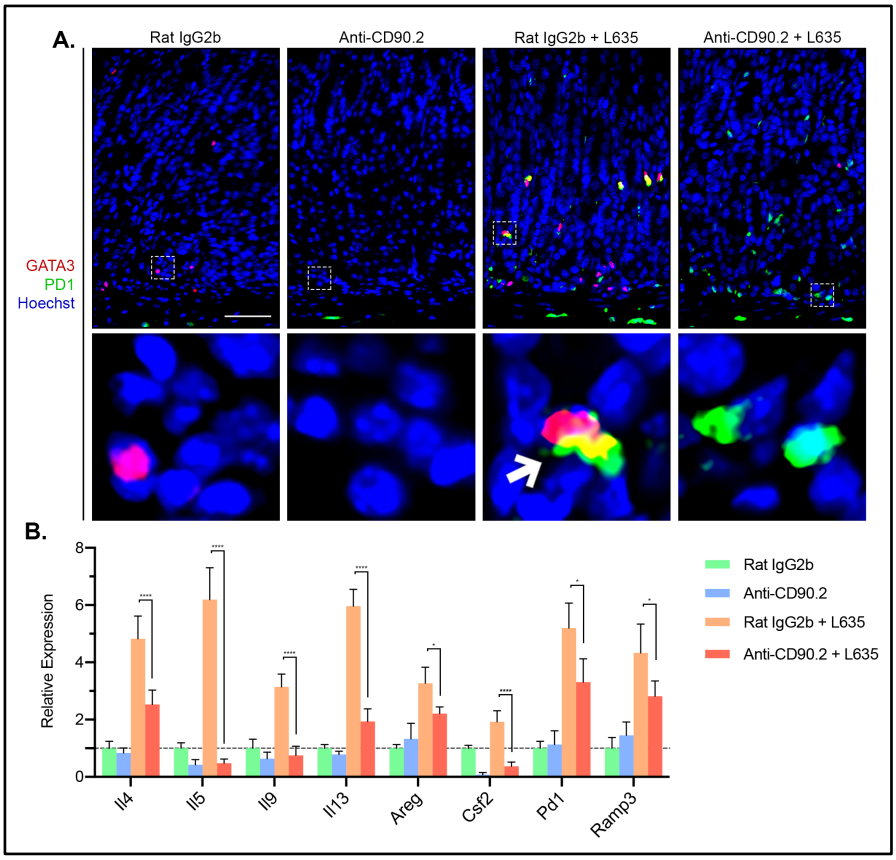

Figure 33. Depletion of ILC2s reduces expression of L635-induced genes.
Rat IgG2b only mice (n=4), Anti-CD90.2 only mice (n=4), Rat IgG2b + L635 mice (n=3), and Anti-CD90.2 + L635 mice (n=3) ***A.*** *Immunofluorescence staining for ILC2 marker GATA3 (red), PD1 (green), with nuclear counter stain Hoechst (blue) (scale bars = 100 μm).* ***B.*** *Relative mRNA expression of ILC2 related proteins (Il4, Il5, Il9, Il13, Areg, Csf2, Pd1, and Ramp3) in each group. Expression values normalized to Rat IgG2b only group. Statistical significance determined by one-way ANOVA with Bonferroni's post-hoc multiple comparisons test. * for p < 0.05 and **** for p < 0.0001. Error bars represent mean ± SD.*

ILC2s are responsible for alteration in tuft cell abundance after oxyntic atrophy.

Tuft cells represent an unusual type of chemosensory epithelial cell present in multiple organs of the digestive system, including the stomach and the intestine (Gerbe et al., 2012; Nabeyama and Leblond, 1974; Saqui-Salces et al., 2011). Doublecortin-like kinase 1 (Dclk1) is considered an effective marker for tuft cells in the mouse

gastrointestinal tract. Our previous studies have shown that loss of parietal cells leads to the reversible expansion of Dclk1-expressing cells in the gastric mucosa (Choi et al., 2015). Interestingly, ILC2-derived IL-13 promotes tuft cell hyperplasia following helminth infection in the small intestine (Howitt et al., 2016; von Moltke et al., 2016). To determine if ILC2s are required for tuft cell hyperplasia following L635-induced parietal cell loss, we performed immunostaining for Dclk1 (Figure 34A). Anti-CD90.2 treatment blocked expansion of the tuft cell lineage following L635-induced parietal cell loss (Figure 34B). These results indicate a role for ILC2s in tuft cell hyperplasia after acute gastric damage.

ILC2s promote infiltration of macrophages and eosinophils into the gastric mucosa.

Our previous investigations determined that L635-induced parietal cell loss results in F4/80-positive macrophage infiltration into the gastric mucosa. RNA sequencing and immunohistochemical data revealed macrophages associated with advanced mucin-secreting metaplasia in L635-treated mice have an M2 polarized phenotype and are considered alternatively activated (Petersen et al., 2014). Alternatively-activated M2 macrophages are typically associated with wound healing and tissue repair. To visualize macrophage infiltration and polarization in ILC2 depleted mice we performed co-immunostaining for the macrophage marker F4/80 with the M2 polarization marker CD163 (Figure 34C). Anti-CD90.2 + L635-treated mice showed significantly decreased macrophage infiltration into the gastric mucosa and very few M2 polarized macrophages were detected (Figure 34D). These data suggest a role for ILC2s in macrophage recruitment and activation after acute gastric damage.

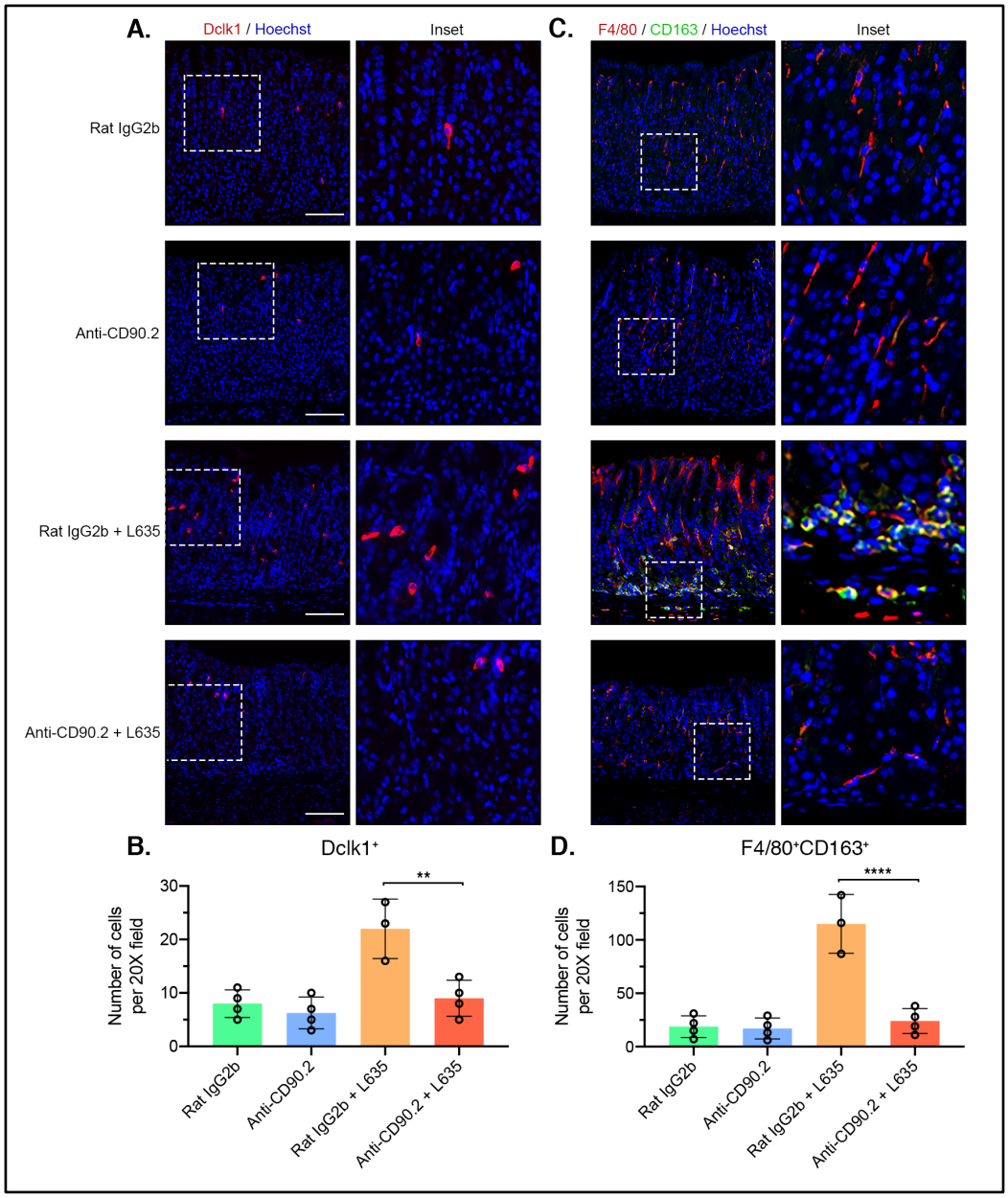

Figure 34. ILC2 depletion blocks tuft cell hyperplasia and macrophage infiltration/ polarization.

A. *Immunofluorescence staining for tuft cell marker Dclk1 (red) with nuclear counter stain Hoechst (blue) (scale bars = 100 μm).* ***B.*** *Quantification of Dclk1-positive tuft cells per 20X objective field.* ***C.*** *Immunofluorescence staining for macrophage/ dendritic cell marker F4/80 (red), alternatively activated macrophage marker CD163 (green), with nuclear counter stain Hoechst (blue) (scale bars = 100 μm).* ***D.*** *Quantification of F4/80 and CD163 dual-positive alternatively activated macrophages per 20X objective field. Statistical significance determined by one-way ANOVA with Bonferroni's post-hoc multiple comparisons test. ** for $p < 0.01$, and **** for $p < 0.0001$. Error bars represent mean ± SD.*

Our previous studies also revealed L635-treated mice have robust eosinophil infiltration (Petersen et al., 2017). Eosinophil recruitment to the gastric mucosa is dependent on IL-5. Therefore, we sought to determine if ILC2s play a role in eosinophil infiltration by performing immunohistochemical staining for the eosinophil marker Major Basic Protein (MBP) (Figure 35A). Anti-CD90.2 treatment blocked eosinophil infiltration following L635-induced parietal cell loss (Figure 35B). These results provide evidence that ILC2s play a role in eosinophil recruitment to the gastric mucosa following acute injury.

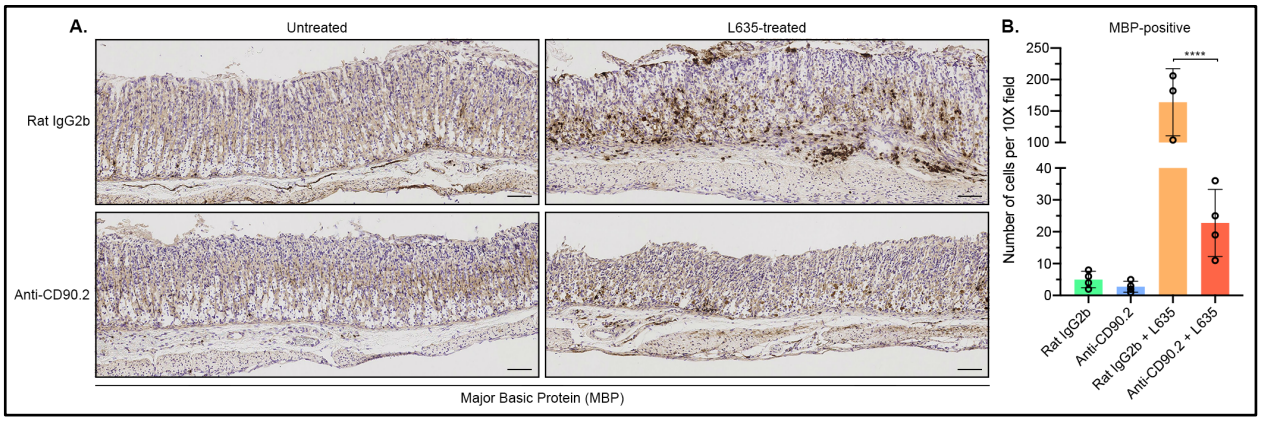

Figure 35. ILC2 depletion inhibits eosinophil infiltration after gastric damage.
A. *Eosinophil specific Major Basic Protein IHC of Rat IgG2b only mice (n=4), Anti-CD90.2 only mice (n=4), Rat IgG2b + L635 mice (n=3), and Anti-CD90.2 + L635 mice (n=3) to visualize eosinophil granules.* ***B.*** *Quantification of MBP-positive eosinophils per 10X objective field. Statistical significance determined by one-way ANOVA with Bonferroni's post-hoc multiple comparisons test. **** for $p < 0.0001$. Error bars represent mean ± SD.*

Depletion of ILC2s inhibits foveolar hyperplasia, proliferation, and SPEM development after injury.

ILC2s have been implicated in maintaining the gastric stem cell niche, so we sought to determine the effect of ILC2 depletion on proliferation in the gastric mucosa (Hayakawa et al., 2015). To do this, we immunostained for the proliferation marker Ki67

(Figure 36A). In the normal oxyntic mucosa, Ki67 labelled stem/progenitor cells are located in the gland isthmus about a third of the way down the gland. Upon gastric injury, chief cells at the base of the glands reprogram and are capable of re-entering into the cell cycle and proliferating (Leushacke et al., 2017; Nam et al., 2010a; Radyk et al., 2017). Additionally, mucin-producing foveolar cells located near the lumen of gastric glands also expand in response to injury, a gastric lesion referred to as foveolar hyperplasia (Nomura et al., 2005). Foveolar cells produce Muc5ac, a mucin recognized by UEA1-lectin in the gastric mucosa. Anti-CD90.2 + L635-treated mice had significantly less proliferation than Rat IgG2b + L635-treated mice (Figure 36B). To evaluate foveolar hyperplasia after L635 treatment, we measured the average thickness of the UEA1-positive foveolar region. The average thickness of the foveolar region of anti-CD90.2 + L635-treated mice was significantly shorter than Rat IgG2b + L635-treated mice (Figure 36C).

The process of chief cell reprogramming requires the downscaling of their mature characteristics. The basic helix-loop-helix transcription factor Mist1 (Bhlha15) controls the secretory architecture of chief cells including cellular organization and production of large zymogenic granules (Ramsey et al., 2007). Loss of Mist1 is a distinct feature of chief cell reprogramming into SPEM. Dual immunofluorescence staining for GIF and Mist1 allows for monitoring of Mist1 loss in zymogenic granule-containing chief cells (Figure 36D). Immunostaining revealed that chief cells from anti-CD90.2 + L635-treated mice retained expression of Mist1 (Figure 36E). In the normal oxyntic mucosa, the expression of TFF2 is restricted to mucous neck cells found in the neck region of oxyntic glands. In L635-treated mice, TFF2 is up-regulated in chief cells at the base of glands as they reprogram into SPEM. In anti-CD90.2 + L635-treated mice, significantly fewer TFF2 and GIF dual-

positive cells at the base of glands were observed (Figure 36F). These results indicate that ILC2s coordinate the initiation of chief cell reprogramming into SPEM.

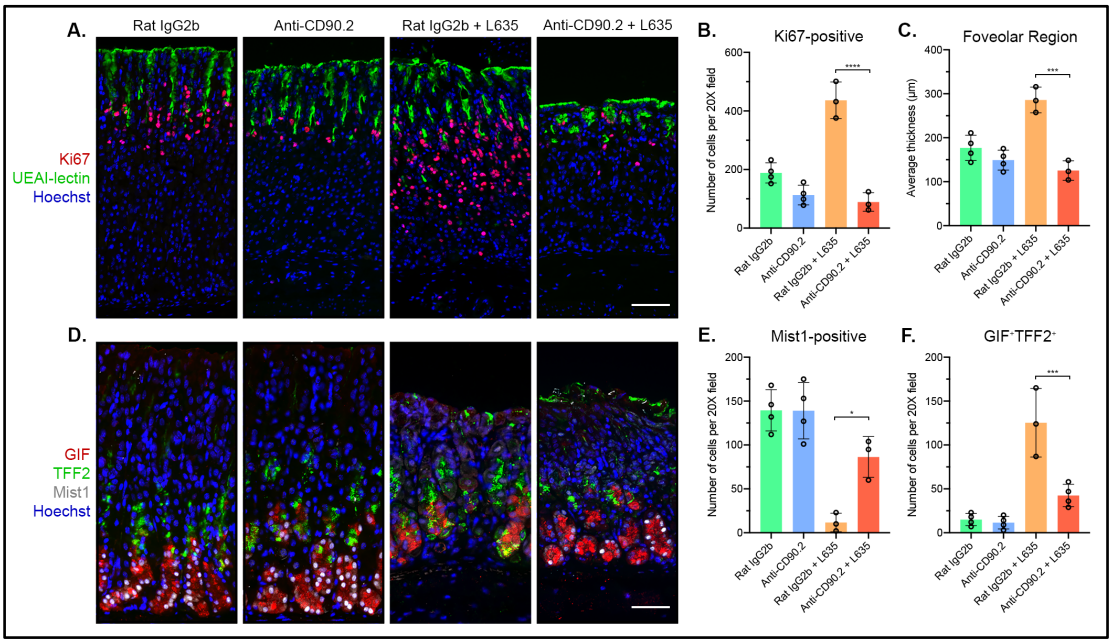

Figure 36. Depletion of ILC2s blocks L635-induction of foveolar hyperplasia, proliferation, and SPEM development.
Rat IgG2b only mice (n=4), Anti-CD90.2 only mice (n=4), Rat IgG2b + L635 mice (n=3), and Anti-CD90.2 + L635 mice (n=3) ***A.*** *Immunofluorescence staining for proliferation marker Ki67 (red), foveolar cell marker UEAI-lectin (green), with nuclear counter stain Hoechst (blue) (scale bars = 100 μm).* ***B.*** *Quantification of Ki67-positive cells per 20X objective field.* ***C.*** *Average thickness (μm) of UEA1-positive foveolar region.* ***D.*** *Immunofluorescence staining for zymogenic granule marker GIF (red), mucus granule marker TFF2 (green), chief cell transcription factor Mist1 (white) with nuclear counter stain Hoechst (blue) (scale bars = 100 μm). Quantification of* ***E.*** *Mist1-positive cells and* ***F.*** *GIF and TFF2 dual-positive (SPEM) cells per 20X objective field. Statistical significance determined by one-way ANOVA with Bonferroni's post-hoc multiple comparisons test. * for $p < 0.05$, *** for $p < 0.001$ and **** for $p < 0.0001$. Error bars represent mean ± SD.*

DISCUSSION

Following significant gastric injury, the epithelium recruits reparative lineages to sites of damage through both the reprogramming and expansion of mucin-secreting lineages (Meyer et al., 2019; Petersen et al., 2017; Willet et al., 2018). Chief cell reprogramming to SPEM is a necessary process for gastric epithelial repair. This process of SPEM development is triggered by damage to gastric epithelium including acute parietal cell loss (Huh et al., 2012; Nam et al., 2010a), ulceration (Bertaux-Skeirik et al., 2015; Engevik et al., 2016), or chronic infection with *Helicobacter* species (Nam et al., 2010a). Previous investigations in the stomach have attempted to identify the mechanisms of gastric repair. We recently identified that an IL-33/IL-13 cytokine-signaling network is necessary and sufficient for the induction of epithelial reprograming following chemically-induced acute parietal cell loss (Petersen et al., 2017). IL-33 and IL-13 knockout mice showed a blockade in SPEM development and have reduced M2-macrophage infiltration and polarization. We also determined that macrophage depletion attenuated advancement of metaplastic lesions (Petersen et al., 2014). The present study identified that ILC2-derived factors are required for the reprogramming of the gastric mucosa after injury. Using *in vivo* mouse models, we have determined that in the absence of ILC2s the development of mucin-secreting metaplasia, expansion of foveolar and tuft cell lineages, and the infiltration and activation of macrophages and eosinophils are all attenuated. These results indicate that ILC2s perform a central role in the coordination of gastric epithelial repair after severe damage.

Tissue resident ILC2s are an intrinsic mucosal source of cytokines including IL-4, IL-5, IL-9, and IL-13 (Guo et al., 2012; Neill et al., 2010). Cytokine production and release are activated by epithelial stress signals including IL-33. We have previously noted that IL-13 deletion, but not loss of IL-4, IL-5 or IL-9 markedly inhibits epithelial reprogramming following acute parietal cell loss (Petersen et al., 2017). The present study indicates that gastric damage triggers a significant accumulation of ILC2s in the mucosa and induces their redistribution to the bases of glands co-incident with the reprogramming of chief cells into SPEM and inflammatory infiltration. This increase in ILC2s was blocked in mice lacking IL-33 mice but did occur in IL-13KO mice following acute gastric injury. These results indicate that IL-33 release is required for activation of ILC2s. Gastric ILC2s showed strong secretion of IL-13 in response to IL-33 *in vitro*. We also found that gastric ILC2s up-regulated IL-13 following injury. When ILC2s were depleted in either wild-type mice or Rag1 knockout mice, chief cell reprogramming to SPEM following acute gastric damage was prominently attenuated. Additionally, we found that ablation of ILC2 cells blocked the expansion of tuft and foveolar cell lineages and the activation of infiltrating macrophages and eosinophils following injury. Collectively, these findings suggest that ILC2s are the major source of IL-13 and are required for the coordinated response and recruitment of reparative cell lineages after severe injury to the gastric epithelium.

Many of the putative roles for ILC2s in gastric mucosal healing demonstrated here are similar to those identified in asthma or allergic airway responses as well as infection-related intestinal repair (Fuchs and Colonna, 2013; Scanlon and McKenzie, 2012). In all cases, activation of ILC2s leads to mucin hypersecretion that is integral to mucosal repair and protection. In addition, a close relationship between ILC2s and populations of sensory

tuft cells appear critical to the coordination of the response. In the intestinal epithelium, release of IL-25 from tuft cells is a critical activator of ILC2s (Howitt et al., 2016; von Moltke et al., 2016). While ILC2s can respond to tuft cell derived signals, in the present investigation the expansion of tuft cell numbers following oxyntic atrophy was dependent on ILC2s. Thus, there appears to be a reciprocal relationship for signaling between tuft cells and ILC2s in the gastric mucosa. Furthermore, ILC2 functional responses appear to have tissue specific characteristics (Ricardo-Gonzalez et al., 2018). While many of the responses observed in activated ILC2 cells overlap with ILC2 responses noted in other tissues, including up-regulation of IL-13, IL-5, and Areg, other highly expressed transcripts appear to be more specific to the gastric ILC2s. In addition to the expansion of ILC2 numbers, single cell sequencing demonstrated that ILC2s markedly up-regulate the expression of cytokines as well as a number of key regulators including *Pd1, Dgat2* and *Ramp3*. How these specific regulators are related to the function of ILC2s in the coordinated response to gastric injury remains to be determined.

In summary, our investigations have demonstrated the importance of ILC2 in the coordinated gastric epithelial response following severe injury. ILC2s elicit a cascade of events including the initiation of chief cell reprogramming, expansion of sensory tuft cells and mucin-secreting foveolar cells, and recruitment of immune cells to the gastric mucosa. All of these mechanisms serve as critical repair mechanisms to coordinate the protection and restoration of the gastric epithelium after severe mucosal injury.

CHAPTER IV:

CONCLUSIONS AND FUTURE DIRECTIONS

CONCLUSIONS

The studies detailed here identify the roles of the oxidative stress and innate immune responses in recruiting reparative cell lineages to protect the gastric epithelium after damage. I determined that an antioxidant system, CD44v9-xCT, was up-regulated early as chief cells transitioned into mucin-secreting SPEM. Inhibition of xCT or siRNA knockdown blocked cystine uptake and decreased glutathione production by metaplastic cells and prevented ROS detoxification and proliferation. Moreover, xCT activity was required for chief cell reprogramming into SPEM after gastric injury *in vivo*. Chief cells from xCT-deficient mice exhibited decreased autophagy, mucin granule formation and proliferation, as well as increased levels of ROS and apoptosis compared to wild-type mice. On the other hand, the anti-inflammatory metabolites of sulfasalazine did not affect SPEM development. The results presented here suggest that maintaining redox balance is crucial for progression through the reprogramming process and that xCT-mediated cystine uptake is required for chief cell plasticity and ROS detoxification in response to damage.

Additionally, I determined there is a significant increase in the number of GATA3-positive ILC2s in the stomach after damage, that is blocked in mice lacking IL-33. I characterized a marker signature of gastric mucosal ILC2s and identified a distinct transcriptional profile of metaplasia-associated ILC2s including *Il5, Il13, Csf2*, *Pd1,* and

Ramp3. Depletion of ILC2s with anti-CD90.2 antibody treatment blocked the development of metaplasia after L635-induced injury in wild-type and Rag1 knockout mice. Additionally, ILC2 depletion prevented foveolar and tuft cell hyperplasia and infiltration/activation of macrophages and eosinophils after injury. Our results suggest that type 2 inflammation and ILC2s are at the center of coordinated gastric epithelial repair. Both the oxidative stress and innate immune responses work to recruit reparative cells to sites of gastric injury, which is crucial for tissue repair. Reparative cell lineages function to (1) maintain redox balance, (2) boost mucin-secretion, and (3) activate an immune response.

Redox balance

Oxidative stress occurs when there is an imbalance between oxidants (such as ROS) and antioxidants (Mittal et al., 2014). ROS are highly reactive molecules that damage and/or alter the function of nucleic acids, proteins, lipids, and carbohydrates (Navarro-Yepes et al., 2014). Under normal conditions, cells balance the production of oxidants and antioxidants to maintain redox equilibrium (Finkel and Holbrook, 2000). Response to gastric injury elevates ROS levels due to increased inflammation and cellular metabolism (Forrester et al., 2018; Ni et al., 2012). Therefore, cells must initiate an oxidative stress response to counteract the oxidative burden (Ishii and Mann, 2014; Ishimoto et al., 2011; Nagano et al., 2013; Sato et al., 2005; Wada, 2013). In particular, zymogenic chief cells up-regulate nutrient transporters to aid in the production of glutathione, a potent antioxidant (Meyer et al., 2019). Glutathione works to combat elevated ROS levels and prevent oxidative stress-related cell death (Franco and Cidlowski, 2009; Rushworth and Megson, 2014). Maintaining redox balance, thus the recruitment of SPEM cells that express antioxidant systems (xCT and CD44v9), is critical

for tissue repair after gastric injury (Meyer et al., 2019). In addition to antioxidant systems, SPEM cells at the sites of mucosal injury up-regulate the expression of mucins.

Mucin-secretion

The gastric mucosa is protected from acid secretion, proteolytic enzymes, bacteria, and noxious agents by a firmly adherent mucus gel. Gastric mucus is composed of two mucin glycoproteins, MUC6 and MUC5AC (Hoffmann, 2015; Nordman et al., 2002). An increased number of mucin-secreting cells is required to protect the stomach following gastric injury. Therefore, digestive enzyme-secreting chief cells reprogram to MUC6-secreting SPEM (Leushacke et al., 2017; Nam et al., 2010b; Radyk et al., 2017). Chief cell reprogramming to SPEM has been called “antralization” or “pseudopyloric” metaplasia as chief cells acquire the characteristics of mucin-secreting cells found in the distal stomach: antral/pyloric glands or Brunner’s glands (Goldenring, 2018). The reprogramming of chief cells occurs through a highly regulated process (Willet et al., 2018). The first step of the reprogramming process is the loss of the transcription factor (Mist1) that governs the secretory architecture of chief cells including cellular organization and that production of large protein-containing granules (Lennerz et al., 2010; Ramsey et al., 2007). Following the loss of Mist1, autophagic and lysosomal pathways are acutely up-regulated in order to target rough endoplasmic reticulum, mitochondria, and secretory granules for degradation (Willet et al., 2018). Next, there are distinct transcriptional changes that include the upregulation of MUC6, TFF2, CD44v9, and AQP5 (Nozaki et al., 2008a; Weis et al., 2014; Weis et al., 2013). Finally, metaplastic cells are capable of re-entering into the cell cycle and proliferating. The results presented here suggest that adaptation to oxidative stress and ILC2-derived cytokines are both required for chief cell

reprogramming to SPEM and the production of MUC6. While mucin-secretion and expansion of the SPEM cell lineage are crucial for tissue repair following injury, if this process is combined with chronic injury and inflammation it can put the individual at risk for developing cancer (Schmidt et al., 1999).

In addition to SPEM formation, MUC5AC-secreting foveolar cells expand in response to gastric injury and increases in gastrin (a hormone which stimulates gastric acid secretion) (Nomura et al., 2005). This gastric lesion is referred to as foveolar hyperplasia and is defined by the increased length of the gastric pit. Similar to SPEM, mucin-secretion and expansion of the foveolar cell lineage is critical for tissue repair following injury. Collectively, upon gastric damage MUC5AC-secreting foveolar cells expand to reinforce the mucus layer that covers the luminal section of the gastric gland, while chief cells reprogram to MUC6-secreting SPEM to build up the mucus layer that coats the basal section of the gastric gland. Both foveolar hyperplasia and SPEM require ILC2 activation to develop. Together, these cells lineages work to protect and drive restoration of the gastric epithelium following injury.

Immune activation

Paradigm-shifting studies over the past several years have altered the view that T lymphocytes are at the center of immune orchestration and have placed special emphasis on cytokine-producing innate lymphoid cells (Neill et al., 2010). ILCs have lymphoid morphology, but lack antigen-specific receptors and conventional lineage markers (lymphoid, myeloid, and erythroid markers) (Eberl et al., 2015). Group 2 ILCs are defined by the transcription factor GATA3 and their ability to produce type 2 signature cytokines IL-4, IL-5, IL-9, and IL-13 (Klein Wolterink et al., 2013; Serafini et al., 2015). ILC2s are

activated by a specialized class of immune regulators known as alarmins. In particular, ILC2s are activated by the epithelial cell-derived alarmins TSLP, IL-25, and IL-33 (Li et al., 2014; Salimi et al., 2013; Stier et al., 2016). In the stomach, IL-33 has been the focus of many investigations as mice lacking IL-33 or the IL-33 receptor have insufficient repair mechanisms following gastric injury (Petersen et al., 2017). Furthermore, chronic administration of IL-33 initiates oxyntic atrophy, metaplasia development, and inflammation (Buzzelli et al., 2015). IL-33 is expressed by epithelial cells where it is stored in the nucleus and is released into the extracellular space following tissue damage (Schwartz et al., 2016). The studies detailed here suggest that ILC2s are at the center of gastric repair mechanisms after injury. Gastric ILC2s respond to IL-33 by producing robust levels of type 2 cytokines, and coordinate chief cell reprogramming to SPEM, foveolar and tuft cell hyperplasia, and recruitment/activation of other immune cell lineages (macrophages and eosinophils).

Previous studies have reported that macrophages are required for the progression of SPEM to a more advanced metaplastic lesion. Macrophage-depleted mice have fewer proliferative SPEM cells as well as fewer intestinal transcripts after injury when compared to control mice. Macrophages that are associated with advanced mucin-secreting metaplasia in the stomach have an M2 polarized phenotype and are considered alternatively activated (Petersen et al., 2014). Monocytes, the precursor to macrophages and dendritic cells, are trafficked to peripheral tissues in response to specific cues such as chemokines (Shi and Pamer, 2011). Monocytes differentiate into M2 macrophages in response to both IL-4 and IL-13 (Fairweather and Cihakova, 2009). Alternatively-activated macrophages are typically associated with type 2 immune responses and tissue repair

(Mantovani et al., 2002; Shapouri-Moghaddam et al., 2018). It has been proposed that M2 macrophages increase fibrosis through the expression of factors such as fibronectin, matrix metalloproteinases, IL-1β, and TGF-β (Bogdan et al., 1992; Martinez et al., 2009). Alternatively-activated macrophages also express scavenger receptors that not only bind pathogens during infection, but also bind host tissue such as apoptotic cells as a part of homeostasis and tissue repair (Kerrigan and Brown, 2009; Kim and Nair, 2019; Nickel et al., 2009; Van Ginderachter et al., 2006). Furthermore, M2 macrophages associated with advanced SPEM may restrict type 1 immune responses and produce IL-33 which can feedback on the system to ramp up type 2 immune activation (Meyer and Goldenring, 2018; Petersen et al., 2017). The data presented here indicate a role for ILC2s in macrophage recruitment and activation after acute gastric injury. Therefore, there may be cross talk between ILC2s and macrophages after damage to the gastric epithelium to coordinate a type 2 immune response and initiate wound healing.

In addition to macrophage recruitment, damage triggers robust eosinophil infiltration (also known as eosinophilia) into the gastric mucosa (Petersen et al., 2017). Eosinophils are a source of granule-derived cationic proteins, chemokines, cytokines, and lipid mediators (Acharya and Ackerman, 2014). Eosinophil-derived mediators have wide-ranging effects and work to maintain normal tissue homeostasis and tissue remodeling/repair (Weller and Spencer, 2017). Like macrophages, the results described here suggest a role for ILC2s in eosinophil recruitment to the gastric epithelium through the secretion of IL-5. While macrophages and eosinophils work to promote tissue repair, both lineages may produce reactive oxygen species that contribute to oxidative stress. Collectively, these results provide evidence that ILC2s, M2 macrophages, and

eosinophils work together to promote a type 2 immune response and wound healing (including reprogramming and/or expansion of reparative epithelial cells, mucin-secretion, angiogenesis, and fibrosis) after acute gastric injury.

FUTURE DIRECTIONS

The studies detailed here identify the roles of the oxidative stress and innate immune responses in recruiting reparative cells to sites of gastric injury. Future investigations should focus on three areas of interest: (1) ILC2-related genes, (2) immune cell interactions, and (3) acinar to ductal metaplasia in the pancreas.

ILC2-related gene studies:

Interleukin-13 (IL-13)

IL-13 signals through a receptor complex of IL4Ra and IL13Ra1 (Hallett et al., 2012). We have previously shown that IL13Ra1 is expressed on the membrane of chief cells, tuft cells, and to a lesser extent foveolar cells (Petersen et al., 2017). Binding of IL-13 to the receptor complex initiates JAK-dependent tyrosine phosphorylation of a transcription factor, STAT6 (Wills-Karp and Finkelman, 2008). Phosphorylated STAT6 subsequently translocates to the nucleus where it can regulate gene expression (Goenka and Kaplan, 2011). It is speculated that IL-13 can also function through the RAS signaling pathway. Both phospho-STAT6 and phospho-ERK (a downstream effector of the RAS signaling pathway) are observed in SPEM cells following acute gastric injury. Other groups have reported that IL-13 produced by ILC2s in the lungs and the intestine can directly stimulate mucin overexpression in epithelial cells (Cohn et al., 1999; Gerbe et al., 2016; Hao et al., 2014; Nikolaidis et al., 2003; Zhu et al., 1999). Mucin overexpression is

a characteristic of metaplasia in the stomach. Therefore, I hypothesize that IL-13 directly signals to chief cells to promote reprogramming and mucin-secretion following injury. To test this hypothesis, I utilized a previously characterized chief cell line to determine if the addition of IL-13 directly influenced the transcriptional profile and protein signature of the cells. Unfortunately, this chief cell line is not fully mature and lacks the expression of the IL-13 receptor. To address if IL-13 will directly influence the transcriptional profile and protein signature of chief cells, future studies should focus on the administration of recombinant IL-13 to mice that have mature chief cells and IL-13 receptor expression.

Programmed Cell Death Protein 1 (PD-1)

The role of ILC2s in initiating and amplifying type 2 inflammation is tightly regulated to block mucosal immune responses from getting out of control. Recent studies on ILC2s in airway inflammation have identified a negative regulatory axis driven by signaling through the cell surface protein programmed cell death protein-1 (PD-1) (Mariotti et al., 2019; Taylor et al., 2017). In addition to ILC2s, PD-1 is expressed on activated T cells, B cells, and macrophages (Jubel et al., 2020). Through single cell RNA sequencing, we identified that PD-1 is one of the top up-regulated genes in gastric ILC2s after L635-induced injury. This was confirmed at the transcript level by qPCR and at the protein level by immunostaining. PD-1 has two ligands, namely PDL1 and PDL2. Previous studies have shown that co-stimulation of PD-1 by either of these ligands acts as a negative regulator of T cell activation by preventing T cell proliferation and/or promoting a regulatory phenotype (Arasanz et al., 2017). In ILC2s, it appears that negative regulation by PD-1 decreases cell number and effector function (Taylor et al., 2017). Interestingly,

we discovered that one of the ligands for PD-1, PDL2, is expressed by acid-secreting parietal cells under homeostatic conditions in the stomach.

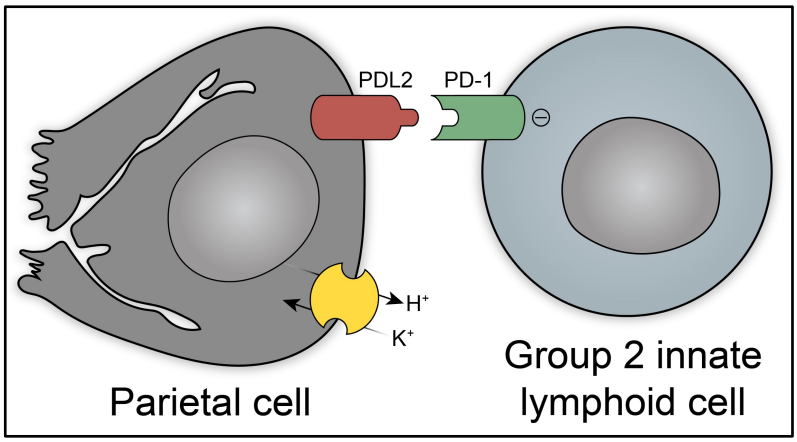

Figure 37. Cross talk between acid-secreting parietal cell and ILC2s.
Diagram of the proposed communication between H^+K^+ ATPase-positive parietal cells and ILC2s via the PD-1/PDL2 negative regulatory axis.

Since gastric injury is often associated with loss of parietal cells, and consequently loss of PDL2, we predicted that communication between ILC2s and parietal cells may be involved in ILC2 activation. We recently obtained mice lacking PDL2 and these mice sporadically develop isolated metaplastic lesions in the stomach, even in the absence of any damaging agents. We predict these metaplastic lesions initiate at sites of local damage that occur naturally in the stomach. However, without PDL2 regulation of ILC2 activation, local damage progresses to gastritis and advanced lesions in the stomach. Aged $PDL2^{-/-}$ mice exhibit small dysplastic lesions in the gastric mucosa that are positive for the dysplastic marker Trop2 and exhibit altered nuclear positioning.

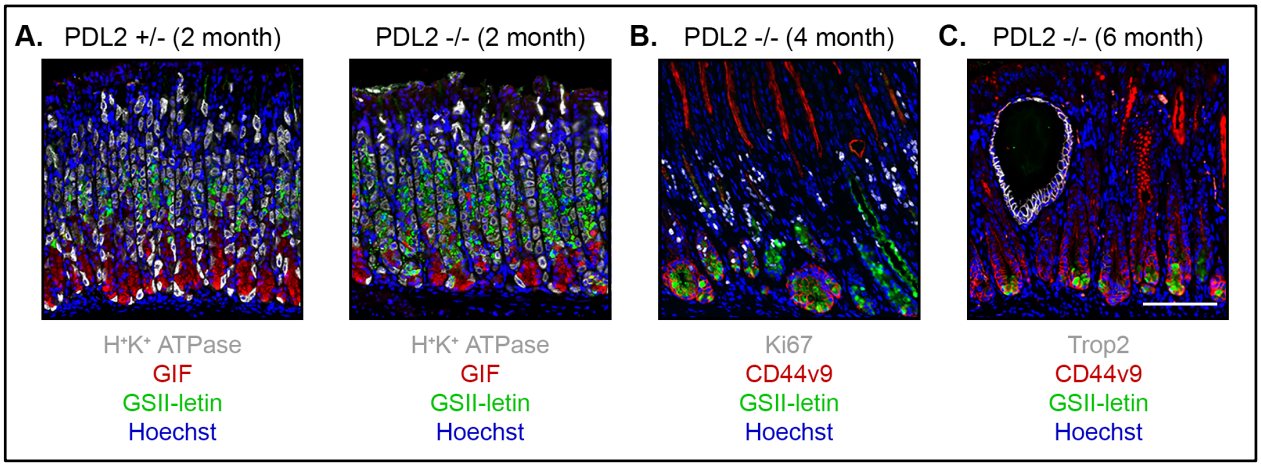

Figure 38. Mice lacking PDL2 spontaneously develop metaplastic and dysplastic lesions in the gastric mucosa.
PDL2$^{+/-}$ and PDL2$^{-/-}$ mice were sacrificed at 2 months, 4 months, and 6 months old. ***A.*** *Immunofluorescence staining for parietal cell marker H+/K+-ATPase (white), zymogenic granule marker GIF (red), and mucin granule marker GSII-lectin (green), with nuclear counterstain Hoechst (blue).* ***B.*** *Immunofluorescence staining for proliferation marker Ki67 (white), metaplastic marker CD44v9 (red), and mucin granule marker GSII-lectin (green), with nuclear counterstain Hoechst (blue).* ***C.*** *Immunofluorescence staining for dysplastic marker Trop2 (white), metaplastic marker CD44v9 (red), and mucin granule marker GSII-lectin (green), with nuclear counterstain Hoechst (blue) (scale bar = 100 μm). While PDL2$^{+/-}$ mice maintained normal glandular architecture, PDL2$^{-/-}$ mice spontaneously developed progressive CD44v9-positive metaplastic and Trop-positive dysplastic lesions in the stomach over time.*

Further studies are needed to determine the cross talk between parietal cells and gastric ILC2s. Future experiments should focus on the response to different types of gastric injury in PDL2$^{-/-}$ mice, including L635 and DMP-777 treatment, ulceration, and *Helicobacter* infection. In particular, the remaining questions pertain to if mice lacking PDL2 negative regulation respond to injury faster, develop more advanced lesions, or exhibit higher levels of inflammation. Furthermore, are mice lacking PDL2 able to recover following the resolution of injury. In addition to using PDL2$^{-/-}$ mice, recombinant PDL2 can be utilized in cell culture or in mice to evaluate ILC2 regulation.

Currently, there is a spotlight on the PD-1 regulatory axis in cancer cell biology as many tumors upregulate PD-1 ligands in order to evade the immune system (Gong et al., 2018; Xu-Monette et al., 2017). A blocking agent against PD-1, such as anti-PD-1 immunotherapy, can be used to disrupt the pathway that shields tumor cells from being targeted by the immune system (Marchetti et al., 2017). Interestingly, many patients receiving anti-PD-1 therapy exhibit immune-related adverse events in the gastrointestinal tract (Zhang et al., 2020). It is likely that PD-1 blockade increase ILC2 activation in these patients, which can trigger metaplasia development and inflammation. A detailed examination of gastric tissues from patients receiving anti-PD-1 therapy is required to understand the role of PD-1 regulation and ILC2s in humans.

Calcitonin Gene-Related Peptide (CGRP)

Neuroimmune interactions have emerged as crucial regulators of type 2 immune responses (Huang et al., 2019; Moriyama and Artis, 2019). Cross talk between neurons and ILC2s has been described in a number of mucosal tissues (Cardoso et al., 2017; Wallrapp et al., 2017). Specifically, studies have shown that the neuropeptide calcitonin gene-related peptide (CGRP) induces marked changes in ILC2 expression programs (Nagashima et al., 2019; Sui et al., 2018; Xu et al., 2019). CGRP can be released by neuroendocrine cells resident in mucosal tissues and signals through a receptor complex made up of CALCRL and RAMP1-3 (Dickerson, 2013; Evans et al., 2000). Interestingly, single cell RNA sequencing revealed that RAMP3 is one of the top up-regulated genes in gastric ILC2s after L635-induced injury. CALCRL and RAMP1 are also expressed by a subset of gastric ILC2s. Future studies should focus on the role CGRP signaling in regulating ILC2 activation in the stomach.

Interleukin-33 (IL-33)

IL-33 functions as a secreted signal released from cells at sites of mucosal damage. We have recently reported that mice lacking IL-33 or a subunit of the IL-33 receptor complex (ST2) fail to develop metaplasia following acute parietal cell loss (Petersen et al., 2017). IL-33 belongs to the IL-1 family of cytokines. Under healthy conditions, IL-33 translocates to the nucleus where it participates in regulating gene expression (Carriere et al., 2007). IL-33 also functions as a stored alarmin that is released when there is cell injury or necrosis that damages the epithelial cell barrier (Buzzelli et al., 2015; Judd et al., 2016; Schwartz et al., 2016). Although not well understood, there are also regulated mechanisms of IL-33 release from stimulated living cells (Byers et al., 2013; Kakkar et al., 2012; Kouzaki et al., 2011). Extracellular IL-33 works to coordinate immune defenses and repair mechanisms, while also triggering adaptive immune responses. IL-33 signals through the IL-33 receptor complex that consists of ST2 and IL1RAcP (Schmitz et al., 2005). In the normal mammalian stomach corpus, IL-33 is expressed in a subset of surface mucous foveolar epithelial cells (Buzzelli et al., 2015; Petersen et al., 2017). Following the administration of L635 and subsequent parietal cell loss, there is an expansion of IL-33 expressing foveolar epithelial cells as well as an inflammatory infiltrate, especially macrophages, that produce IL-33. IL-33 release and signaling after epithelial injury results in the upregulation of type II cytokines, including IL-13 (Petersen et al., 2017). One of the major remaining questions is what initially triggers IL-33 release after acute gastric injury. While parietal cell death is hallmark of gastric damage, parietal cells do not express IL-33. In the gastric mucosa IL-33 is expressed by MUC5AC-secreting foveolar cells. It has been proposed that IL-33 release can be

stimulated by mechanical stress and/or extracellular ATP in living cells (Kakkar et al., 2012; Kouzaki et al., 2011). Further studies are required to determine what stimulates IL-33 release following acute gastric injury.

Interleukin-25 and Thymic Stromal Lymphopoietin (IL-25 and TSLP)

Similar to IL-33, Interleukin-25 and Thymic Stromal Lymphopoietin (IL-25 and TSLP respectively) act as epithelial alarmins that stimulate ILC2 activation (Roan et al., 2019; Vannella et al., 2016). However, their role in the initiation, maintenance, and progression of type 2 inflammation after acute gastric injury is less clear. These alarmins are released from the epithelium and local stromal compartments in response to external insults when cells are damaged or stressed. Like IL-33, IL-25 and TSLP can trigger the production of type 2 cytokines. It has been proposed that IL-25, IL-33, and TSLP induce distinct activation profiles in ILC2s (Camelo et al., 2017). Through single cell RNA sequencing, we determined that gastric ILC2s express both the IL-25 and TSLP receptors. IL-25 is expressed by tuft cells, which expand after gastric injury (Gronke and Diefenbach, 2016). In the intestine, tuft cell-derived IL-25 regulates ILC2 activation (von Moltke et al., 2016). A closer examination of the reciprocal relationship and cross talk between tuft cells and ILC2s in the stomach is needed. On the other hand, it has been shown that *Helicobacter* infection induces the production of TSLP by gastric epithelial cells (Kido et al., 2010). Future studies should focus on the cell types in the stomach that express IL-25 and TSLP and determine their role in type 2 inflammation, ILC2 activation, and tissue repair following gastric damage.

Immune cell interaction studies:

Epithelial tissues, including the stomach, act as a physical barrier between our bodies and the external environment (Hunt et al., 2015). The traditional view of the gastric mucosa is a protective out layer of epithelial cells that is supported by a layer of immune cells searching for areas where the integrity of the outer layer has been compromised (Larsen et al., 2020; Naik et al., 2018). However, instead of separating these two elements, they should be looked at as a single integrated system. The immune cells that respond to gastric injury (ILC2s, macrophages, and eosinophils) accumulate at the base of gastric glands, co-incident with the development of SPEM. While many of the studies presented here are centered on the cross talk between epithelial cells and immune cells, the direct cell-to-cell contact between epithelial cells and immune cells has not been addressed. Future studies should investigate if gastric immune cells exhibit processes and what epithelial cells they associate with. Emphasis should be placed on the localization, shape, and extensions from each immune cell lineage. Furthermore, direct cell interactions between immune cells and other immune cell lineages should be examined. Many of these questions can be addressed by co-culturing ILC2s, macrophages, and/or eosinophils with normal gastric organoids or metaplastic organoids.

Acinar to ductal metaplasia studies:

Reprogramming of mature, differentiated cells promotes regeneration and is an important repair process in tissues that lack an active adult stem cell compartment such as the pancreas (Murtaugh and Keefe, 2015). In the pancreas, injury and inflammation trigger digestive enzyme-secreting acinar cells to reprogram into a metaplastic cell

lineage analogous to SPEM, a process described as acinar to ductal metaplasia or ADM (De La et al., 2008; Jensen et al., 2005; Shi et al., 2013). ADM cells acquire morphological and molecular characteristics hybrid between acinar cells and duct cells (the cells that line the ducts that transport acinar cell-secreted enzymes toward the intestine) (Puri et al., 2015). Like SPEM, acinar cell reprogramming requires the downscaling of transcription factors and proteins that govern acinar maturation, architecture, and function. ADM cells exhibit low levels of digestive enzyme granules along with abundant mucin (MUC1 and MUC6) granules (Iovanna et al., 1992). Although acinar and duct cells are largely mitotically quiescent, ADM cells re-enter the cell cycle and proliferate (Pinho et al., 2011). Furthermore, chronic inflammation and/or underlying mutations can push ADM cells to increase proliferation and eventually undergo neoplastic transformation to pancreatic intraepithelial neoplasia (PanIN). PanINs are a precursor to invasive pancreatic cancer (Storz, 2017). Defining tumor-initiating events is crucial for the development of early detection methods and effective treatments in the pancreas.

It has been reported that CD44v9, a protein involved in the oxidative stress response, is expressed on the membrane of ADM cells and in PanIN lesions (Kiuchi et al., 2015; Mills and Sansom, 2015; Ringel et al., 2001). Future studies should investigate whether acinar cells rely on the CD44v9-xCT antioxidant system for reprogramming. To address this question, daily injections of cerulein (a rapid method to induce large-scale pancreatic damage) can be administered to xCT knockout mice or in combination with sulfasalazine treatment. Interestingly, alternatively activated macrophages and IL-13 signaling are also required for the progression of ADM in the pancreas (Liou et al., 2017;

Liou et al., 2013). Additional studies should address the role of ILC2s in acinar cell reprogramming, type 2 inflammation, and tissue repair in response to pancreatic injury.

In conclusion, it appears that in response to gastric injury there are several epithelial-immune cell circuits that synergize to promote repair in the stomach. The data presented here suggest that oxidative stress and innate immune responses are crucial for the stomach to effectively repair after damage.

REFERENCES

Acharya, K.R., and Ackerman, S.J. (2014). Eosinophil granule proteins: form and function. J Biol Chem *289*, 17406-17415.

Annibale, B., Esposito, G., and Lahner, E. (2020). A current clinical overview of atrophic gastritis. Expert Rev Gastroenterol Hepatol *14*, 93-102.

Arasanz, H., Gato-Canas, M., Zuazo, M., Ibanez-Vea, M., Breckpot, K., Kochan, G., and Escors, D. (2017). PD1 signal transduction pathways in T cells. Oncotarget *8*, 51936-51945.

Beasley, D.E., Koltz, A.M., Lambert, J.E., Fierer, N., and Dunn, R.R. (2015). The Evolution of Stomach Acidity and Its Relevance to the Human Microbiome. PLoS One *10*, e0134116.

Bernink, J.H., Germar, K., and Spits, H. (2014). The role of ILC2 in pathology of type 2 inflammatory diseases. Curr Opin Immunol *31*, 115-120.

Bertaux-Skeirik, N., Feng, R., Schumacher, M.A., Li, J., Mahe, M.M., Engevik, A.C., Javier, J.E., Peek, R.M., Jr., Ottemann, K., Orian-Rousseau, V.*, et al.* (2015). CD44 plays a functional role in Helicobacter pylori-induced epithelial cell proliferation. PLoS Pathog *11*, e1004663.

Bogdan, C., Paik, J., Vodovotz, Y., and Nathan, C. (1992). Contrasting mechanisms for suppression of macrophage cytokine release by transforming growth factor-beta and interleukin-10. J Biol Chem *267*, 23301-23308.

Burkitt, M.D., Duckworth, C.A., Williams, J.M., and Pritchard, D.M. (2017). Helicobacter pylori-induced gastric pathology: insights from in vivo and ex vivo models. Dis Model Mech *10*, 89-104.

Buzzelli, J.N., Chalinor, H.V., Pavlic, D.I., Sutton, P., Menheniott, T.R., Giraud, A.S., and Judd, L.M. (2015). IL33 Is a Stomach Alarmin That Initiates a Skewed Th2 Response to Injury and Infection. Cell Mol Gastroenterol Hepatol *1*, 203-221 e203.

Byers, D.E., Alexander-Brett, J., Patel, A.C., Agapov, E., Dang-Vu, G., Jin, X., Wu, K., You, Y., Alevy, Y., Girard, J.P.*, et al.* (2013). Long-term IL-33-producing epithelial progenitor cells in chronic obstructive lung disease. J Clin Invest *123*, 3967-3982.

Camelo, A., Rosignoli, G., Ohne, Y., Stewart, R.A., Overed-Sayer, C., Sleeman, M.A., and May, R.D. (2017). IL-33, IL-25, and TSLP induce a distinct phenotypic and activation profile in human type 2 innate lymphoid cells. Blood Adv *1*, 577-589.

Cardoso, V., Chesne, J., Ribeiro, H., Garcia-Cassani, B., Carvalho, T., Bouchery, T., Shah, K., Barbosa-Morais, N.L., Harris, N., and Veiga-Fernandes, H. (2017). Neuronal regulation of type 2 innate lymphoid cells via neuromedin U. Nature *549*, 277-281.

Carriere, V., Roussel, L., Ortega, N., Lacorre, D.A., Americh, L., Aguilar, L., Bouche, G., and Girard, J.P. (2007). IL-33, the IL-1-like cytokine ligand for ST2 receptor, is a chromatin-associated nuclear factor in vivo. Proc Natl Acad Sci U S A *104*, 282-287.

Choi, E., Hendley, A.M., Bailey, J.M., Leach, S.D., and Goldenring, J.R. (2016). Expression of Activated Ras in Gastric Chief Cells of Mice Leads to the Full Spectrum of Metaplastic Lineage Transitions. Gastroenterology *150*, 918-930 e913.

Choi, E., Petersen, C.P., Lapierre, L.A., Williams, J.A., Weis, V.G., Goldenring, J.R., and Nam, K.T. (2015). Dynamic expansion of gastric mucosal doublecortin-like kinase 1-expressing cells in response to parietal cell loss is regulated by gastrin. Am J Pathol *185*, 2219-2231.

Chung, W.J., Lyons, S.A., Nelson, G.M., Hamza, H., Gladson, C.L., Gillespie, G.Y., and Sontheimer, H. (2005). Inhibition of cystine uptake disrupts the growth of primary brain tumors. J Neurosci *25*, 7101-7110.

Coffey, R.J., Romano, M., Polk, W.H., and Dempsey, P.J. (1992). Roles for transforming growth factor-alpha in gastric physiology and pathophysiology. Yale J Biol Med *65*, 693-704; discussion 621-693.

Cohn, L., Homer, R.J., MacLeod, H., Mohrs, M., Brombacher, F., and Bottomly, K. (1999). Th2-induced airway mucus production is dependent on IL-4Ralpha, but not on eosinophils. J Immunol *162*, 6178-6183.

Correa, P. (1988). A human model of gastric carcinogenesis. Cancer Res *48*, 3554-3560.

Correa, P., Piazuelo, M.B., and Wilson, K.T. (2010). Pathology of gastric intestinal metaplasia: clinical implications. Am J Gastroenterol *105*, 493-498.

De Bundel, D., Schallier, A., Loyens, E., Fernando, R., Miyashita, H., Van Liefferinge, J., Vermoesen, K., Bannai, S., Sato, H., Michotte, Y.*, et al.* (2011). Loss of system x(c)- does not induce oxidative stress but decreases extracellular glutamate in hippocampus and influences spatial working memory and limbic seizure susceptibility. J Neurosci *31*, 5792-5803.

De La, O.J., Emerson, L.L., Goodman, J.L., Froebe, S.C., Illum, B.E., Curtis, A.B., and Murtaugh, L.C. (2008). Notch and Kras reprogram pancreatic acinar cells to ductal intraepithelial neoplasia. Proc Natl Acad Sci U S A *105*, 18907-18912.

de Martel, C., Ferlay, J., Franceschi, S., Vignat, J., Bray, F., Forman, D., and Plummer, M. (2012). Global burden of cancers attributable to infections in 2008: a review and synthetic analysis. Lancet Oncol *13*, 607-615.

Dickerson, I.M. (2013). Role of CGRP-receptor component protein (RCP) in CLR/RAMP function. Curr Protein Pept Sci *14*, 407-415.

Eberl, G., Colonna, M., Di Santo, J.P., and McKenzie, A.N. (2015). Innate lymphoid cells. Innate lymphoid cells: a new paradigm in immunology. Science *348*, aaa6566.

Engelbertsen, D., Foks, A.C., Alberts-Grill, N., Kuperwaser, F., Chen, T., Lederer, J.A., Jarolim, P., Grabie, N., and Lichtman, A.H. (2015). Expansion of CD25+ Innate Lymphoid Cells Reduces Atherosclerosis. Arterioscler Thromb Vasc Biol *35*, 2526-2535.

Engevik, A.C., Feng, R., Choi, E., White, S., Bertaux-Skeirik, N., Li, J., Mahe, M.M., Aihara, E., Yang, L., DiPasquale, B.*, et al.* (2016). The Development of Spasmolytic Polypeptide/TFF2-Expressing Metaplasia (SPEM) During Gastric Repair Is Absent in the Aged Stomach. Cell Mol Gastroenterol Hepatol *2*, 605-624.

Evans, B.N., Rosenblatt, M.I., Mnayer, L.O., Oliver, K.R., and Dickerson, I.M. (2000). CGRP-RCP, a novel protein required for signal transduction at calcitonin gene-related peptide and adrenomedullin receptors. J Biol Chem *275*, 31438-31443.

Fairweather, D., and Cihakova, D. (2009). Alternatively activated macrophages in infection and autoimmunity. J Autoimmun *33*, 222-230.

Finkel, T., and Holbrook, N.J. (2000). Oxidants, oxidative stress and the biology of ageing. Nature *408*, 239-247.

Forrester, S.J., Kikuchi, D.S., Hernandes, M.S., Xu, Q., and Griendling, K.K. (2018). Reactive Oxygen Species in Metabolic and Inflammatory Signaling. Circ Res *122*, 877-902.

Franco, R., and Cidlowski, J.A. (2009). Apoptosis and glutathione: beyond an antioxidant. Cell Death Differ *16*, 1303-1314.

Fu, D.A., and Campbell-Thompson, M. (2017). Periodic Acid-Schiff Staining with Diastase. Methods Mol Biol *1639*, 145-149.

Fuchs, A., and Colonna, M. (2013). Innate lymphoid cells in homeostasis, infection, chronic inflammation and tumors of the gastrointestinal tract. Curr Opin Gastroenterol *29*, 581-587.

Gerbe, F., Sidot, E., Smyth, D.J., Ohmoto, M., Matsumoto, I., Dardalhon, V., Cesses, P., Garnier, L., Pouzolles, M., Brulin, B.*, et al.* (2016). Intestinal epithelial tuft cells initiate type 2 mucosal immunity to helminth parasites. Nature *529*, 226-230.

Goenka, S., and Kaplan, M.H. (2011). Transcriptional regulation by STAT6. Immunol Res *50*, 87-96.

Goldenring, J.R. (2018). Pyloric metaplasia, pseudopyloric metaplasia, ulcer-associated cell lineage and spasmolytic polypeptide-expressing metaplasia: reparative lineages in the gastrointestinal mucosa. J Pathol *245*, 132-137.

Goldenring, J.R., and Nam, K.T. (2010). Oxyntic atrophy, metaplasia, and gastric cancer. Prog Mol Biol Transl Sci *96*, 117-131.

Goldenring, J.R., Nam, K.T., Wang, T.C., Mills, J.C., and Wright, N.A. (2010). Spasmolytic polypeptide-expressing metaplasia and intestinal metaplasia: time for reevaluation of metaplasias and the origins of gastric cancer. Gastroenterology *138*, 2207-2210, 2210 e2201.

Goldenring, J.R., Ray, G.S., Coffey, R.J., Meunier, P.C., Haley, P.J., Barnes, T.B., and Car, B.D. (2000). Reversible drug-induced oxyntic atrophy in rats. Gastroenterology *118*, 1080-1093.

Gong, J., Chehrazi-Raffle, A., Reddi, S., and Salgia, R. (2018). Development of PD-1 and PD-L1 inhibitors as a form of cancer immunotherapy: a comprehensive review of registration trials and future considerations. J Immunother Cancer *6*, 8.

Gour, N., Smole, U., Yong, H.M., Lewkowich, I.P., Yao, N., Singh, A., Gabrielson, E., Wills-Karp, M., and Lajoie, S. (2018). C3a is required for ILC2 function in allergic airway inflammation. Mucosal Immunol *11*, 1653-1662.

Gout, P.W., Buckley, A.R., Simms, C.R., and Bruchovsky, N. (2001). Sulfasalazine, a potent suppressor of lymphoma growth by inhibition of the x(c)- cystine transporter: a new action for an old drug. Leukemia *15*, 1633-1640.

Gronke, K., and Diefenbach, A. (2016). Tuft cell-derived IL-25 activates and maintains ILC2. Immunol Cell Biol *94*, 221-223.

Guo, L., Junttila, I.S., and Paul, W.E. (2012). Cytokine-induced cytokine production by conventional and innate lymphoid cells. Trends Immunol *33*, 598-606.

Habib, E., Linher-Melville, K., Lin, H.X., and Singh, G. (2015). Expression of xCT and activity of system xc(-) are regulated by NRF2 in human breast cancer cells in response to oxidative stress. Redox Biol *5*, 33-42.

Halldorsdottir, A.M., Sigurdardottrir, M., Jonasson, J.G., Oddsdottir, M., Magnusson, J., Lee, J.R., and Goldenring, J.R. (2003). Spasmolytic polypeptide-expressing metaplasia (SPEM) associated with gastric cancer in Iceland. Dig Dis Sci *48*, 431-441.

Hallett, M.A., Venmar, K.T., and Fingleton, B. (2012). Cytokine stimulation of epithelial cancer cells: the similar and divergent functions of IL-4 and IL-13. Cancer Res *72*, 6338-6343.

Hao, Y., Kuang, Z., Jing, J., Miao, J., Mei, L.Y., Lee, R.J., Kim, S., Choe, S., Krause, D.C., and Lau, G.W. (2014). Mycoplasma pneumoniae modulates STAT3-STAT6/EGFR-FOXA2 signaling to induce overexpression of airway mucins. Infect Immun *82*, 5246-5255.

Hardbower, D.M., de Sablet, T., Chaturvedi, R., and Wilson, K.T. (2013). Chronic inflammation and oxidative stress: the smoking gun for Helicobacter pylori-induced gastric cancer? Gut Microbes *4*, 475-481.

Hayakawa, Y., Ariyama, H., Stancikova, J., Sakitani, K., Asfaha, S., Renz, B.W., Dubeykovskaya, Z.A., Shibata, W., Wang, H., Westphalen, C.B.*, et al.* (2015). Mist1 Expressing Gastric Stem Cells Maintain the Normal and Neoplastic Gastric Epithelium and Are Supported by a Perivascular Stem Cell Niche. Cancer Cell *28*, 800-814.

Hoffmann, W. (2015). TFF2, a MUC6-binding lectin stabilizing the gastric mucus barrier and more (Review). Int J Oncol *47*, 806-816.

Howitt, M.R., Lavoie, S., Michaud, M., Blum, A.M., Tran, S.V., Weinstock, J.V., Gallini, C.A., Redding, K., Margolskee, R.F., Osborne, L.C.*, et al.* (2016). Tuft cells, taste-chemosensory cells, orchestrate parasite type 2 immunity in the gut. Science *351*, 1329-1333.

Huang, Y., Zhao, C., and Su, X. (2019). Neuroimmune regulation of lung infection and inflammation. QJM *112*, 483-487.

Huh, W.J., Khurana, S.S., Geahlen, J.H., Kohli, K., Waller, R.A., and Mills, J.C. (2012). Tamoxifen induces rapid, reversible atrophy, and metaplasia in mouse stomach. Gastroenterology *142*, 21-24 e27.

Hunt, R.H., Camilleri, M., Crowe, S.E., El-Omar, E.M., Fox, J.G., Kuipers, E.J., Malfertheiner, P., McColl, K.E., Pritchard, D.M., Rugge, M.*, et al.* (2015). The stomach in health and disease. Gut *64*, 1650-1668.

Iovanna, J.L., Lechene de la Porte, P., and Dagorn, J.C. (1992). Expression of genes associated with dedifferentiation and cell proliferation during pancreatic regeneration following acute pancreatitis. Pancreas *7*, 712-718.

Isacke, C.M., and Yarwood, H. (2002). The hyaluronan receptor, CD44. Int J Biochem Cell Biol *34*, 718-721.

Ishii, T., and Mann, G.E. (2014). Redox status in mammalian cells and stem cells during culture in vitro: critical roles of Nrf2 and cystine transporter activity in the maintenance of redox balance. Redox Biol *2*, 786-794.

Ishimoto, T., Nagano, O., Yae, T., Tamada, M., Motohara, T., Oshima, H., Oshima, M., Ikeda, T., Asaba, R., Yagi, H.*, et al.* (2011). CD44 variant regulates redox status in cancer cells by stabilizing the xCT subunit of system xc(-) and thereby promotes tumor growth. Cancer Cell *19*, 387-400.

Jensen, J.N., Cameron, E., Garay, M.V., Starkey, T.W., Gianani, R., and Jensen, J. (2005). Recapitulation of elements of embryonic development in adult mouse pancreatic regeneration. Gastroenterology *128*, 728-741.

Jones, T.R., Kang, I.H., Wheeler, D.B., Lindquist, R.A., Papallo, A., Sabatini, D.M., Golland, P., and Carpenter, A.E. (2008). CellProfiler Analyst: data exploration and analysis software for complex image-based screens. BMC Bioinformatics *9*, 482.

Jubel, J.M., Barbati, Z.R., Burger, C., Wirtz, D.C., and Schildberg, F.A. (2020). The Role of PD-1 in Acute and Chronic Infection. Front Immunol *11*, 487.

Judd, L.M., Heine, R.G., Menheniott, T.R., Buzzelli, J., O'Brien-Simpson, N., Pavlic, D., O'Connor, L., Al Gazali, K., Hamilton, O., Scurr, M.*, et al.* (2016). Elevated IL-33 expression is associated with pediatric eosinophilic esophagitis, and exogenous IL-33 promotes eosinophilic esophagitis development in mice. Am J Physiol Gastrointest Liver Physiol *310*, G13-25.

Kakkar, R., Hei, H., Dobner, S., and Lee, R.T. (2012). Interleukin 33 as a mechanically responsive cytokine secreted by living cells. J Biol Chem *287*, 6941-6948.

Kerrigan, A.M., and Brown, G.D. (2009). C-type lectins and phagocytosis. Immunobiology *214*, 562-575.

Khurana, S.S., Riehl, T.E., Moore, B.D., Fassan, M., Rugge, M., Romero-Gallo, J., Noto, J., Peek, R.M., Jr., Stenson, W.F., and Mills, J.C. (2013). The hyaluronic acid receptor CD44 coordinates normal and metaplastic gastric epithelial progenitor cell proliferation. J Biol Chem *288*, 16085-16097.

Kido, M., Tanaka, J., Aoki, N., Iwamoto, S., Nishiura, H., Chiba, T., and Watanabe, N. (2010). Helicobacter pylori promotes the production of thymic stromal lymphopoietin by gastric epithelial cells and induces dendritic cell-mediated inflammatory Th2 responses. Infect Immun *78*, 108-114.

Kim, B.S., Wang, K., Siracusa, M.C., Saenz, S.A., Brestoff, J.R., Monticelli, L.A., Noti, M., Tait Wojno, E.D., Fung, T.C., Kubo, M.*, et al.* (2014). Basophils promote innate lymphoid cell responses in inflamed skin. J Immunol *193*, 3717-3725.

Kim, S.Y., and Nair, M.G. (2019). Macrophages in wound healing: activation and plasticity. Immunol Cell Biol *97*, 258-267.

Kiuchi, S., Ikeshita, S., Miyatake, Y., and Kasahara, M. (2015). Pancreatic cancer cells express CD44 variant 9 and multidrug resistance protein 1 during mitosis. Exp Mol Pathol *98*, 41-46.

Klein Wolterink, R.G., Serafini, N., van Nimwegen, M., Vosshenrich, C.A., de Bruijn, M.J., Fonseca Pereira, D., Veiga Fernandes, H., Hendriks, R.W., and Di Santo, J.P. (2013). Essential, dose-dependent role for the transcription factor Gata3 in the development of IL-5+ and IL-13+ type 2 innate lymphoid cells. Proc Natl Acad Sci U S A *110*, 10240-10245.

Kouzaki, H., Iijima, K., Kobayashi, T., O'Grady, S.M., and Kita, H. (2011). The danger signal, extracellular ATP, is a sensor for an airborne allergen and triggers IL-33 release and innate Th2-type responses. J Immunol *186*, 4375-4387.

Larsen, S.B., Cowley, C.J., and Fuchs, E. (2020). Epithelial cells: liaisons of immunity. Curr Opin Immunol *62*, 45-53.

Lei, A.H., Xiao, Q., Liu, G.Y., Shi, K., Yang, Q., Li, X., Liu, Y.F., Wang, H.K., Cai, W.P., Guan, Y.J.*, et al.* (2018). ICAM-1 controls development and function of ILC2. J Exp Med *215*, 2157-2174.

Lennerz, J.K., Kim, S.H., Oates, E.L., Huh, W.J., Doherty, J.M., Tian, X., Bredemeyer, A.J., Goldenring, J.R., Lauwers, G.Y., Shin, Y.K.*, et al.* (2010). The transcription factor MIST1 is a novel human gastric chief cell marker whose expression is lost in metaplasia, dysplasia, and carcinoma. Am J Pathol *177*, 1514-1533.

Leushacke, M., Tan, S.H., Wong, A., Swathi, Y., Hajamohideen, A., Tan, L.T., Goh, J., Wong, E., Denil, S., Murakami, K.*, et al.* (2017). Lgr5-expressing chief cells drive epithelial regeneration and cancer in the oxyntic stomach. Nat Cell Biol.

Li, D., Guabiraba, R., Besnard, A.G., Komai-Koma, M., Jabir, M.S., Zhang, L., Graham, G.J., Kurowska-Stolarska, M., Liew, F.Y., McSharry, C.*, et al.* (2014). IL-33 promotes ST2-dependent lung fibrosis by the induction of alternatively activated macrophages and innate lymphoid cells in mice. J Allergy Clin Immunol *134*, 1422-1432 e1411.

Liou, G.Y., Bastea, L., Fleming, A., Doppler, H., Edenfield, B.H., Dawson, D.W., Zhang, L., Bardeesy, N., and Storz, P. (2017). The Presence of Interleukin-13 at Pancreatic ADM/PanIN Lesions Alters Macrophage Populations and Mediates Pancreatic Tumorigenesis. Cell Rep *19*, 1322-1333.

Liou, G.Y., Doppler, H., Necela, B., Krishna, M., Crawford, H.C., Raimondo, M., and Storz, P. (2013). Macrophage-secreted cytokines drive pancreatic acinar-to-ductal metaplasia through NF-kappaB and MMPs. J Cell Biol *202*, 563-577.

Ma, J., Shen, H., Kapesa, L., and Zeng, S. (2016). Lauren classification and individualized chemotherapy in gastric cancer. Oncol Lett *11*, 2959-2964.

Mantovani, A., Sozzani, S., Locati, M., Allavena, P., and Sica, A. (2002). Macrophage polarization: tumor-associated macrophages as a paradigm for polarized M2 mononuclear phagocytes. Trends Immunol *23*, 549-555.

Marchetti, A., Di Lorito, A., and Buttitta, F. (2017). Why anti-PD1/PDL1 therapy is so effective? Another piece in the puzzle. J Thorac Dis *9*, 4863-4866.

Mariotti, F.R., Quatrini, L., Munari, E., Vacca, P., and Moretta, L. (2019). Innate Lymphoid Cells: Expression of PD-1 and Other Checkpoints in Normal and Pathological Conditions. Front Immunol *10*, 910.

Martinez, F.O., Helming, L., and Gordon, S. (2009). Alternative activation of macrophages: an immunologic functional perspective. Annu Rev Immunol *27*, 451-483.

McCullagh, E.A., and Featherstone, D.E. (2014). Behavioral characterization of system xc- mutant mice. Behav Brain Res *265*, 1-11.

Meyer, A.R., Engevik, A.C., Willet, S.G., Williams, J.A., Zou, Y., Massion, P.P., Mills, J.C., Choi, E., and Goldenring, J.R. (2019). Cystine/Glutamate Antiporter (xCT) Is Required for Chief Cell Plasticity After Gastric Injury. Cell Mol Gastroenterol Hepatol *8*, 379-405.

Meyer, A.R., and Goldenring, J.R. (2018). Injury, repair, inflammation and metaplasia in the stomach. J Physiol.

Mills, J.C., and Sansom, O.J. (2015). Reserve stem cells: Differentiated cells reprogram to fuel repair, metaplasia, and neoplasia in the adult gastrointestinal tract. Sci Signal *8*, re8.

Mittal, M., Siddiqui, M.R., Tran, K., Reddy, S.P., and Malik, A.B. (2014). Reactive oxygen species in inflammation and tissue injury. Antioxid Redox Signal *20*, 1126-1167.

Monticelli, L.A., Sonnenberg, G.F., Abt, M.C., Alenghat, T., Ziegler, C.G., Doering, T.A., Angelosanto, J.M., Laidlaw, B.J., Yang, C.Y., Sathaliyawala, T.*, et al.* (2011). Innate lymphoid cells promote lung-tissue homeostasis after infection with influenza virus. Nat Immunol *12*, 1045-1054.

Moriyama, S., and Artis, D. (2019). Neuronal regulation of group 2 innate lymphoid cells and type 2 inflammation. Adv Immunol *143*, 1-9.

Moro, K., Yamada, T., Tanabe, M., Takeuchi, T., Ikawa, T., Kawamoto, H., Furusawa, J., Ohtani, M., Fujii, H., and Koyasu, S. (2010). Innate production of T(H)2 cytokines by adipose tissue-associated c-Kit(+)Sca-1(+) lymphoid cells. Nature *463*, 540-544.

Murtaugh, L.C., and Keefe, M.D. (2015). Regeneration and repair of the exocrine pancreas. Annu Rev Physiol *77*, 229-249.

Nagane, M., Kanai, E., Shibata, Y., Shimizu, T., Yoshioka, C., Maruo, T., and Yamashita, T. (2018). Sulfasalazine, an inhibitor of the cystine-glutamate antiporter, reduces DNA damage repair and enhances radiosensitivity in murine B16F10 melanoma. PLoS One *13*, e0195151.

Nagano, O., Okazaki, S., and Saya, H. (2013). Redox regulation in stem-like cancer cells by CD44 variant isoforms. Oncogene *32*, 5191-5198.

Nagashima, H., Mahlakoiv, T., Shih, H.Y., Davis, F.P., Meylan, F., Huang, Y., Harrison, O.J., Yao, C., Mikami, Y., Urban, J.F., Jr.*, et al.* (2019). Neuropeptide CGRP Limits Group 2 Innate Lymphoid Cell Responses and Constrains Type 2 Inflammation. Immunity *51*, 682-695 e686.

Naik, S., Larsen, S.B., Cowley, C.J., and Fuchs, E. (2018). Two to Tango: Dialog between Immunity and Stem Cells in Health and Disease. Cell *175*, 908-920.

Nam, K.T., Lee, H.-J., Sousa, J.F., Weis, V.G., O'Neal, R.L., Finke, P.E., Romero-Gallo, J., Shi, G., Mills, J.C., Peek, R.M.*, et al.* (2010a). Mature chief cells are cryptic progenitors for metaplasia in the stomach. Gastroenterology *139*, 2028-2037.

Nam, K.T., Lee, H.J., Sousa, J.F., Weis, V.G., O'Neal, R.L., Finke, P.E., Romero-Gallo, J., Shi, G., Mills, J.C., Peek, R.M., Jr.*, et al.* (2010b). Mature chief cells are cryptic progenitors for metaplasia in the stomach. Gastroenterology *139*, 2028-2037 e2029.

Nashed, M.G., Ungard, R.G., Young, K., Zacal, N.J., Seidlitz, E.P., Fazzari, J., Frey, B.N., and Singh, G. (2017). Behavioural Effects of Using Sulfasalazine to Inhibit Glutamate Released by Cancer Cells: A Novel target for Cancer-Induced Depression. Sci Rep *7*, 41382.

Navarro-Yepes, J., Burns, M., Anandhan, A., Khalimonchuk, O., del Razo, L.M., Quintanilla-Vega, B., Pappa, A., Panayiotidis, M.I., and Franco, R. (2014). Oxidative stress, redox signaling, and autophagy: cell death versus survival. Antioxid Redox Signal *21*, 66-85.

Neill, D.R., Wong, S.H., Bellosi, A., Flynn, R.J., Daly, M., Langford, T.K., Bucks, C., Kane, C.M., Fallon, P.G., Pannell, R.*, et al.* (2010). Nuocytes represent a new innate effector leukocyte that mediates type-2 immunity. Nature *464*, 1367-1370.

Ni, J., Mei, M., and Sun, L. (2012). Oxidative DNA damage and repair in chronic atrophic gastritis and gastric cancer. Hepatogastroenterology *59*, 671-675.

Nickel, T., Schmauss, D., Hanssen, H., Sicic, Z., Krebs, B., Jankl, S., Summo, C., Fraunberger, P., Walli, A.K., Pfeiler, S.*, et al.* (2009). oxLDL uptake by dendritic cells induces upregulation of scavenger-receptors, maturation and differentiation. Atherosclerosis *205*, 442-450.

Nikolaidis, N.M., Zimmermann, N., King, N.E., Mishra, A., Pope, S.M., Finkelman, F.D., and Rothenberg, M.E. (2003). Trefoil factor-2 is an allergen-induced gene regulated by Th2 cytokines and STAT6 in the lung. Am J Respir Cell Mol Biol *29*, 458-464.

Nomura, S., Yamaguchi, H., Ogawa, M., Wang, T.C., Lee, J.R., and Goldenring, J.R. (2005). Alterations in gastric mucosal lineages induced by acute oxyntic atrophy in wild-type and gastrin-deficient mice. Am J Physiol Gastrointest Liver Physiol *288*, G362-375.

Nordman, H., Davies, J.R., Lindell, G., de Bolos, C., Real, F., and Carlstedt, I. (2002). Gastric MUC5AC and MUC6 are large oligomeric mucins that differ in size, glycosylation and tissue distribution. Biochem J *364*, 191-200.

Nozaki, K., Ogawa, M., Williams, J.A., Lafleur, B.J., Ng, V., Drapkin, R.I., Mills, J.C., Konieczny, S.F., Nomura, S., and Goldenring, J.R. (2008a). A molecular signature of

gastric metaplasia arising in response to acute parietal cell loss. Gastroenterology *134*, 511-522.

Nozaki, K., Ogawa, M., Williams, J.A., LaFleur, B.J., Ng, V., Drapkin, R.I., Mills, J.C., Konieczny, S.F., Nomura, S., and Goldenring, J.R. (2008b). A molecular signature of gastric metaplasia arising in response to acute parietal cell loss. Gastroenterology, 511-521.

Peppercorn, M.A. (1984). Sulfasalazine. Pharmacology, clinical use, toxicity, and related new drug development. Ann Intern Med *101*, 377-386.

Petersen, C.P., Meyer, A.R., De Salvo, C., Choi, E., Schlegel, C., Petersen, A., Engevik, A.C., Prasad, N., Levy, S.E., Peebles, R.S.*, et al.* (2017). A signalling cascade of IL-33 to IL-13 regulates metaplasia in the mouse stomach. Gut *67*, 805-817.

Petersen, C.P., Weis, V.G., Nam, K.T., Sousa, J.F., Fingleton, B., and Goldenring, J.R. (2014). Macrophages promote progression of spasmolytic polypeptide-expressing metaplasia after acute loss of parietal cells. Gastroenterology *146*, 1727-1738 e1728.

Picelli, S., Faridani, O.R., Bjorklund, A.K., Winberg, G., Sagasser, S., and Sandberg, R. (2014). Full-length RNA-seq from single cells using Smart-seq2. Nat Protoc *9*, 171-181.

Pinho, A.V., Rooman, I., Reichert, M., De Medts, N., Bouwens, L., Rustgi, A.K., and Real, F.X. (2011). Adult pancreatic acinar cells dedifferentiate to an embryonic progenitor phenotype with concomitant activation of a senescence programme that is present in chronic pancreatitis. Gut *60*, 958-966.

Poynter, D., Selway, S.A., Papworth, S.A., and Riches, S.R. (1986). Changes in the gastric mucosa of the mouse associated with long lasting unsurmountable histamine H2 blockade. Gut *27*, 1338-1346.

Prochazka, L., Tesarik, R., and Turanek, J. (2014). Regulation of alternative splicing of CD44 in cancer. Cell Signal *26*, 2234-2239.

Puri, S., Folias, A.E., and Hebrok, M. (2015). Plasticity and dedifferentiation within the pancreas: development, homeostasis, and disease. Cell Stem Cell *16*, 18-31.

Radyk, M.D., Burclaff, J., Willet, S.G., and Mills, J.C. (2017). Metaplastic Cells in the Stomach Arise, Independently of Stem Cells, via Dedifferentiation or Transdifferentiation of Chief Cells. Gastroenterology.

Ramsey, V.G., Doherty, J.M., Chen, C.C., Stappenbeck, T.S., Konieczny, S.F., and Mills, J.C. (2007). The maturation of mucus-secreting gastric epithelial progenitors into digestive-enzyme secreting zymogenic cells requires Mist1. Development *134*, 211-222.

Ricardo-Gonzalez, R.R., Van Dyken, S.J., Schneider, C., Lee, J., Nussbaum, J.C., Liang, H.E., Vaka, D., Eckalbar, W.L., Molofsky, A.B., Erle, D.J.*, et al.* (2018). Tissue signals imprint ILC2 identity with anticipatory function. Nat Immunol *19*, 1093-1099.

Riera, K.M., Jang, B., Min, J., Roland, J.T., Yang, Q., Fesmire, W.T., Camilleri-Broet, S., Ferri, L., Kim, W.H., Choi, E.*, et al.* (2020). Trop2 is upregulated in the transition to dysplasia in the metaplastic gastric mucosa. J Pathol.

Ringel, J., Jesnowski, R., Schmidt, C., Ringel, J., Kohler, H.J., Rychly, J., Batra, S.K., and Lohr, M. (2001). CD44 in normal human pancreas and pancreatic carcinoma cell lines. Teratog Carcinog Mutagen *21*, 97-106.

Roan, F., Obata-Ninomiya, K., and Ziegler, S.F. (2019). Epithelial cell-derived cytokines: more than just signaling the alarm. J Clin Invest *129*, 1441-1451.

Robinette, M.L., Fuchs, A., Cortez, V.S., Lee, J.S., Wang, Y., Durum, S.K., Gilfillan, S., Colonna, M., and Immunological Genome, C. (2015). Transcriptional programs define molecular characteristics of innate lymphoid cell classes and subsets. Nat Immunol *16*, 306-317.

Roediger, B., Kyle, R., Le Gros, G., and Weninger, W. (2014). Dermal group 2 innate lymphoid cells in atopic dermatitis and allergy. Curr Opin Immunol *31*, 108-114.

Roediger, B., and Weninger, W. (2015). Group 2 innate lymphoid cells in the regulation of immune responses. Adv Immunol *125*, 111-154.

Roth, K.A., Kapadia, S.B., Martin, S.M., and Lorenz, R.G. (1999). Cellular immune responses are essential for the development of Helicobacter felis-associated gastric pathology. J Immunol *163*, 1490-1497.

Rushworth, G.F., and Megson, I.L. (2014). Existing and potential therapeutic uses for N-acetylcysteine: the need for conversion to intracellular glutathione for antioxidant benefits. Pharmacol Ther *141*, 150-159.

Saenz, J.B., and Mills, J.C. (2018). Acid and the basis for cellular plasticity and reprogramming in gastric repair and cancer. Nat Rev Gastroenterol Hepatol *15*, 257-273.

Salimi, M., Barlow, J.L., Saunders, S.P., Xue, L., Gutowska-Owsiak, D., Wang, X., Huang, L.C., Johnson, D., Scanlon, S.T., McKenzie, A.N.*, et al.* (2013). A role for IL-25 and IL-33-driven type-2 innate lymphoid cells in atopic dermatitis. J Exp Med *210*, 2939-2950.

Sato, H., Shiiya, A., Kimata, M., Maebara, K., Tamba, M., Sakakura, Y., Makino, N., Sugiyama, F., Yagami, K., Moriguchi, T.*, et al.* (2005). Redox imbalance in cystine/glutamate transporter-deficient mice. J Biol Chem *280*, 37423-37429.

Satoh-Takayama, N., Kato, T., Motomura, Y., Kageyama, T., Taguchi-Atarashi, N., Kinoshita-Daitoku, R., Kuroda, E., Di Santo, J.P., Mimuro, H., Moro, K.*, et al.* (2020). Bacteria-Induced Group 2 Innate Lymphoid Cells in the Stomach Provide Immune Protection through Induction of IgA. Immunity.

Scanlon, S.T., and McKenzie, A.N. (2012). Type 2 innate lymphoid cells: new players in asthma and allergy. Curr Opin Immunol *24*, 707-712.

Schmidt, P.H., Lee, J.R., Joshi, V., Playford, R.J., Poulsom, R., Wright, N.A., and Goldenring, J.R. (1999). Identification of a metaplastic cell lineage associated with human gastric adenocarcinoma. Lab Invest *79*, 639-646.

Schmitz, J., Owyang, A., Oldham, E., Song, Y., Murphy, E., McClanahan, T.K., Zurawski, G., Moshrefi, M., Qin, J., Li, X.*, et al.* (2005). IL-33, an interleukin-1-like cytokine that signals via the IL-1 receptor-related protein ST2 and induces T helper type 2-associated cytokines. Immunity *23*, 479-490.

Schneider, C.A., Rasband, W.S., and Eliceiri, K.W. (2012). NIH Image to ImageJ: 25 years of image analysis. Nat Methods *9*, 671-675.

Schwartz, C., O'Grady, K., Lavelle, E.C., and Fallon, P.G. (2016). Interleukin 33: an innate alarm for adaptive responses beyond Th2 immunity-emerging roles in obesity, intestinal inflammation, and cancer. Eur J Immunol *46*, 1091-1100.

Serafini, N., Vosshenrich, C.A., and Di Santo, J.P. (2015). Transcriptional regulation of innate lymphoid cell fate. Nat Rev Immunol *15*, 415-428.

Shapouri-Moghaddam, A., Mohammadian, S., Vazini, H., Taghadosi, M., Esmaeili, S.A., Mardani, F., Seifi, B., Mohammadi, A., Afshari, J.T., and Sahebkar, A. (2018). Macrophage plasticity, polarization, and function in health and disease. J Cell Physiol *233*, 6425-6440.

Sharma, P., and Montgomery, E. (2013). Gastrointestinal dysplasia. Pathology *45*, 273-285.

Shi, C., and Pamer, E.G. (2011). Monocyte recruitment during infection and inflammation. Nat Rev Immunol *11*, 762-774.

Shi, G., DiRenzo, D., Qu, C., Barney, D., Miley, D., and Konieczny, S.F. (2013). Maintenance of acinar cell organization is critical to preventing Kras-induced acinar-ductal metaplasia. Oncogene *32*, 1950-1958.

Sipponen, P., and Maaroos, H.I. (2015). Chronic gastritis. Scand J Gastroenterol *50*, 657-667.

Siska, P.J., Kim, B., Ji, X., Hoeksema, M.D., Massion, P.P., Beckermann, K.E., Wu, J., Chi, J.T., Hong, J., and Rathmell, J.C. (2016). Fluorescence-based measurement of cystine uptake through xCT shows requirement for ROS detoxification in activated lymphocytes. J Immunol Methods *438*, 51-58.

Sousa, J.F., Ham, A.J., Whitwell, C., Nam, K.T., Lee, H.J., Yang, H.K., Kim, W.H., Zhang, B., Li, M., LaFleur, B.*, et al.* (2012). Proteomic profiling of paraffin-embedded samples identifies metaplasia-specific and early-stage gastric cancer biomarkers. Am J Pathol *181*, 1560-1572.

Spits, H., and Di Santo, J.P. (2011). The expanding family of innate lymphoid cells: regulators and effectors of immunity and tissue remodeling. Nat Immunol *12*, 21-27.

Stier, M.T., Bloodworth, M.H., Toki, S., Newcomb, D.C., Goleniewska, K., Boyd, K.L., Quitalig, M., Hotard, A.L., Moore, M.L., Hartert, T.V.*, et al.* (2016). Respiratory syncytial virus infection activates IL-13-producing group 2 innate lymphoid cells through thymic stromal lymphopoietin. J Allergy Clin Immunol *138*, 814-824 e811.

Storz, P. (2017). Acinar cell plasticity and development of pancreatic ductal adenocarcinoma. Nat Rev Gastroenterol Hepatol *14*, 296-304.

Sui, P., Wiesner, D.L., Xu, J., Zhang, Y., Lee, J., Van Dyken, S., Lashua, A., Yu, C., Klein, B.S., Locksley, R.M.*, et al.* (2018). Pulmonary neuroendocrine cells amplify allergic asthma responses. Science *360*.

Taylor, S., Huang, Y., Mallett, G., Stathopoulou, C., Felizardo, T.C., Sun, M.A., Martin, E.L., Zhu, N., Woodward, E.L., Elias, M.S.*, et al.* (2017). PD-1 regulates KLRG1(+) group 2 innate lymphoid cells. J Exp Med *214*, 1663-1678.

Vaahtera, L., Brosche, M., Wrzaczek, M., and Kangasjarvi, J. (2014). Specificity in ROS signaling and transcript signatures. Antioxid Redox Signal *21*, 1422-1441.

Van Ginderachter, J.A., Movahedi, K., Hassanzadeh Ghassabeh, G., Meerschaut, S., Beschin, A., Raes, G., and De Baetselier, P. (2006). Classical and alternative activation of mononuclear phagocytes: picking the best of both worlds for tumor promotion. Immunobiology *211*, 487-501.

Vannella, K.M., Ramalingam, T.R., Borthwick, L.A., Barron, L., Hart, K.M., Thompson, R.W., Kindrachuk, K.N., Cheever, A.W., White, S., Budelsky, A.L.*, et al.* (2016). Combinatorial targeting of TSLP, IL-25, and IL-33 in type 2 cytokine-driven inflammation and fibrosis. Sci Transl Med *8*, 337ra365.

von Moltke, J., Ji, M., Liang, H.E., and Locksley, R.M. (2016). Tuft-cell-derived IL-25 regulates an intestinal ILC2-epithelial response circuit. Nature *529*, 221-225.

Wada, T. (2013). Functional role of CD44v-xCT system in the development of spasmolytic polypeptide-expressing metaplasia Cancer Science *104*, 1323-1329.

Wada, T., Ishimoto, T., Seishima, R., Tsuchihashi, K., Yoshikawa, M., Oshima, H., Oshima, M., Masuko, T., Wright, N.A., Furuhashi, S.*, et al.* (2013). Functional role of CD44v-xCT system in the development of spasmolytic polypeptide-expressing metaplasia. Cancer Sci *104*, 1323-1329.

Wallrapp, A., Burkett, P.R., Riesenfeld, S.J., Kim, S.J., Christian, E., Abdulnour, R.E., Thakore, P.I., Schnell, A., Lambden, C., Herbst, R.H.*, et al.* (2019). Calcitonin Gene-Related Peptide Negatively Regulates Alarmin-Driven Type 2 Innate Lymphoid Cell Responses. Immunity *51*, 709-723 e706.

Wallrapp, A., Riesenfeld, S.J., Burkett, P.R., Abdulnour, R.E., Nyman, J., Dionne, D., Hofree, M., Cuoco, M.S., Rodman, C., Farouq, D.*, et al.* (2017). The neuropeptide NMU amplifies ILC2-driven allergic lung inflammation. Nature *549*, 351-356.

Warzecha, C.C., Shen, S., Xing, Y., and Carstens, R.P. (2009). The epithelial splicing factors ESRP1 and ESRP2 positively and negatively regulate diverse types of alternative splicing events. RNA Biol *6*, 546-562.

Weis, V.G., Knowles, B.C., Choi, E., Goldstein, A.E., Williams, J.A., Manning, E.H., Roland, J.T., Lapierre, L.A., and Goldenring, J.R. (2016). Loss of MYO5B in mice recapitulates Microvillus Inclusion Disease and reveals an apical trafficking pathway distinct to neonatal duodenum. Cell Mol Gastroenterol Hepatol *2*, 131-157.

Weis, V.G., Petersen, C.P., Mills, J.C., Tuma, P.L., Whitehead, R.H., and Goldenring, J.R. (2014). Establishment of novel in vitro mouse chief cell and SPEM cultures identifies MAL2 as a marker of metaplasia in the stomach. Am J Physiol Gastrointest Liver Physiol *307*, G777-792.

Weis, V.G., Petersen, C.P., Weis, J.A., Meyer, A.R., Choi, E., Mills, J.C., and Goldenring, J.R. (2017). Maturity and age influence chief cell ability to transdifferentiate into metaplasia. Am J Physiol Gastrointest Liver Physiol *312*, G67-G76.

Weis, V.G., Sousa, J.F., LaFleur, B.J., Nam, K.T., Weis, J.A., Finke, P.E., Ameen, N.A., Fox, J.G., and Goldenring, J.R. (2013). Heterogeneity in mouse spasmolytic polypeptide-expressing metaplasia lineages identifies markers of metaplastic progression. Gut *62*, 1270-1279.

Weller, P.F., and Spencer, L.A. (2017). Functions of tissue-resident eosinophils. Nat Rev Immunol *17*, 746-760.

Willet, S.G., Lewis, M.A., Miao, Z.F., Liu, D., Radyk, M.D., Cunningham, R.L., Burclaff, J., Sibbel, G., Lo, H.G., Blanc, V.*, et al.* (2018). Regenerative proliferation of differentiated cells by mTORC1-dependent paligenosis. EMBO J *37*.

Wills-Karp, M., and Finkelman, F.D. (2008). Untangling the complex web of IL-4- and IL-13-mediated signaling pathways. Sci Signal *1*, pe55.

Xu, H., Ding, J., Porter, C.B.M., Wallrapp, A., Tabaka, M., Ma, S., Fu, S., Guo, X., Riesenfeld, S.J., Su, C.*, et al.* (2019). Transcriptional Atlas of Intestinal Immune Cells Reveals that Neuropeptide alpha-CGRP Modulates Group 2 Innate Lymphoid Cell Responses. Immunity *51*, 696-708 e699.

Xu-Monette, Z.Y., Zhang, M., Li, J., and Young, K.H. (2017). PD-1/PD-L1 Blockade: Have We Found the Key to Unleash the Antitumor Immune Response? Front Immunol *8*, 1597.

Yae, T., Tsuchihashi, K., Ishimoto, T., Motohara, T., Yoshikawa, M., Yoshida, G.J., Wada, T., Masuko, T., Mogushi, K., Tanaka, H.*, et al.* (2012). Alternative splicing of CD44 mRNA by ESRP1 enhances lung colonization of metastatic cancer cell. Nat Commun *3*, 883.

Yamaguchi, H., Goldenring, J.R., Kaminishi, M., and Lee, J.R. (2002). Identification of spasmolytic polypeptide expressing metaplasia (SPEM) in remnant gastric cancer and surveillance postgastrectomy biopsies. Dig Dis Sci *47*, 573-578.

Yang, I., Nell, S., and Suerbaum, S. (2013). Survival in hostile territory: the microbiota of the stomach. FEMS Microbiol Rev *37*, 736-761.

Zavros, Y. (2017). Initiation and Maintenance of Gastric Cancer: A Focus on CD44 Variant Isoforms and Cancer Stem Cells. Cell Mol Gastroenterol Hepatol *4*, 55-63.

Zhang, F., Kumano, M., Beraldi, E., Fazli, L., Du, C., Moore, S., Sorensen, P., Zoubeidi, A., and Gleave, M.E. (2014). Clusterin facilitates stress-induced lipidation of LC3 and autophagosome biogenesis to enhance cancer cell survival. Nature communications *5*, 5775.

Zhang, M.L., Neyaz, A., Patil, D., Chen, J., Dougan, M., and Deshpande, V. (2020). Immune-related adverse events in the gastrointestinal tract: diagnostic utility of upper gastrointestinal biopsies. Histopathology *76*, 233-243.

Zhang, Y., Chen, J.N., Dong, M., Zhang, Z.G., Zhang, Y.W., Wu, J.Y., Du, H., Li, H.G., Huang, Y., and Shao, C.K. (2017). Clinical significance of spasmolytic polypeptide-expressing metaplasia and intestinal metaplasia in Epstein-Barr virus-associated and Epstein-Barr virus-negative gastric cancer. Hum Pathol *63*, 128-138.

Zhu, Z., Homer, R.J., Wang, Z., Chen, Q., Geba, G.P., Wang, J., Zhang, Y., and Elias, J.A. (1999). Pulmonary expression of interleukin-13 causes inflammation, mucus hypersecretion, subepithelial fibrosis, physiologic abnormalities, and eotaxin production. J Clin Invest *103*, 779-788.